

UNCLASSIFIED

AD NUMBER
AD866372
NEW LIMITATION CHANGE
TO Approved for public release, distribution unlimited
FROM Distribution authorized to U.S. Gov't. agencies and their contractors; Administrative/Operational Use; NOV 1969. Other requests shall be referred to Air Force Flight Dynamics Lab., Wright-Patterson AFB, OH 45433.
AUTHORITY
AFFDL ltr, 25 Oct 1972

THIS PAGE IS UNCLASSIFIED

AFFDL-TR-69-79

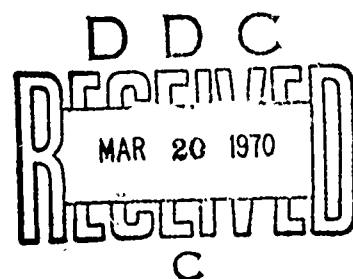
AD 866372

DEVELOPMENT OF HIGH ALTITUDE CLEAR AIR TURBULENCE MODELS

EDWARD V. ASHBURN, DAVID E. WACO AND F. A. MITCHELL
Lockheed-California Company

TECHNICAL REPORT AFFDL-TR-69-79

NOVEMBER 1969



This document is subject to special export controls and each transmittal to foreign governments or foreign nationals may be made only with prior approval of the Air Force Flight Dynamics Laboratory (FDTE), Wright-Patterson AFB, Ohio 45433.

Reproduced by the
CLEARINGHOUSE
for Federal Scientific & Technical
Information Springfield Va 22151

AIR FORCE FLIGHT DYNAMICS LABORATORY
AIR FORCE SYSTEMS COMMAND
WRIGHT-PATTERSON AIR FORCE BASE, OHIO

ACU	
CFSTI	SECTION <input type="checkbox"/>
ROC	DIFF SECTION <input checked="" type="checkbox"/>
UNCLASSIFIED	<input type="checkbox"/>
JUSTIFICATION	
DISTRIBUTION AVAILABILITY CODES	
DIST.	AVAIL. or SPECIAL
2	

NOTICE

When Government drawings, specifications, or other data are used for any purpose other than in connection with a definitely related Government procurement operation, the United States Government thereby incurs no responsibility nor any obligation whatsoever; and the fact that the government may have formulated, furnished, or in any way supplied the said drawings, specifications, or other data, is not to be regarded by implication or otherwise as in any manner licensing the holder or any other person or corporation, or conveying any rights or permission to manufacture, use, or sell any patented invention that may in any way be related thereto.

This document is subject to export controls and each transmittal to foreign governments or foreign nationals may be made only with prior approval of the Air Force Flight Dynamics Laboratory (AFFDL), Wright-Patterson Air Force Base, Ohio 45433.

Copies of this report should not be returned unless return is required by security considerations, contractual obligations, or notice on a specific document,

AFFDL-TR-69-79

DEVELOPMENT OF HIGH ALTITUDE CLEAR AIR TURBULENCE MODELS

EDWARD V. ASHBURN, DAVID E. WACO AND F. A. MITCHELL

Lockheed-California Company

This document is subject to special export controls and each transmittal to foreign governments or foreign nationals may be made only with prior approval of the Air Force Flight Dynamics Laboratory (FDTE), Wright-Patterson AFB, Ohio 45433.

FOREWORD

This report was prepared by the Lockheed-California Company, Burbank, California for the Air Force Flight Dynamics Laboratory, Wright-Patterson Air Force Base, Ohio under Contract F33615-69-C-1033. The contract title is "Improved HICAT Models for Aircraft Design and Operation". The contract was initiated under Project No. 1367, "Structural Design Criteria", Task No. 136702, "Aerospace Vehicle Structural Loads Criteria". The Lockheed-California Company report number is LR 22630. The report covers work conducted from 1 October 1968 to 30 September 1969.

The contract was administered by the Air Force Flight Dynamics Laboratory, Wright-Patterson Air Force Base, Ohio with Mr. Paul L. Hasty (FDTE) as Project Engineer. The Lockheed-California Company Principal Investigator was Mr. Edward V. Ashburn. Special acknowledgements are due to Dr. Arnold Court, consultant for the program and to the following Lockheed-California Company personnel: Dr. D.T. Perkins, Division Scientist, Physical and Life Sciences Laboratory; Mr. D.T. Prophet, Mr. S. I. Adelfang, Mr. C.A. Melvin, Mr. W.M. Crooks and Mr. J.M. Rapp.

This report was submitted by the authors in September 1969.

This technical report has been reviewed and is approved.


Gordon R. Negaard, Major, USAF
Chief, Design Criteria Branch
Structures Division

ABSTRACT

The high altitude clear air turbulence data were divided into subsets defined by season, altitude, topography and flight heading. The shape of the power spectral density curves are shown to be a function of topography with corresponding "scale lengths" of 500 feet for flights over water and flatland and increasing to 4000 feet for flights over high mountains. The areas under the power spectral density curves (140 to 2000 ft wavelength) are shown to have a log-normal distribution. Eight functions of atmospheric temperature and wind were found to be significantly correlated with high altitude clear air turbulence. Turbulence was observed twice as often with head winds than it was with tail winds. The probability of a turbulent region equaling or exceeding a given length, d , may be expressed as $109 \exp(-0.038d)$ where $d > 2.6$ nm. Over thunderstorms the intensity of the turbulence and the length of the turbulent regions decreased with increasing height above the cloud top.

TABLE OF CONTENTS

Section	Page
I INTRODUCTION	1
II FREQUENCY DISTRIBUTIONS OF THE DATA RELATING TO HIGH ALTITUDE CLEAR AIR TURBULENCE	2
Summary	2
Frequency Distributions	2
III RELATIONSHIPS BETWEEN HICAT AND THE UNDERLYING TOPOGRAPHY	9
Summary	9
The Ratio of Flight Miles in HICAT to the Total Flight Miles as a Function of Topography	10
Power Spectral Density Shapes as a Function of Topography	16
The Variation of Gust Velocities with Topography	27
Variation of U_V with Topography and Altitude	31
IV THE DISTRIBUTION OF LENGTHS OF HIGH ALTITUDE CLEAR AIR TURBULENT REGIONS	37
Summary	37
Discussion	37
V HICAT FLIGHTS AND THUNDERSTORMS	40
Summary	40
Discussion	40
VI CORRELATION OF HICAT WITH FUNCTIONS OF ATMOSPHERE TEMPERATURES AND WINDS	42
Summary	42
Selection of the Sample and Description of the Tests	42
Results of Applying Chi-Square and Kolmogorov Tests	42
In-Flight Measured Temperature Gradients	49
VII CORRELATION BETWEEN HICAT AND HEAD WIND AND TAIL WIND	58
Summary	58
Discussion	58

TABLE OF CONTENTS (Continued)

Section		Page
VIII	EXCEEDANCE PROBABILITY OF RMS (2000) FOR THE THREE COMPONENTS OF THE GUST VELOCITY BY SEASON AND BY ALTITUDE	62
	Summary	62
	Discussion	62
IX	DISTRIBUTION OF HICAT FLIGHT MILES AND TURBULENT FLIGHT MILES IN THE UNITED STATES	66
	Summary	66
	Discussion	66
X	MODELS AND EXAMPLES	68
XI	CONCLUSIONS	70
	REFERENCES	72

LIST OF ILLUSTRATIONS

Figure		Page
1	Distribution by Seasons of Number of Observations of HICAT.	4
2	Distribution by Seasons of the Number of Observations of cg Acceleration and U_{DE} (max).	5
3	Distribution by Seasons of Number of Observations of Aircraft Heading, Ambient Temperature and Wind.	6
4	Distributions by Altitude of Number of Observations of RMS (2000).	7
5	Distribution by Season and Altitude of Number of Observations of High Altitude Clear Air Turbulence.	8
6	Distribution of the Number of Observations of Turbulence by Topography and by Season.	11
7	Distribution of Number of Observations of Turbulence Over Water by Season and Altitude.	12
8	Distribution of Number of Observations of Turbulence Over Flatland by Season and Altitude.	13
9	Distribution of Number of Observations of Turbulence Over Low Mountains by Season and Altitude.	14
10	Distribution of Number of Observations of Turbulence Over High Mountains by Season and Altitude.	15
11	Distribution of Total Flight Miles and Turbulent Flight Miles by Terrain for Ferry Flights and All Flights.	17
12	Distribution of Total Flight Miles and Turbulent Flight Miles by Terrain for Edwards, Hickam, Christchurch and Laverton.	18
13	Distribution of Total Flight Miles and Turbulent Flight Miles by Terrain for Barksdale, Caribou, Albrook and Patrick.	19
14	Distribution of Total Flight Miles and Turbulent Flight Miles by Terrain for Hanscom, Ramey, Elmendorf and Bedford.	20
15	Normalized Power Spectral Curves for All Flatland Cases with Long Wavelength Limit of 10,000 ft.	24
16	Normalized Power Spectral Curves for All Low Mountain Cases with Long Wavelength Limit of 10,000 ft.	25
17	Normalized Power Spectral Curves for All High Mountain Cases with Long Wavelength Limit of 10,000 ft.	26
18	Normalized Spectra for Three Particular Cases of High Altitude Clear Air Turbulence.	28
19	Time Histories of U_v for the Three Spectra Shown in Figure 18.	29

LIST OF ILLUSTRATIONS (Continued)

Figure		Page
20	Distribution of the Number of Observations of Turbulence by RMS (2000) Magnitude and Topography.	30
21	Percentage Exceedance of RMS (2000) for the U_V Component for Four Categories of Topography.	32
22	Percentage Exceedance of RMS (2000) for the U_L Component for Four Categories of Topography.	33
23	Percentage Exceedance of RMS (2000) for the U_F Component for Four Categories of Topography.	34
24	Percentage Exceedance of RMS (2000) for the U_V Component for Two Categories of Topography.	35
25	Histograms of Temperature Variables for Turbulent and Non-Turbulent Cases.	45
26	Histograms of Wind Variables and Richardson's Number for Turbulent and Non-Turbulent Cases.	46
27	Cumulative Frequency Distribution of Temperature Variables for Turbulent and Non-Turbulent Cases.	47
28	Cumulative Frequency Distribution of Wind Variables and Richardson's Number for Turbulent and Non-Turbulent Cases.	48
29	Minimum Vertical Potential Temperature Gradient as a Function of Vertical Vector Wind Shear.	50
30	Correlation Between In-Flight Measured Temperature and Gust Velocity Changes.	51
31	Time Histories of Gust Velocity and Temperature Variations for Smooth (A) and Turbulent (B) Flights Over Southeast Australia.	52
32	Time Histories of Gust Velocity and Temperature Variations for Flights Over Southeast Australia (A) and Albuquerque, New Mexico (B).	53
33	Time Histories of Gust Velocity and Temperature Variations for Flights Over Little Rock, Arkansas (A) and Southeast Australia (B).	54
34	Time Histories of Gust Velocity and Temperature Variations for Two Flights Over the Lee Side of the Sierra Nevada Mountains, California.	55
35	Time Histories of Gust Velocity and Temperature Variations for a Flight Over the Lee Side of the Rocky Mountains Near Denver, Colorado.	56

LIST OF ILLUSTRATIONS (Continued)

Figure		Page
36	Histogram of the Difference in Angle Between Heading and Wind for the HICAT Turbulence Cases.	59
37	Change in WU-2 Observed Wind Direction (ΔW) as a Function of Change in Aircraft True Heading (ΔTH) for All Runs with Change in Altitude ≤ 1000 feet and Wind Velocity ≥ 10 knots.	60
38	Cumulative Distribution of RMS (2000) Gust Velocity.	63
39	Distribution of HICAT Flight and Turbulent Flight Miles in the United States.	67
40	Percentage of Flight Miles for Which Given Value of σ_w^2 is Equalled or Exceeded.	69
Table		Page
I	RATIO (PERCENTAGE) OF TURBULENT FLIGHT MILES TO TOTAL FLIGHT MILES	10
II (a)	AVERAGE VALUES OF THE RATIO OF U_V , U_F , AND U_L AT RMS (2000), RMS (4000), RMS (10,000), AND RMS (20,000) TO RMS (1000)	21
II (b)	THEORETICAL VALUES OF THE RATIOS OF RMS (2000), RMS (4000), RMS (10,000) AND RMS (20,000) TO RMS (1000) FOR VARIOUS L'S OF THE MILD KNEE EQUATION WITH $M = -5/3$	22
III	THE RATIO OF RMS (100,000)/RMS (2000) FOR VARIOUS VALUES OF SCALE LENGTH, L, COMPUTED FROM THE "MILD KNEE" EQUATION WITH SLOPE $M = -5/3$	27
IV	AVERAGE VALUES OF THE RATIO OF U_V RMS (2000), RMS (4000), AND RMS (10,000) TO U_V RMS (1000) FOR GIVEN ALTITUDE BANDS	31
V	NUMBER OF OCCURRENCES BY TERRAIN OR RUNS WITH U_V RMS (2000) GREATER THAN LISTED VALUES FOR GIVEN ALTITUDE BANDS	36
VI	MEAN LENGTHS OF TURBULENT REGIONS AS A FUNCTION OF ALTITUDE	37
VII	MEAN LENGTHS OF TURBULENT REGIONS AS A FUNCTION OF SEASON	38

LIST OF ILLUSTRATIONS (Continued)

Table		Page
VIII	CHARACTERISTICS OF TURBULENCE ABOVE THUNDERSTORMS	40
IX	CHI-SQUARE (χ^2) AND KOLMOGOROV-SMIRNOV (K-S) TESTS APPLIED TO METEOROLOGICAL VARIABLES FOR HICAT FLIGHTS	44
X	CONTINGENCY TABLE SHOWING WIND DIRECTION AND AIRCRAFT HEADING CATEGORIES (349 RUNS)	61
XI	CALCULATED VALUES FOR CONSTANTS IN EXCEEDANCE EQUATION	62
XII	RMS (2000) EXCEEDANCE GUST VELOCITIES (FT/SEC)	65

SYMBOLS

d	Length of turbulence region in nautical miles.
g	Acceleration of gravity (ft/sec ²).
L	Scale length of turbulence in feet
P _d	Probability (percentage) of length of turbulence region exceeding given value.
Ri	Richardson's number.
RMS ()	Root mean square of the area (ft/sec) under the power spectral density curve truncated at wavelength given in parentheses.
T	Temperature (°C).
U _{de}	Derived equivalent gust velocity (ft/sec); positive upward.
U _{dc} (max)	The maximum derived equivalent gust velocity is the value, expressed in ft/sec of the largest positive peak increment of vertical cg normal acceleration observed during a processed turbulent run.
U _F	Longitudinal gust component (ft/sec) in earth reference axes measured in the horizontal plane parallel to the average grid heading of the aircraft over duration of the "run"; positive aft.
U _L	Lateral gust component (ft/sec) in earth reference axes measured in the horizontal plane and perpendicular to the average grid heading of the aircraft over the duration of the "run"; positive to the left.
U _V	Vertical gust component (ft/sec) in the earth reference axes measured perpendicular to the horizontal plane; positive upward.
V	Wind speed in knots.
z	Vertical axis.
λ	Wavelength in feet.
θ	Potential temperature (°K) of the atmosphere.

SECTION I

INTRODUCTION

The HICAT flight program effort required the measurement of clear air turbulence velocity components at altitudes of 45,000 to 70,000 feet at thirteen geographic areas. Instruments carried aboard the U-2 aircraft consisted of a pulse code modulation system, an inertial navigation system, aerodynamic and aircraft response sensors including a fixed vane gust probe, oscillograph recorder, and a digital magnetic tape recorder. These instruments made it possible to obtain clear air turbulence measurements in the wavelength range from approximately 100 to 50,000 feet. The data obtained from the HICAT flight program were published by Crooks et al (1,2). This present report consists of an extensive analysis of the meteorological and geophysical conditions associated with high altitude clear air turbulence where the basic data relating to the turbulence were obtained from the HICAT flight program reports. The principal objective in this analysis was to provide information for use in the design, development and operation of advanced aerospace vehicles. This report is a relatively large extension and amplification of a previous report by Ashburn et al (3) that was published before all the HICAT flight program data were available.

A description of the HICAT data sample and discussions of the power spectral density, meteorological and topographic correlations with HICAT, and the percentage of the time in turbulence are presented in the following sections. Each of the sections begins with a summary.

SECTION II

FREQUENCY DISTRIBUTIONS OF THE DATA RELATING TO HIGH ALTITUDE CLEAR AIR TURBULENCE

Summary

In the HICAT flight program there were nearly 1000 distinct observations of clear air turbulence. The distribution of these observations by season and altitude is as follows:

1. For the winter season there is a sharp maximum at the altitude band 50,100-55,000 ft.
2. For the spring season there is a lower but broader maximum with nearly an equal number of observations in the two altitude bands 50,100-55,000 ft and 55,100-60,000 ft.
3. For the summer season the maximum number of observations is in the 50,100-55,000 ft range but the maximum number is approximately one third of the maximum number for the winter season.
4. For the autumn season the distribution is intermediate between those found for the winter and spring.
5. The RMS (2000) values were computed for approximately 20% of the observations.

Frequency Distributions

The set of data relating to high altitude clear air turbulence that was presented in the reports by Crooks et al (1,2) was, for the purposes of this report, divided into subsets such as season, altitude interval, location, etc. This section consists of a display of the frequency distributions derived from the number of observations per season and altitude intervals. This display serves three purposes. First, it clearly shows the size of the samples available for analysis. Secondly, it indicates the extent to which the unions of subsets (such as season, altitude, location, etc.) provide adequate sample size. Thirdly, it may serve as a guide for planning future HICAT measurement programs.

Figure 1a shows the distribution by season of the total number of observations ("runs" as defined by Crooks (1)) of high altitude clear air turbulence and Figure 1b shows the distribution by season of the number of turbulence cases for which the RMS (2000) for the three components of the true gust velocities were computed. The data for Figures 1-5 were taken from the HICAT Test Summary Tables given by Crooks (1,2). The relatively small number of cases of HICAT for the summer may be explained, in part, by fewer flights in summer because in the northern hemisphere summer of 1966 the flight activity was in the southern hemisphere. In this report the seasons are defined as follows:

Months	Northern Hemisphere	Southern Hemisphere
December - February	Winter	Summer
March - May	Spring	Autumn
June - August	Summer	Winter
September - November	Autumn	Spring

Figures 2a and 2b illustrate the distribution by season of the number of observations of the cg acceleration (maximum) and the $U_{de}(\max)$. Figures 3a, b and c illustrate the distribution of the number of observations of aircraft heading, ambient temperature and wind respectively. The distribution by altitude interval of observations of the RMS (2000) of the three components of the true gust velocity is shown in Figure 4. In Figure 5 the union of the subsets of season and altitude is shown. This figure clearly indicates that the distribution of the number of observations by seasons varies significantly from one altitude band to another.

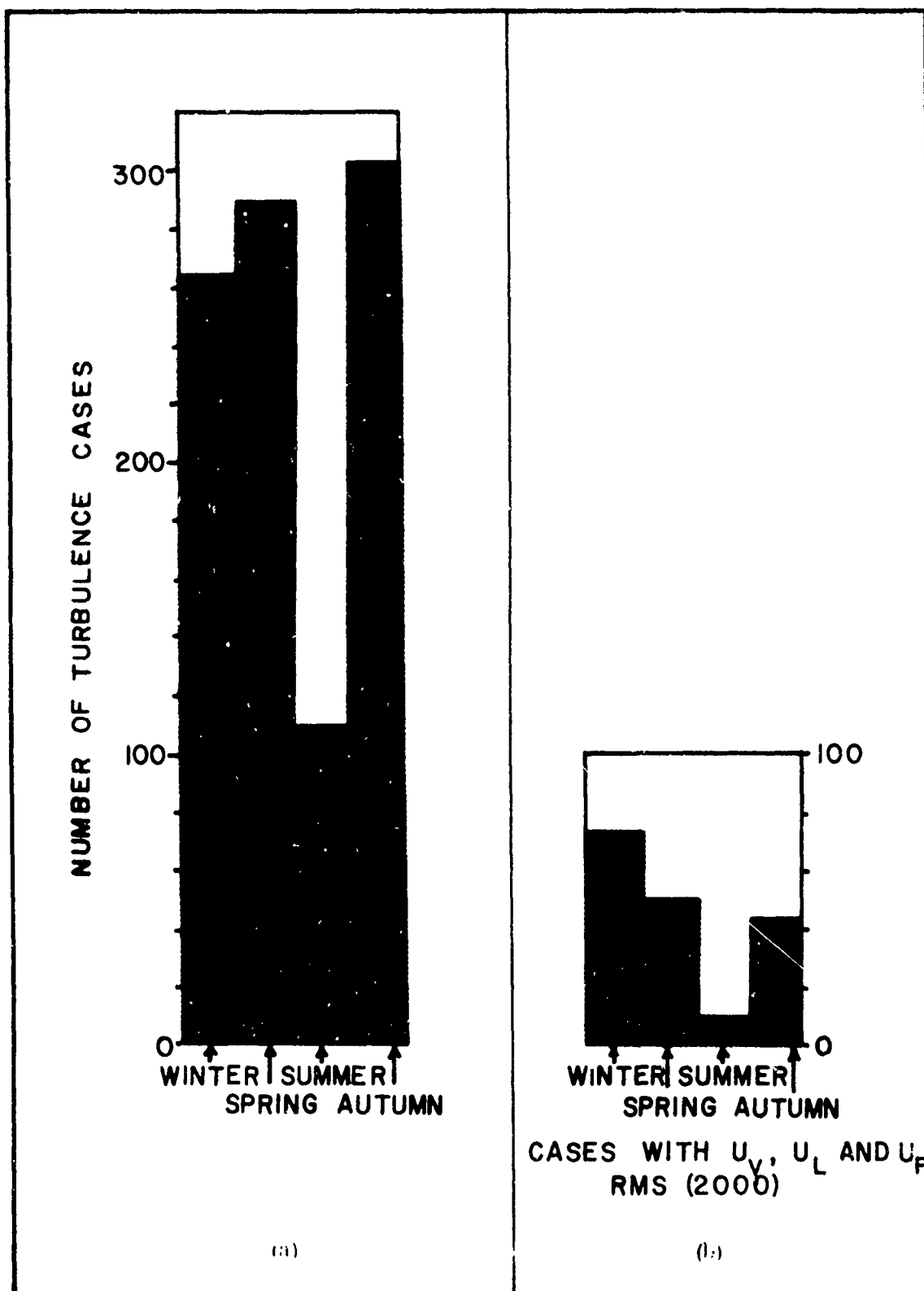


Figure 1. Distribution by Seasons of Number of Observations of HICAT.

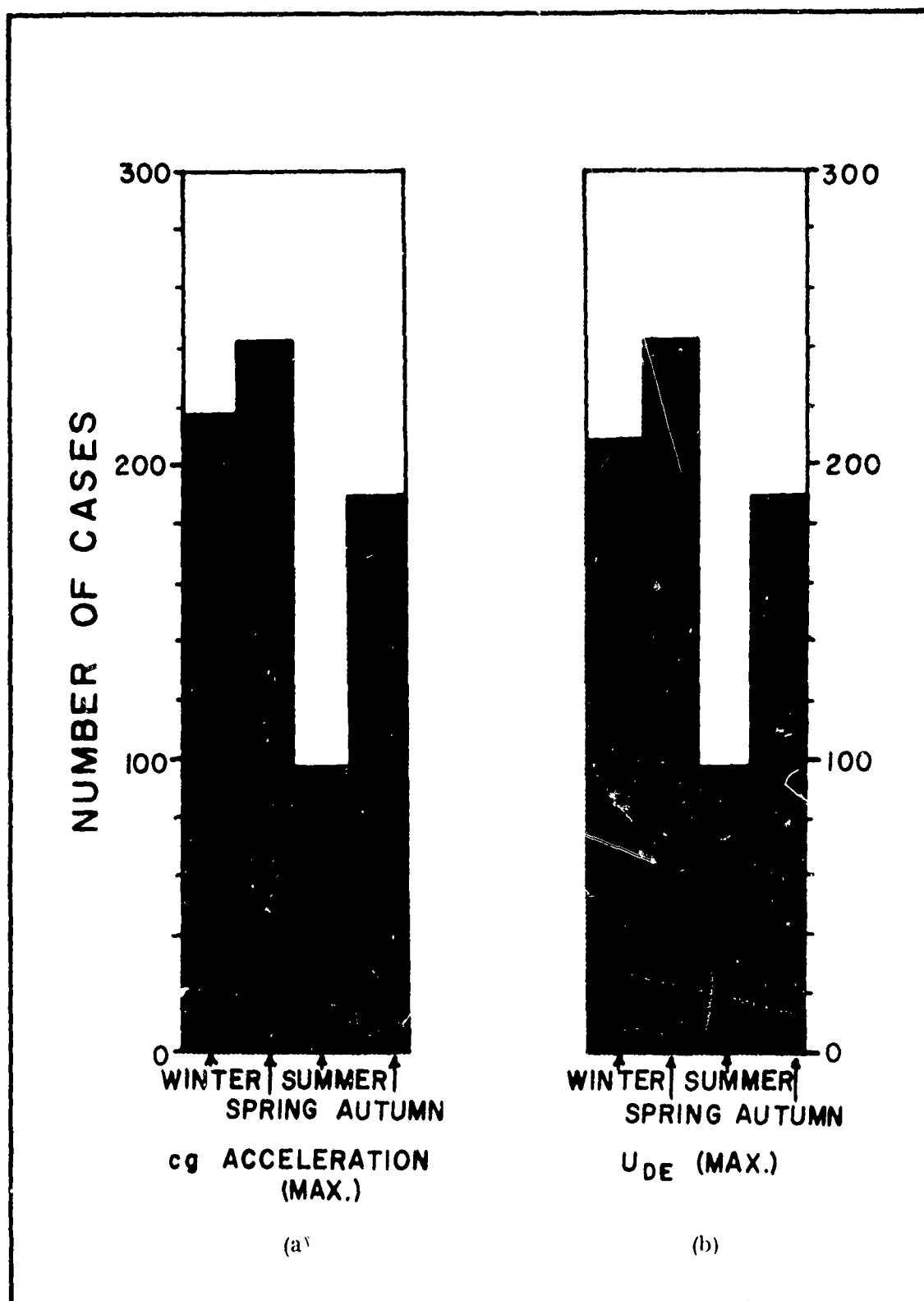


Figure 2. Distribution by Seasons of the Number of Observations of cg Acceleration and U_{de}

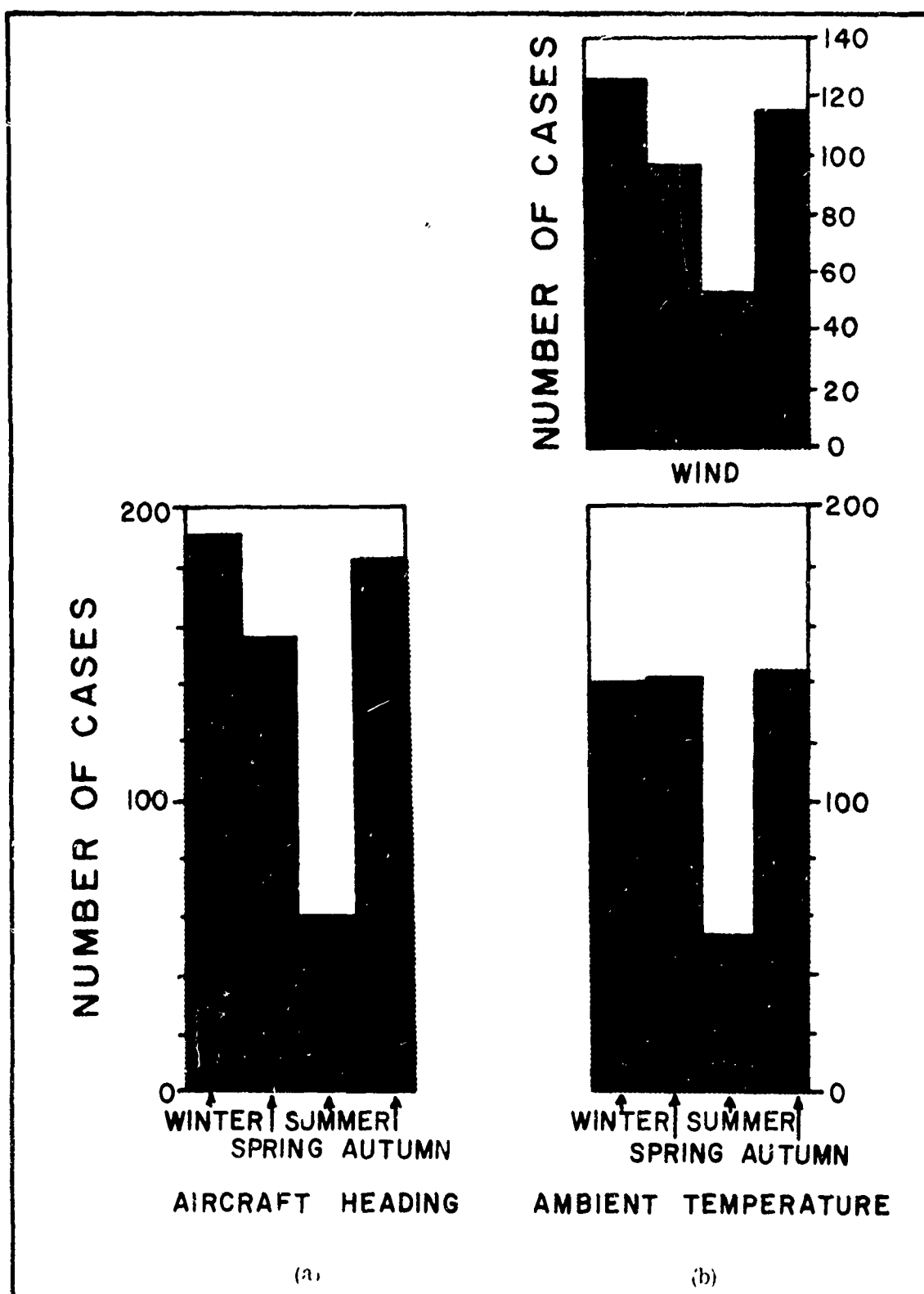


Figure 3. Distribution by Seasons of Number of Observations of Aircraft Heading, Ambient Temperature and Wind.

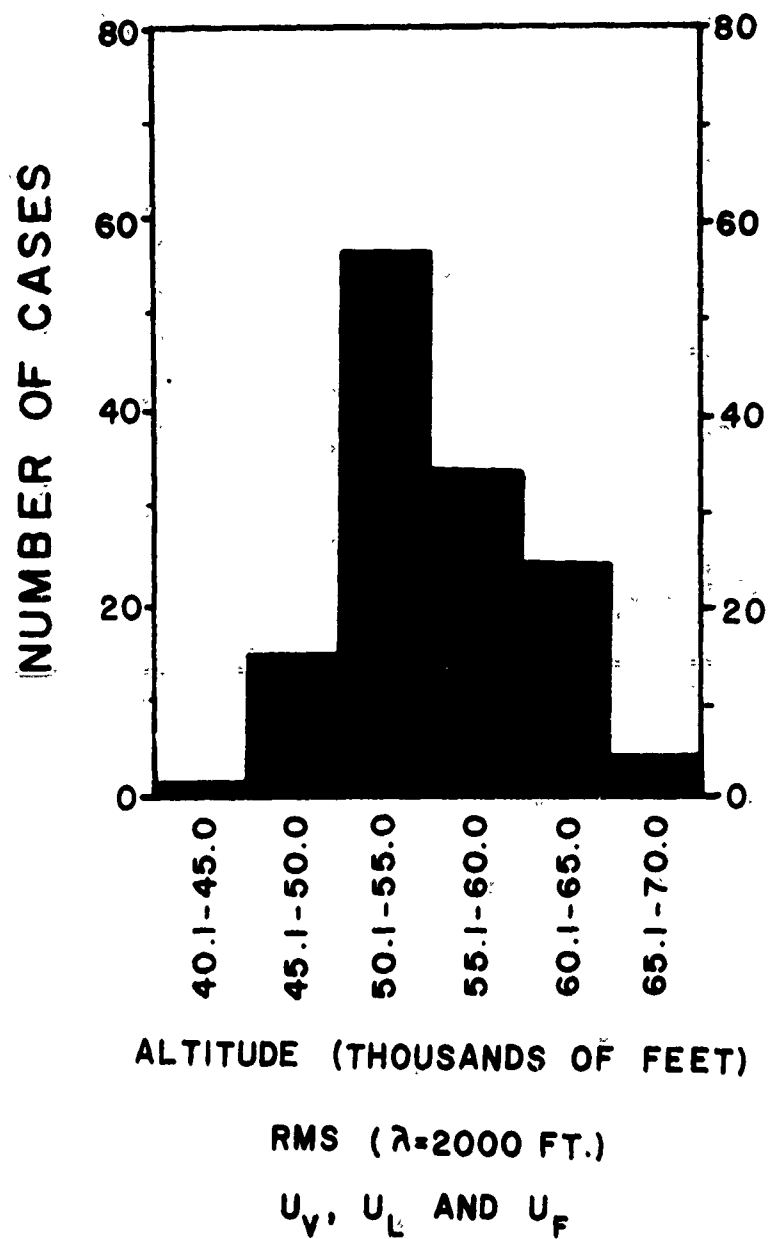


Figure 4. Distributions by Altitude of Number of Observations of RMS(2000).

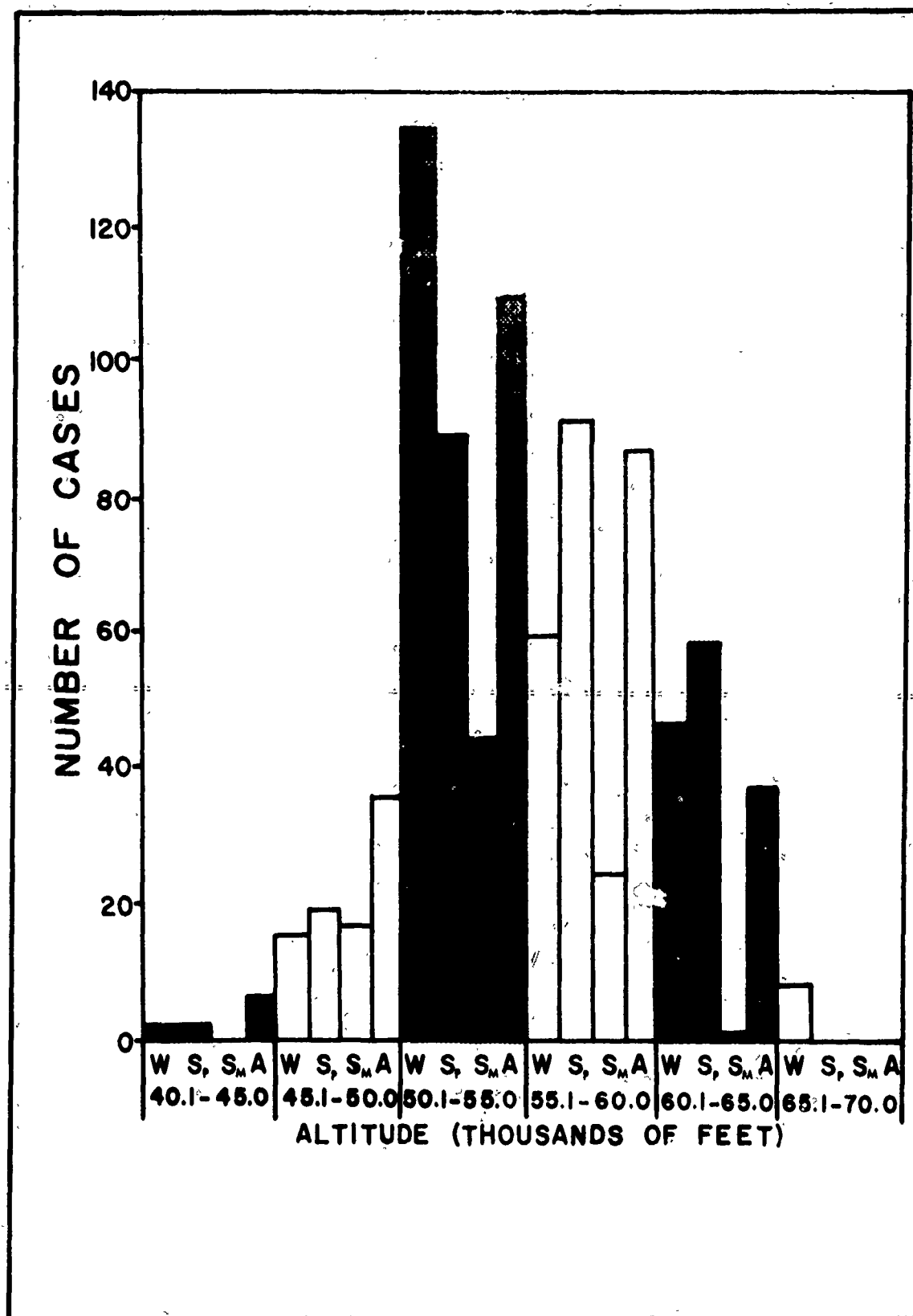


Figure 5. Distribution by Season and Altitude of Number of Observations of High Altitude Clear Air Turbulence.

SECTION III

RELATIONSHIPS BETWEEN HICAT AND THE UNDERLYING TOPOGRAPHY

Summary

The flight track maps for HICAT flights 54 through 285 were reexamined in detail. The total flight miles above 40,000 feet altitude and flight miles in turbulence were determined. Repeat flights through what were presumed to be the same turbulent regions were eliminated. In addition, all cases classified by Crooks et al (1) as "very light" turbulence were treated as non-turbulent. Four categories of underlying topography were used. These were (1) water, (2) flatland (local relief differences less than 3000 ft in altitude), (3) low mountains (local relief differences 3000 to 7000 ft in altitude), and (4) high mountains (local relief differences greater than 7000 ft in altitude). The field of view of both mountain categories was designated as 50 miles upwind from the nadir point.

This analysis indicated that for those cases of turbulence that Crooks et al (1) classified as equal to or greater than "light" the ratio of turbulent flight miles to total flight miles was 33% greater over low mountains than over flatlands or water. This ratio increased to 82% for high mountains relative to flatlands or water. For those cases that Crooks et al (1) classified as moderate or greater turbulence, the ratio of the turbulent flight miles to total flight miles for the mountain cases was three to four times that found for flights over flatland or water.

Curves showing the percentage of the time that given values of the RMS (2000) for the true gust velocities are exceeded indicated significant differences between flights over mountains and flights over flatland or water. Relatively high values of the RMS (2000) were observed more frequently over mountainous terrain than over flatlands or water. These exceedance curves also indicate that if turbulence exists at all in flights over mountains the RMS (2000) is most likely to be relatively high compared to the mean for turbulent cases including all types of terrain.

A detailed examination of the slopes of the power spectral density curves indicated that when the cases were restricted to those with RMS (2000) greater than 1.0 ft/sec the mountain cases showed a significantly greater slope at wavelengths greater than 1000 ft. The lateral (U_L) and longitudinal (U_F) components of the gust velocity showed consistently larger increases in the slope than the vertical component (U_V) for both topographic groups. The "scale length" as determined by the power spectral density curves for U_V appeared to be around 4000 ft for "high mountain" cases, 2000 ft for low mountains and 500 ft for flatlands. There was no significant change in the spectral shape characteristics with flight altitude for either the mountain or the flatland cases.

The distribution of RMS (2000) values of U_V showed no significant change with altitude for the mountain cases and a relatively large decrease with altitude above flatlands.

The Ratio of Flight Miles in HICAT to the Total Flight Miles as a Function of Topography

Flight track maps and topographic maps were used to determine the HICAT Project flight miles over four categories of topography for the HICAT flights 54 through 285. The four categories of topography were defined as follows:

Water

Flatland (local relief differences < 3000 ft)

Low mountains (local relief differences 3000 to 7000 ft)

High mountains (local relief differences > 7000 ft)

In the previous analysis (Ashburn et al (3)) of HICAT data only one mountain category was used. The present analysis also differs from the previous one in the assignment of flight miles through patterns and the choice of category for marginal cases.

The field of view for both mountain classes was designated as 50 miles upwind. If a mountain range was upwind and within 50 miles of the nadir point of the U-2's flight path, the observation was placed in one of the mountain classes. Small islands or isolated peaks on plains were classified as water or flatland, respectively.

Figure 6 shows the seasonal and topographic distribution of the number of cases of high altitude clear air turbulence. The number of cases is nearly equal for each of the seasons for the observations of turbulence over water but the number of cases per season varies greatly for the flatland, low mountain, and high mountain categories. The distributions of the number of observations for each of the four topographic categories by season and altitude are presented in Figures 7-10. Significantly different distributions are evident. For the cases of turbulence observed over high mountains, the relatively high number of cases in the winter category and the relatively small number of cases in the summer category is a dominant feature of the distribution.

The ratio, expressed in percentage, of turbulent flight miles to total flight miles for the four categories of topography are shown in Table I. When repeat passes were flown through what was presumed to be the same turbulent region, both flight and turbulence miles were reduced by an appropriate amount to approximate only one pass through the turbulence.

TABLE I

RATIO (PERCENTAGE) OF TURBULENT FLIGHT MILES TO TOTAL FLIGHT MILES				
	<u>TOPOGRAPHIC CATEGORY</u>			
Turbulence Intensity	Water	Flatland	Low Mountains	High Mountains
≥ Light	2.7	2.7	3.6	4.9
≥ Moderate	0.5	0.5	1.5	1.8

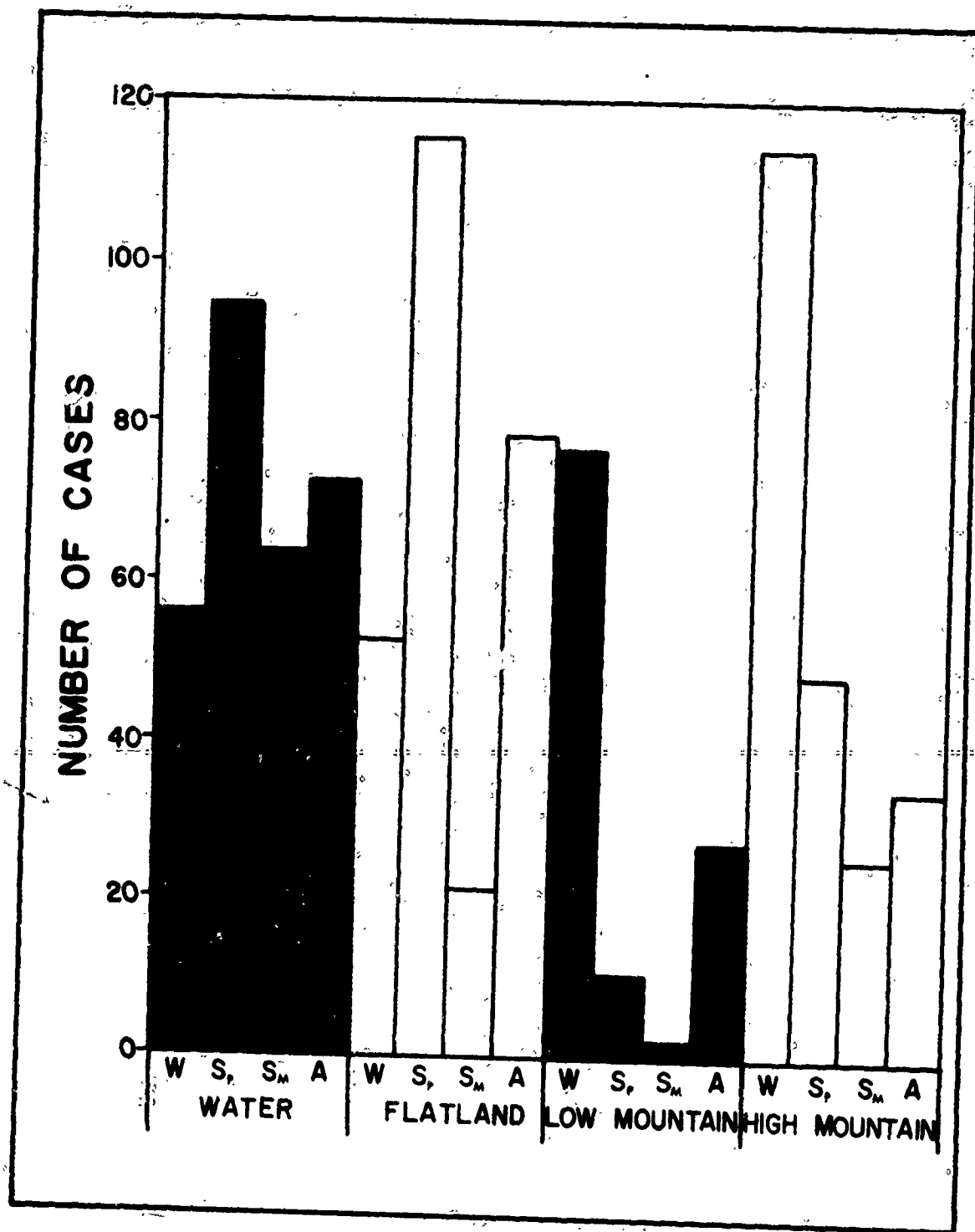


Figure 6. Distribution of the Number of Observations of Turbulence by Topography and by Season.

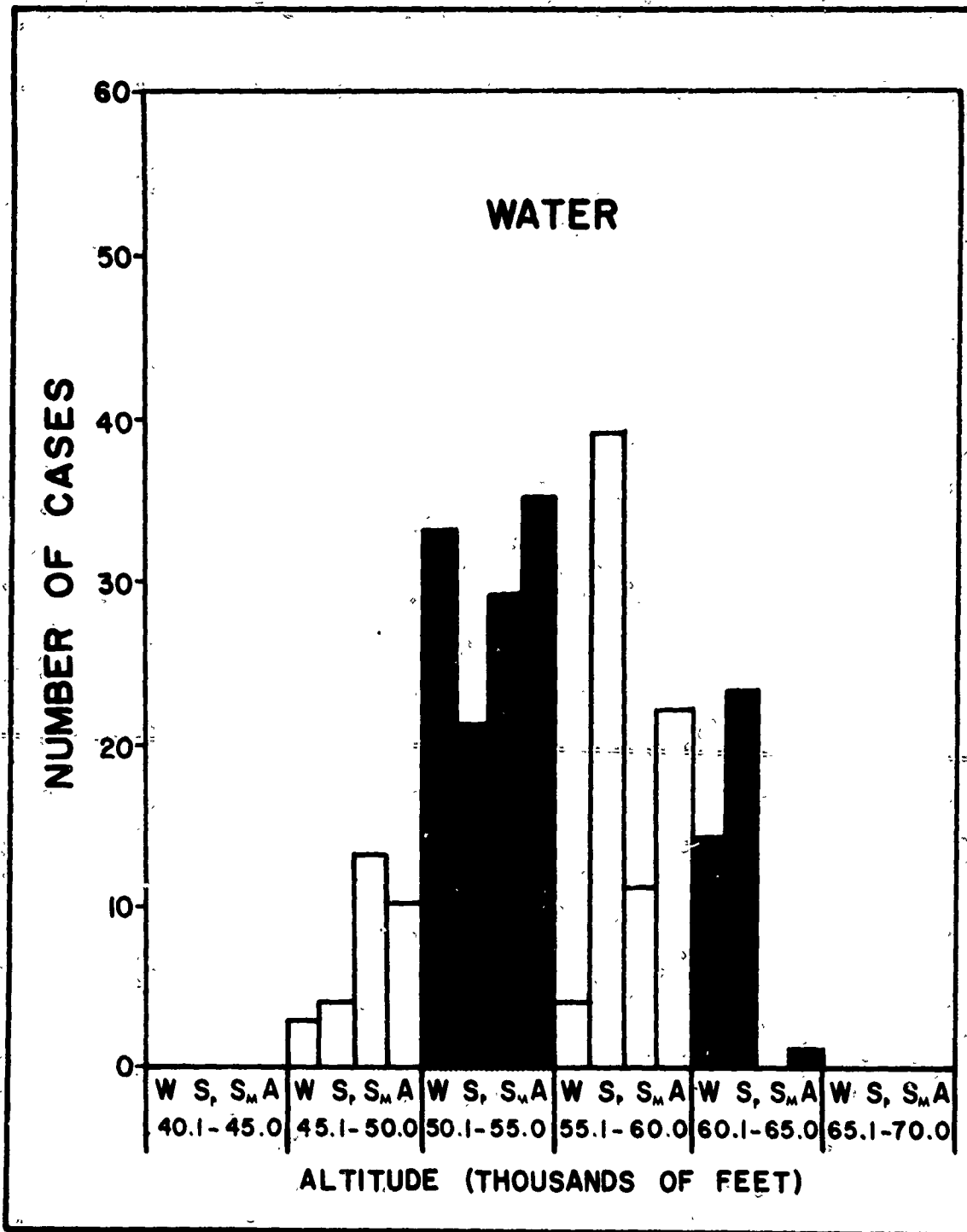


Figure 7. Distribution of Number of Observations of Turbulence Over Water by Season and Altitude.

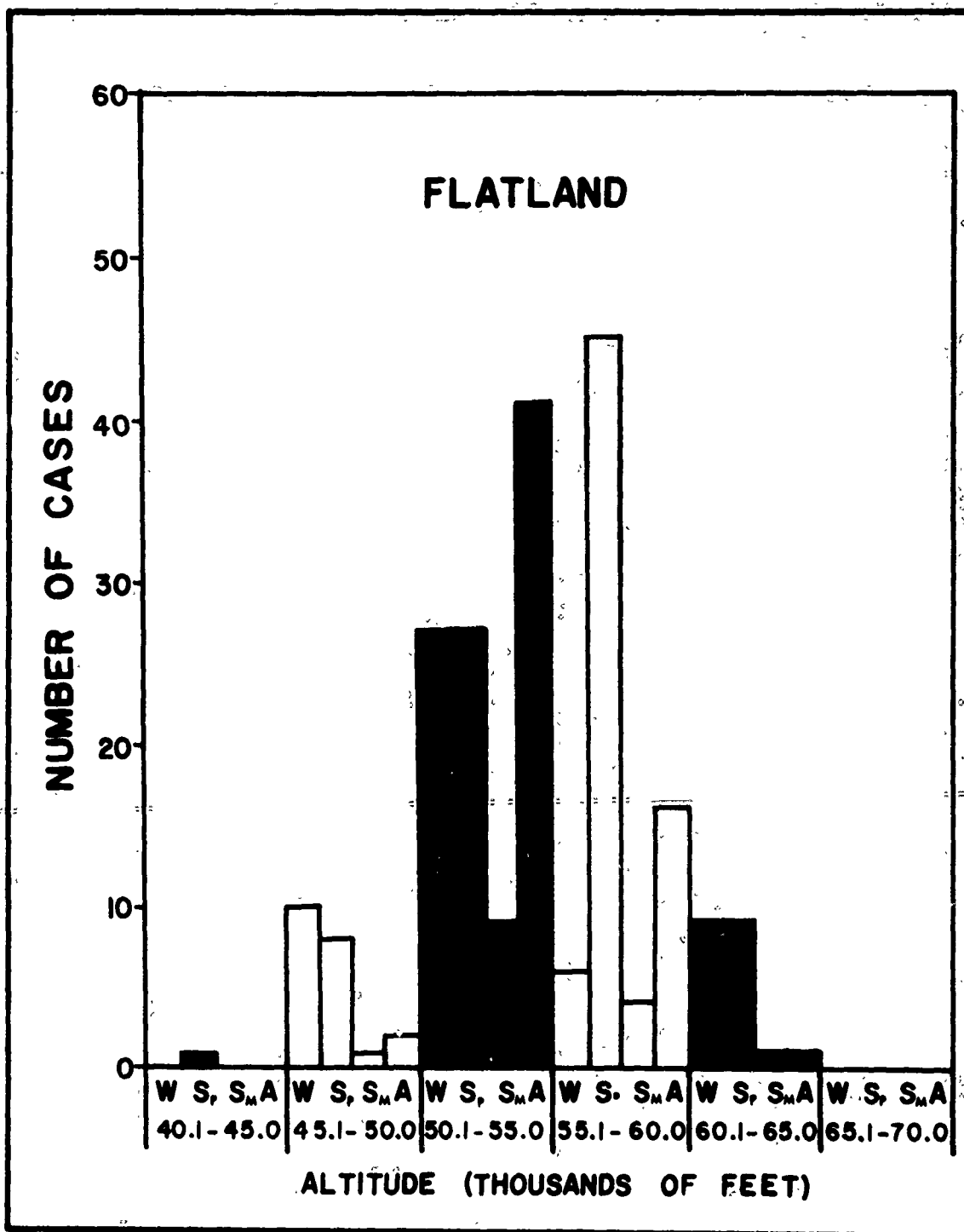


Figure 8. Distribution of Number of Observations of Turbulence Over Flatland by Season and Altitude.

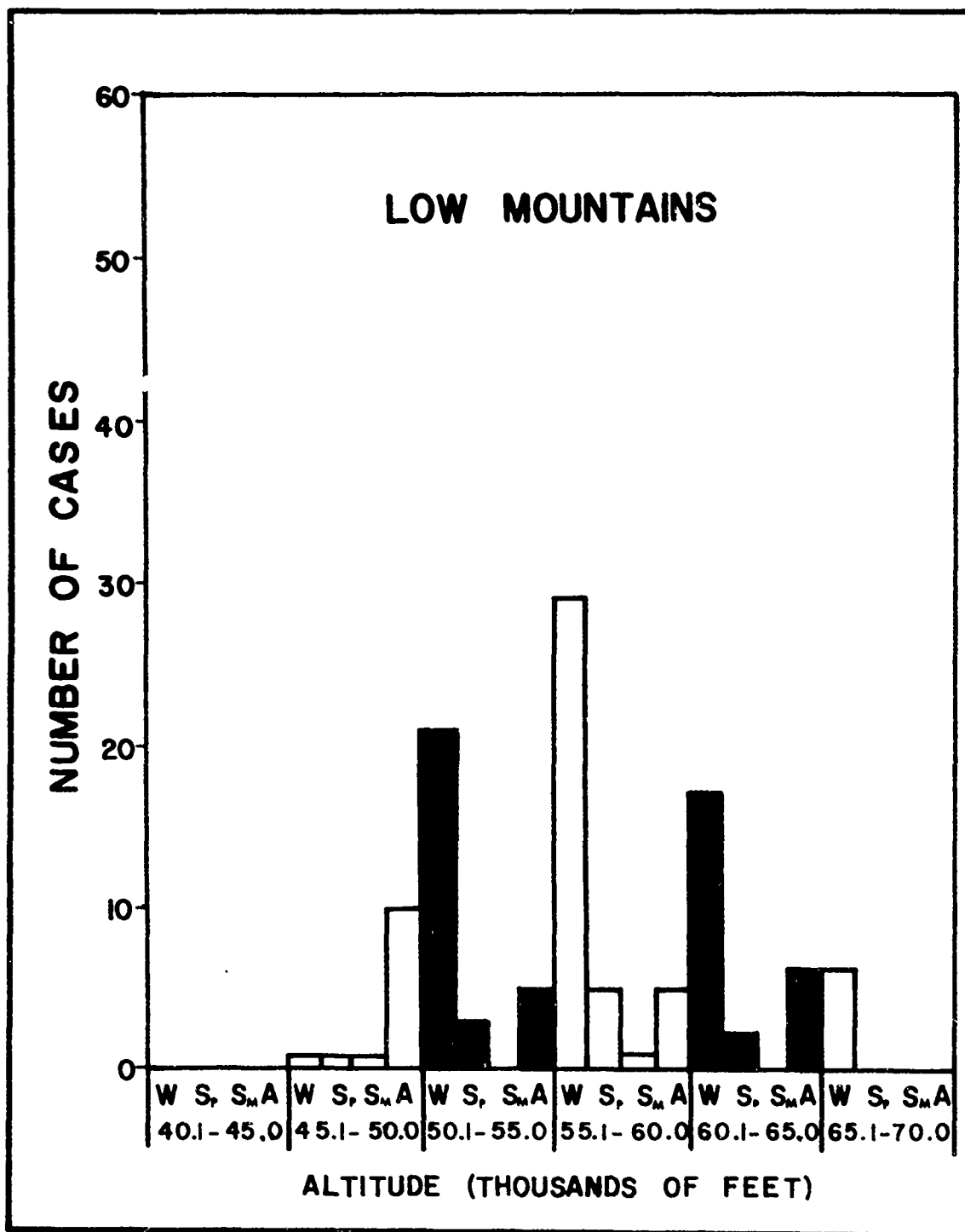


Figure 9. Distribution of Number of Observations of Turbulence Over Low Mountains by Season and Altitude.

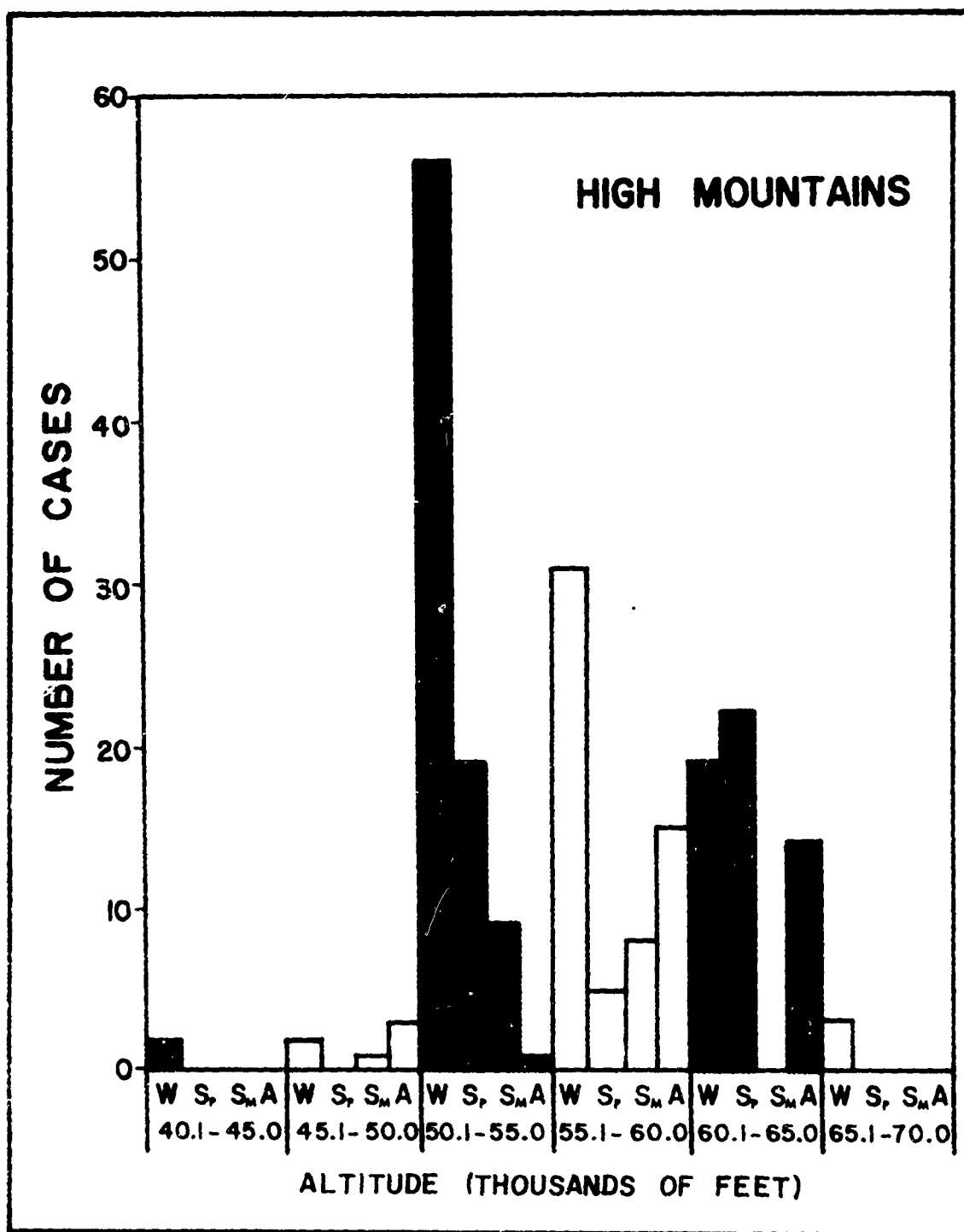


Figure 10. Distribution of Number of Observations of Turbulence Over High Mountains by Season and Altitude.

The results shown in Table I indicate that the percentage occurrence of HICAT is related to the topography immediately below the aircraft. The figures are based on flights for all seasons and over several geographical areas. There was 33% more turbulence \geq light per flight mile over low mountains and 82% more over high mountains than over water or flatland. The percentage for moderate or greater turbulence increased by a factor of more than three for flights over mountains.

Figures 11-14 present the number of flight miles and turbulent flight miles by terrain for the ferry flights, all flights, and for flights made from each of the various bases of operation.

Power Spectral Density Shapes as a Function of Topography

The discussion and data presented in the preceding paragraphs provide evidence that high altitude clear air turbulence is, in part, a function of the underlying topography. Throughout that discussion the turbulence was defined in descriptive terms as severe, moderate, light, etc. These descriptive terms were related by Crooks et al (1, 2) to a semi-quantitative measure of the cg acceleration of the aircraft. In the following paragraphs the turbulence is defined more explicitly in terms of the true gust velocities. The gust velocity power spectra are correlated with topography.

One of the most important objectives of the HICAT program was to derive gust velocity spectra for turbulence waves ranging from 100 feet to as much as 50,000 feet in length. Determinations of spectra with uniform statistical reliability require that turbulence sample lengths increase in proportion to the largest wavelength of interest in the spectrum. Because patches of turbulence and hence recordings of turbulence vary considerably in length, some patches are too short for a reliable long wave spectrum analysis but are quite adequate for a medium or short wave analysis.

The square root of the integral of the spectral curve from the short wavelength limit to the longest wavelength of interest for the design and operation of aircraft is an important quantity but one that is rarely obtainable from the direct measurements. To make it possible to compare spectra with different long wavelengths limits the root mean square (RMS) values were computed by Crooks et al (1, 2) for the following long wavelength limits: 1000, 2000, 4000, 10,000, 20,000, and 40,000 feet. The short wavelength limit was established at 140 feet. Crooks et al (1, 2) also presented a detailed discussion of methods of comparing spectra and of obtaining average spectra. Throughout their work all the HICAT spectra were treated as one set. In the following discussion the HICAT data were divided into subsets that were related to the underlying topography.

The ratios of the RMS at $\lambda = 2000$ ft, $\lambda = 4000$ ft, $\lambda = 10,000$ ft, and $\lambda = 20,000$ ft [abbreviated RMS (2000), RMS (4000), etc.] to RMS at $\lambda = 1000$ ft were used as quantitative measures of the shape of the spectra. Table II presents the average values of these ratios for two categories of topography and for three values of the maximum wavelength of the spectra. Only those cases for which RMS (2000) > 1 ft/sec were used because the errors are relatively large for values less than 1 ft/sec. To increase the sample size only two categories of topography were used. The sample size decreased with increasing maximum wavelength. In the mountain category the ratios of the RMS values increased more rapidly with increasing wavelength than for the water-flatland category. The spectra of the lateral (U_L) and longitudinal (U_F)

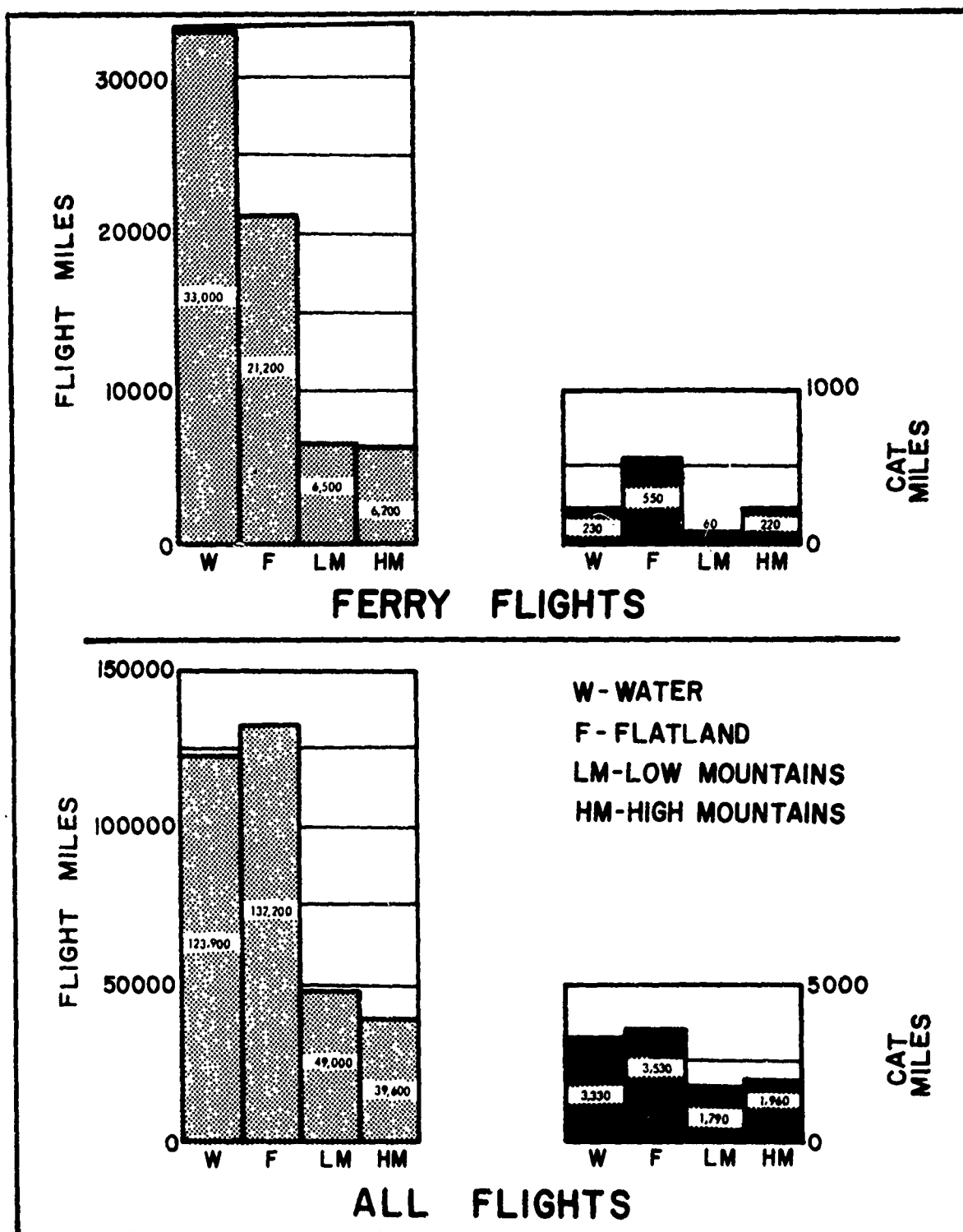


Figure 11. Distribution of Total Flight Miles and Turbulent Flight Miles by Terrain for Ferry Flights and All Flights.

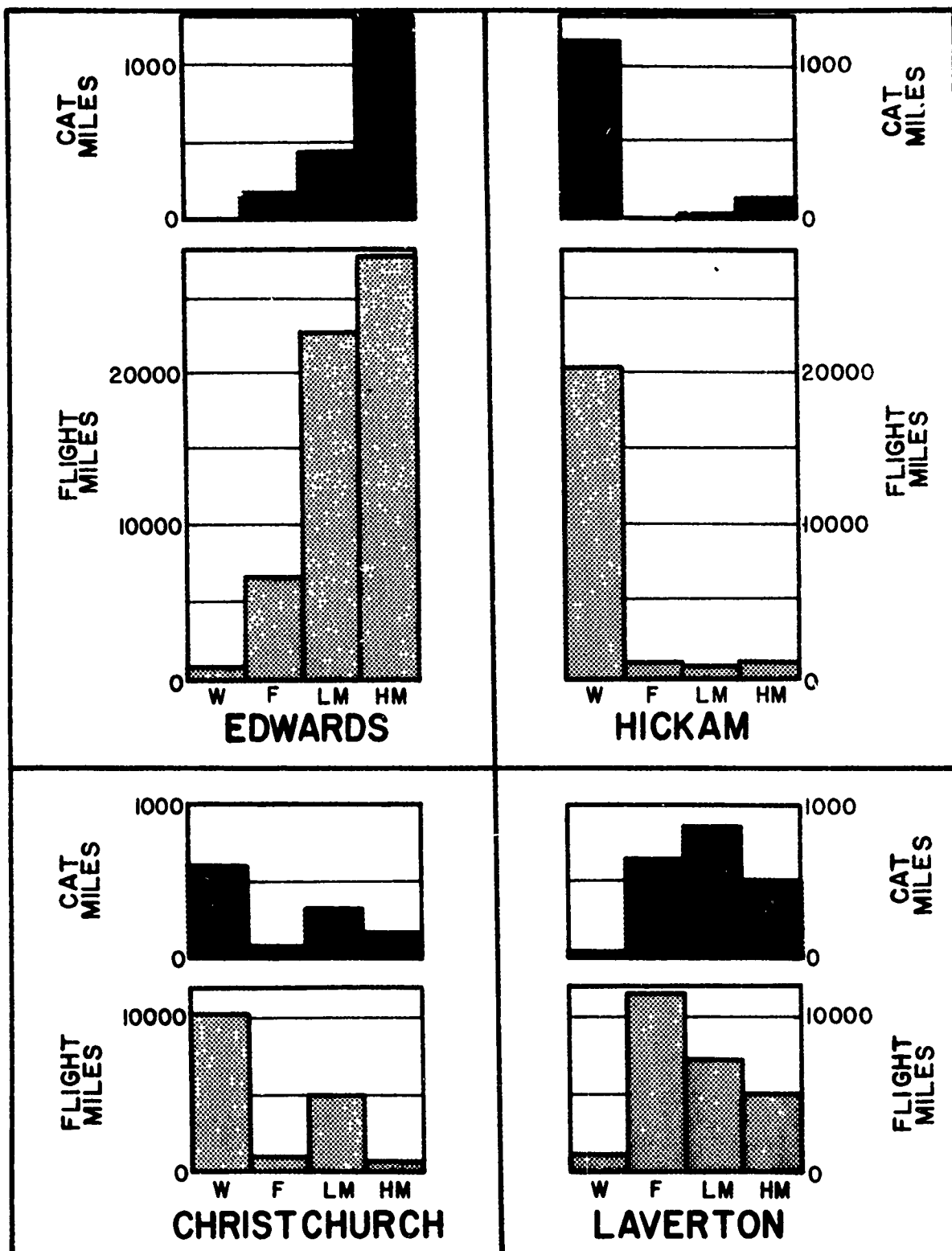


Figure 12. Distribution of Total Flight Miles and Turbulent Flight Miles by Terrain for Edwards, Hickam, Christchurch and Laverton.

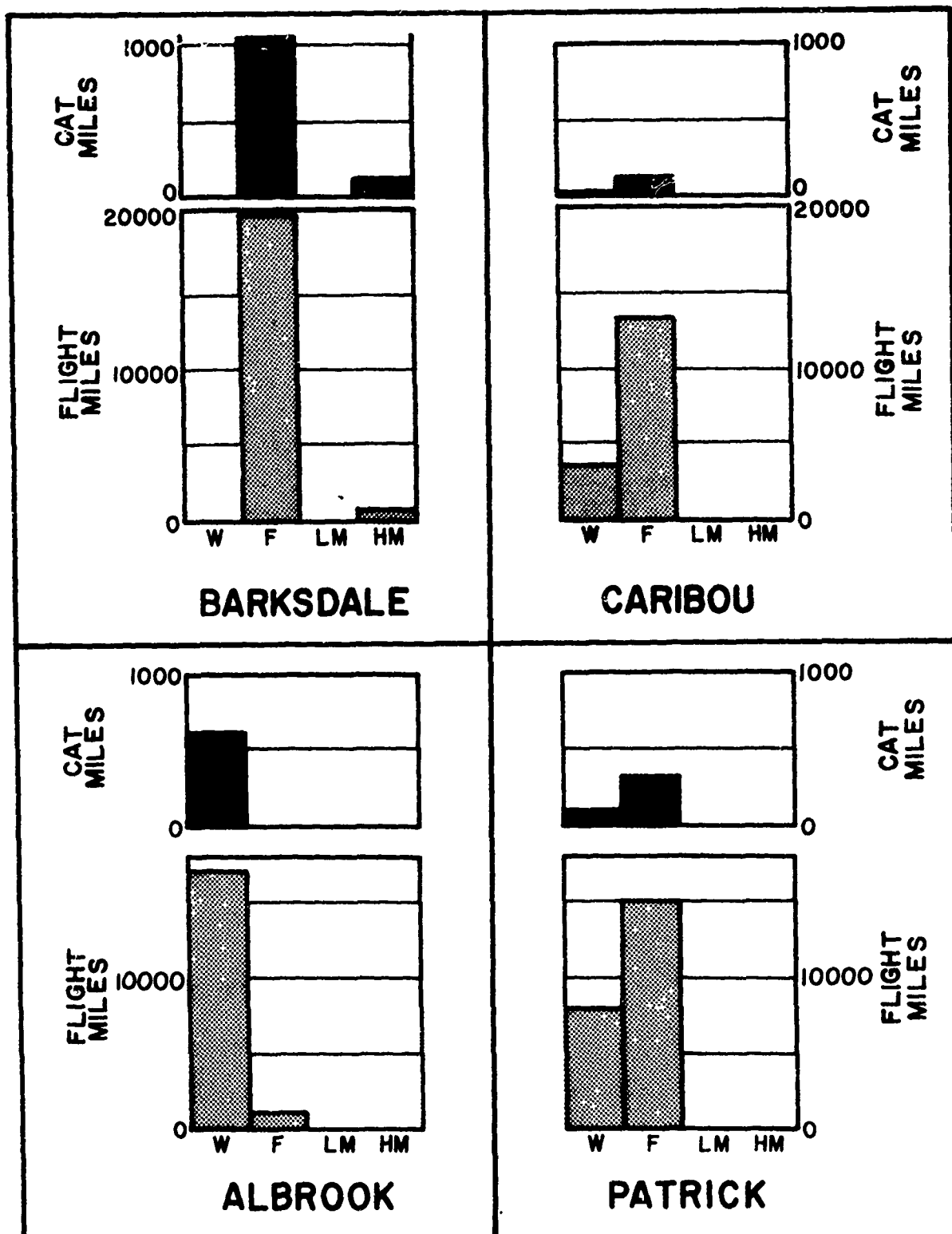


Figure 13. Distribution of Total Flight Miles and Turbulent Flight Miles by Terrain for Barksdale, Caribou, Albrook and Patrick.

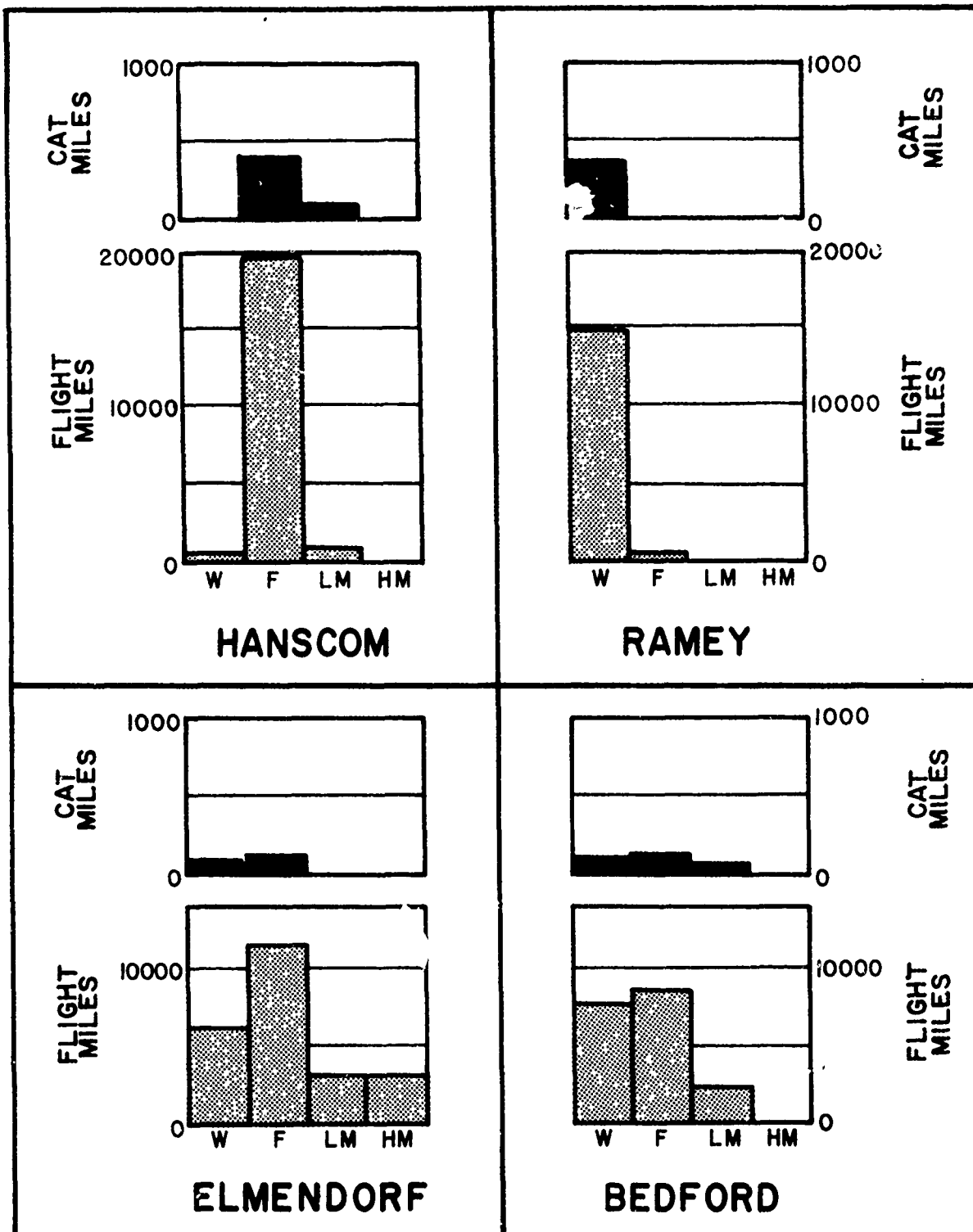


Figure 14. Distribution of Total Flight Miles and Turbulent Flight Miles by Terrain for Hanscom, Ramey, Elmendorf and Bedford.

TABLE II (a)

AVERAGE VALUES OF THE RATIO OF U_V , U_F , AND U_L AT RMS (2000), RMS (4000), RMS (10,000), AND RMS (20,000) TO RMS (1000)							
		Water, Flatland			Mountains		
		U_V	U_F	U_L	U_V	U_F	U_L
λ max 4000 ft	Samples	(13)	(31)	(44)	(40)	(54)	(55)
	$\frac{\text{RMS (2000)}}{\text{RMS (1000)}}$	1.23	1.26	1.25	1.29	1.32	1.30
	$\frac{\text{RMS (4000)}}{\text{RMS (1000)}}$	1.48	1.57	1.55	1.65	1.69	1.77
λ max 10,000 ft	Samples	(8)	(14)	(16)	(16)	(19)	(20)
	$\frac{\text{RMS (2000)}}{\text{RMS (1000)}}$	1.19	1.25	1.25	1.29	1.32	1.28
	$\frac{\text{RMS (4000)}}{\text{RMS (1000)}}$	1.37	1.52	1.54	1.63	1.67	1.75
	$\frac{\text{RMS (10,000)}}{\text{RMS (1000)}}$	1.65	1.95	1.91	2.06	2.31	2.45
λ max 20,000 ft	Samples	(2)	(4)	(4)	(4)	(5)	(5)
	$\frac{\text{RMS (2000)}}{\text{RMS (1000)}}$	1.21	1.29	1.24	1.31	1.34	1.29
	$\frac{\text{RMS (4000)}}{\text{RMS (1000)}}$	1.36	1.53	1.50	1.72	1.75	1.76
	$\frac{\text{RMS (10,000)}}{\text{RMS (1000)}}$	1.54	1.80	1.71	2.25	2.51	2.50
	$\frac{\text{RMS (20,000)}}{\text{RMS (1000)}}$	1.67	2.01	1.86	2.66	3.19	3.11

TABLE II (b)

THEORETICAL VALUES OF THE RATIOS OF RMS (2000), RMS (4000), RMS (10,000) AND RMS (20,000) TO RMS (1000) FOR VARIOUS L'S OF THE MILD KNEE EQUATION WITH $M = -5/3$						
	Scale Length in Feet					
	500	1000	2000	4000	6000	8000
$\frac{\text{RMS (2000)}}{\text{RMS (1000)}}$	1.23	1.26	1.30	1.32	1.33	1.33
$\frac{\text{RMS (4000)}}{\text{RMS (1000)}}$	1.42	1.48	1.60	1.67	1.72	1.72
$\frac{\text{RMS (10,000)}}{\text{RMS (1000)}}$	1.60	1.78	1.96	2.17	2.25	2.29
$\frac{\text{RMS (20,000)}}{\text{RMS (1000)}}$	1.68	1.92	2.22	2.55	2.58	2.66

components of the gust velocity show consistently larger increases in RMS ratios than the spectra of the vertical (U_V) component for both terrain groups.

The increase in the RMS ratios with increasing wavelength was computed for the theoretical representations of turbulence that were discussed in detail by Crooks et al (1,2). Table II also includes the calculated ratios for the "mild knee" equation with the slope m of the short wavelength region equal to $-5/3$. The "mild knee" equation is

$$\varphi(\Omega) = \frac{\text{Constant}}{1 + (\Omega L)^{-m}} \quad (1)$$

where $\varphi(\Omega)$ is the power spectral function, Ω is the reduced frequency ($2\pi/\lambda$) and L is the scale of the turbulence. Of the various equations described by Crooks et al (1,2) this equation appeared to best fit the HICAT spectra data for the three components of the gust velocity presented in Table II.

Average RMS increases for the vertical component water and flatland samples, when compared with the mild knee equation values, appear to suggest an L of 500 ft or slightly higher. Mountain samples show a trend toward much larger L 's of 2000 to 4000 ft for the samples with $\lambda_{\max} = 4000$ ft and 10,000 ft and between 6000 ft and 8000 ft for the four samples with $\lambda_{\max} = 20,000$ ft.

Increases in RMS with λ show less dropoff of energy at longer wavelengths for the lateral and longitudinal gust components than with the vertical component. Consequently, L 's are somewhat larger, near 2000 ft for the flatland-water samples and above 6000 ft for the mountains.

Table III gives the ratios of RMS (100,000)/RMS (2000) for the various values of the scale length L computed from Equation (1). Estimation of RMS (100,000) may be made for any given spectra by multiplying its RMS (2000) value by a number selected on the relation of the cutoff spectra to theoretical curves. For example, given two spectra, one derived from turbulence measurements over water and one over high mountains, if both have a U_V RMS (2000) = 1.00, the RMS (100,000) values would be 1.43 and 2.37 for the water and high mountain cases, respectively. These figures were derived by using the appropriate terrain-related L 's in Table III, the RMS (100,000) value being based on the longest wavelength commonly observed in mountain waves. The RMS (2000) values were chosen because enough of these were computed from the HICAT flight data to constitute an adequate sample whereas the sample size became very small for RMS values with the long wavelength greater than 2000 ft.

Normalized power spectral density curves constitute a second method of estimating scale lengths. To apply this method, power spectral density curves for the 23 U_V samples with $\lambda_{\max} = 10,000$ ft were normalized by dividing the density estimates by the square of RMS (2000). The normalization factor RMS (2000) was arbitrarily chosen. Normalization permits a comparison of spectral shapes at all wavelengths. Curves were faired by hand to eliminate irregularities.

The total sample was distributed into three groups: flatland (7), low mountains (7), and high mountains (9). There were no water samples that met the requirements of RMS (2000) > 1.0 and $\lambda_{\max} = 10,000$ ft. The normalized groups of curves are presented in Figures 15 to 17.

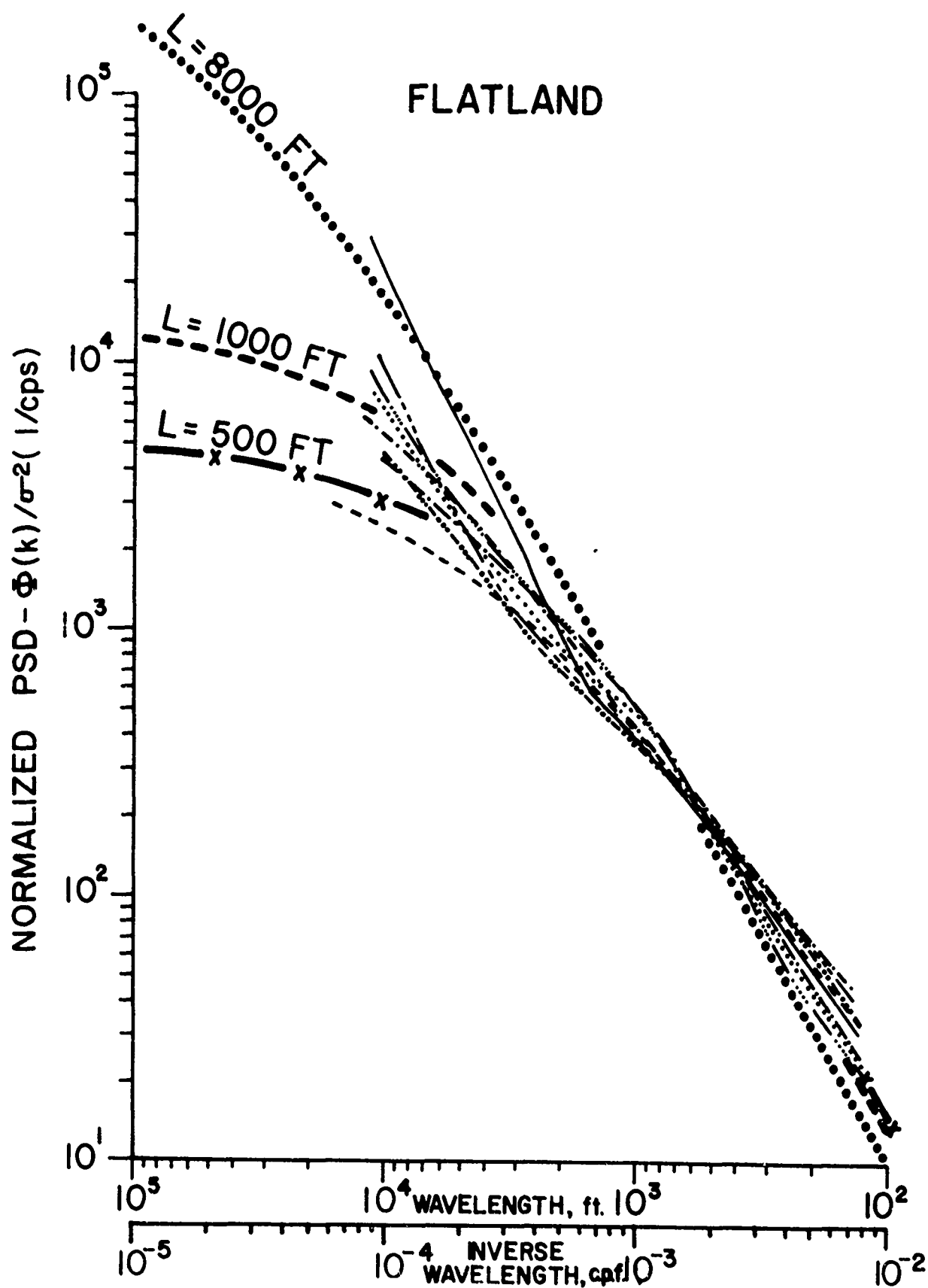


Figure 15. Normalized Power Spectral Curves for All Flatland Cases with Long Wavelength Limit of 10,000 ft.

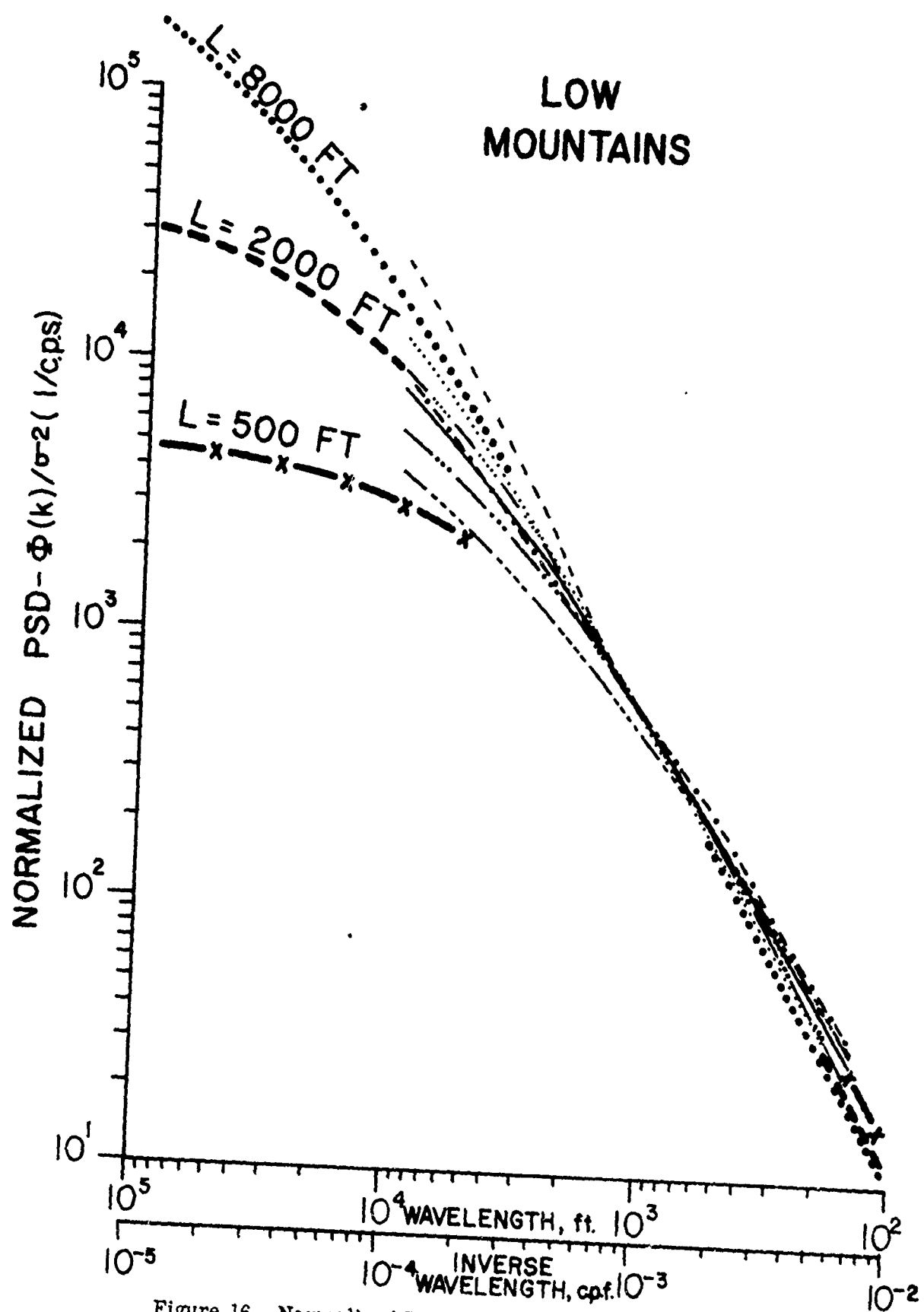


Figure 16. Normalized Power Spectral Curves for All Low Mountain Cases with Long Wavelength Limit of 10,000 ft.

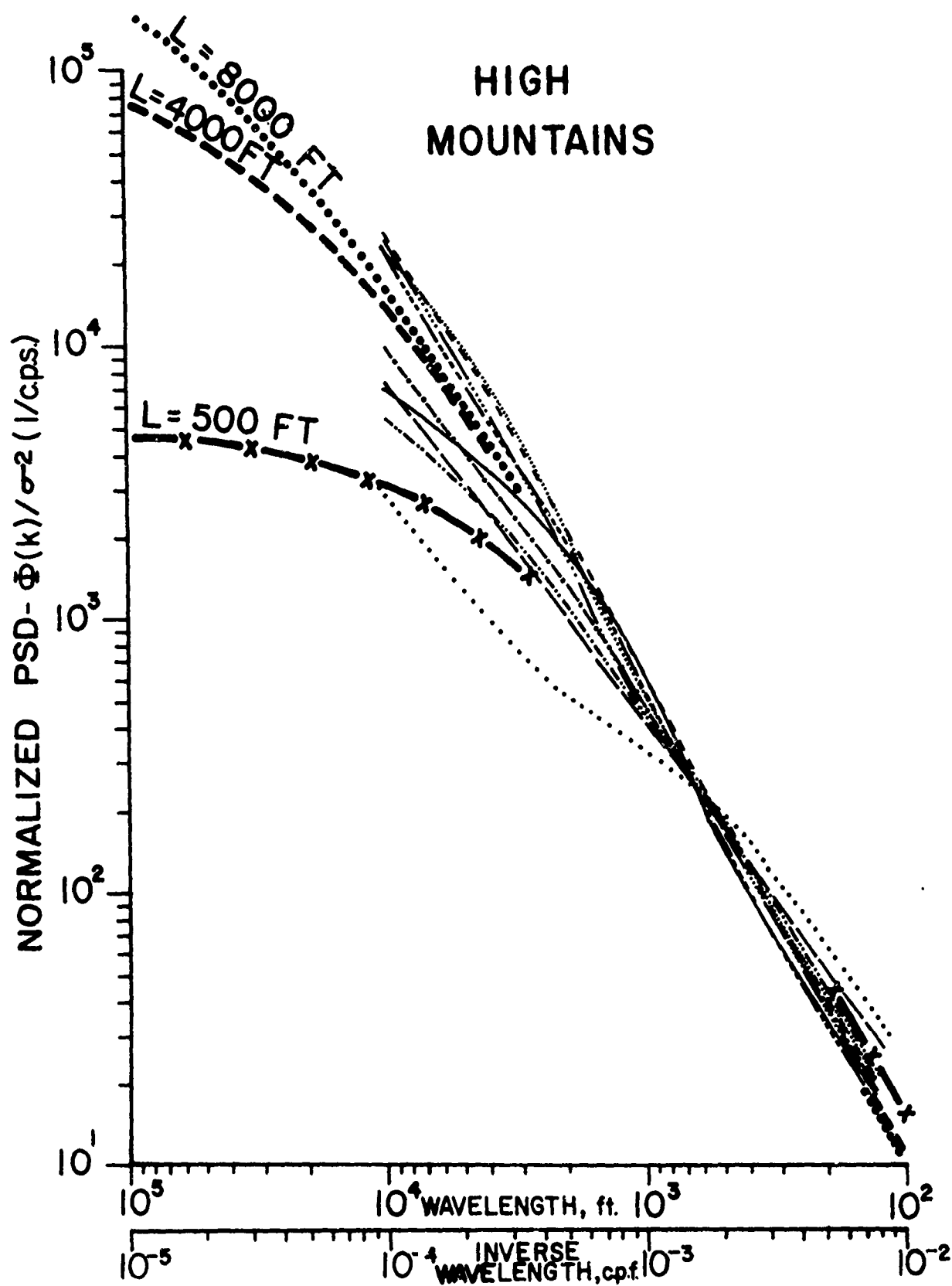


Figure 17. Normalized Power Spectral Curves for All High Mountain Cases with Long Wavelength Limit of 10,000 ft.

TABLE III

THE RATIO OF RMS (100,000)/RMS (2000) FOR VARIOUS VALUES OF SCALE LENGTH, L, COMPUTED FROM THE "MILD KNEE" EQUATION WITH SLOPE $M = -5/3$							
	Scale Length in Feet						
	500	1000	2000	4000	6000	8000	∞
$\frac{\text{RMS (100,000)}}{\text{RMS (2000)}}$	1.43	1.65	1.94	2.37	2.58	2.75	3.98

All but one of the high mountain spectra show a rather small departure from the $-5/3$ slope at longer wavelengths. The scale length associated with these spectra appears to average around 6000 ft with four samples showing $L > 8000$ ft. All of the mountain spectra were derived from flight data obtained over the Rocky Mountains.

The flatland and low mountain spectra show a more rapid change in slope at longer wavelengths. The $-5/3$ law appears to hold only at the short wavelength end of the spectrum for the flatland cases.

Three particular cases of normalized spectra are shown in Figure 18. These spectra were derived from data used to make the time histories of the gust velocities shown in Figure 19. The differences in the spectra and their time histories obtained from flights over the three types of topography are clearly apparent. Flight 198 run 12, the flatland case, was over a squall line but the significance of this is not known.

The Variation of Gust Velocities with Topography

The turbulent regions explored in the HICAT flight program were rarely of sufficient length to provide data to determine the power spectral density curves out to the long wavelengths needed for an adequate description of the gust velocities. Figure 20 however, indicates that a reasonable sample size was obtained for the RMS (2000) values. Hence, statistically significant exceedance data for the RMS (2000) values may be obtained and these then may be combined with the ratios of RMS (100,000) to RMS (2000) given in the preceding paragraphs to provide useful exceedance gust data. The details of the procedure adopted are as follows.

The sample chosen for analysis consisted of all those values of RMS (2000) that were 0.5 ft/sec or greater. There were 39 of these cases for the water category, 60 for the flatland, 33 over low mountains and 84 over high mountains. Observations (runs) resulting from repetitive search flight patterns were not eliminated because their elimination would reduce the sample size significantly. In addition, the elimination of the repetitive patterns would require a subjective judgment for the selection of the most representative "run" and under some rules of selection would eliminate the highest values of the RMS (2000). The percentages at which the curves intercept the line $\text{RMS (2000)} = 0.5 \text{ ft/sec}$ taken from Table I are 2.7%, 2.7%, 3.6% and 4.9% for water, flatland, low mountains and high mountains respectively.

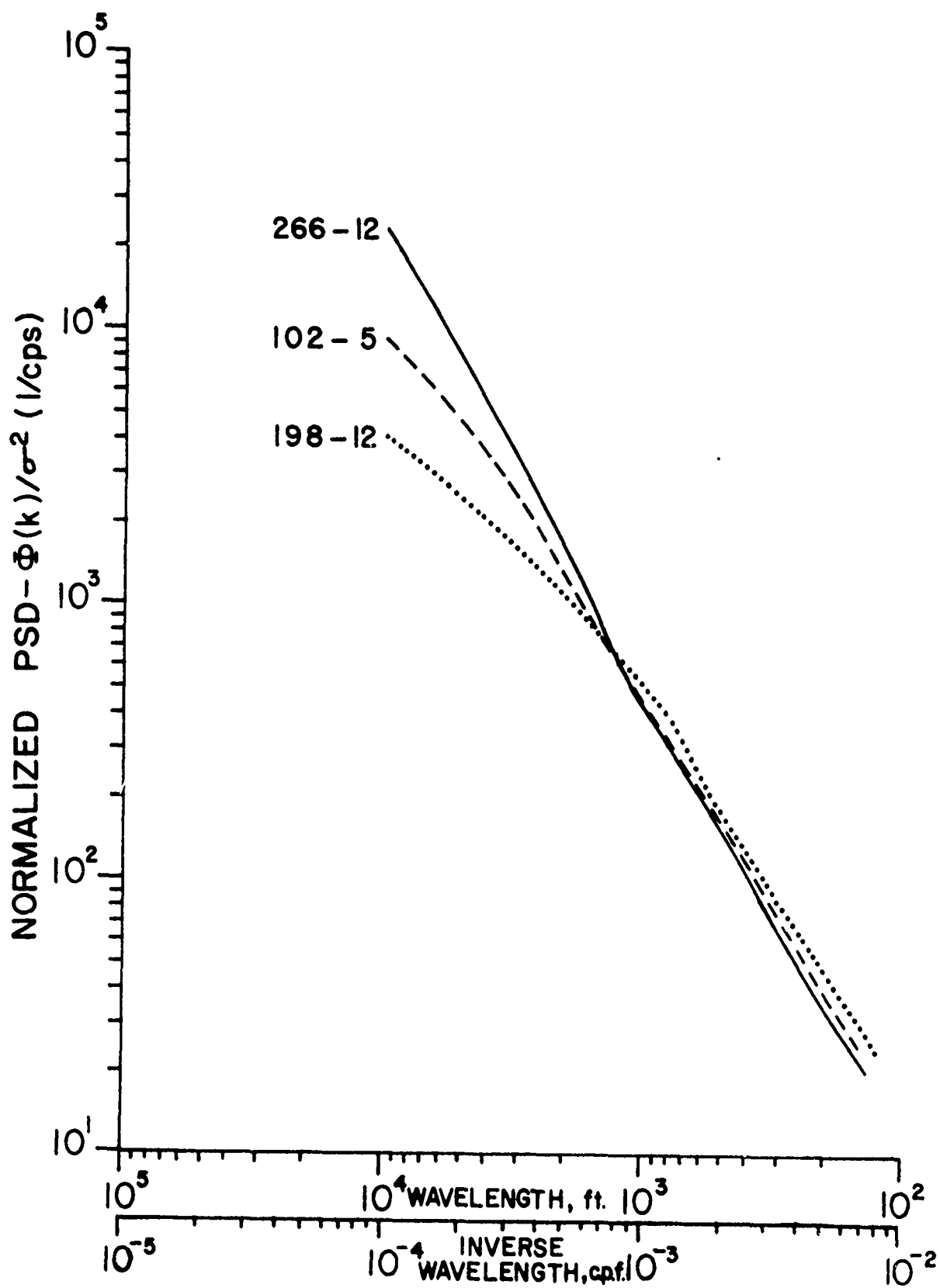


Figure 18. Normalized Spectra for Three Particular Cases of High Altitude Clear Air Turbulence.

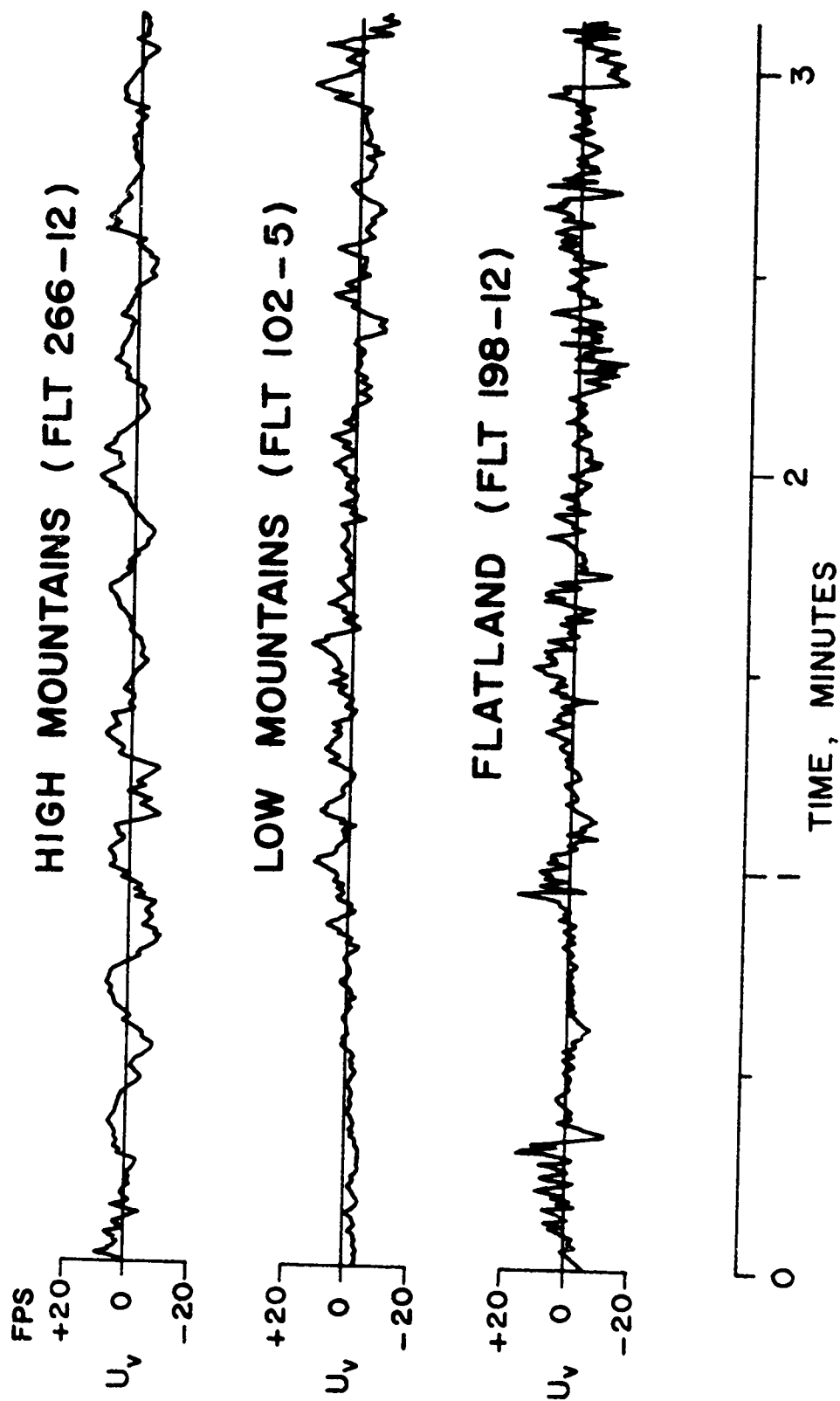


Figure 19. Time Histories of U_v for the Three Spectra Shown in Figure 18.

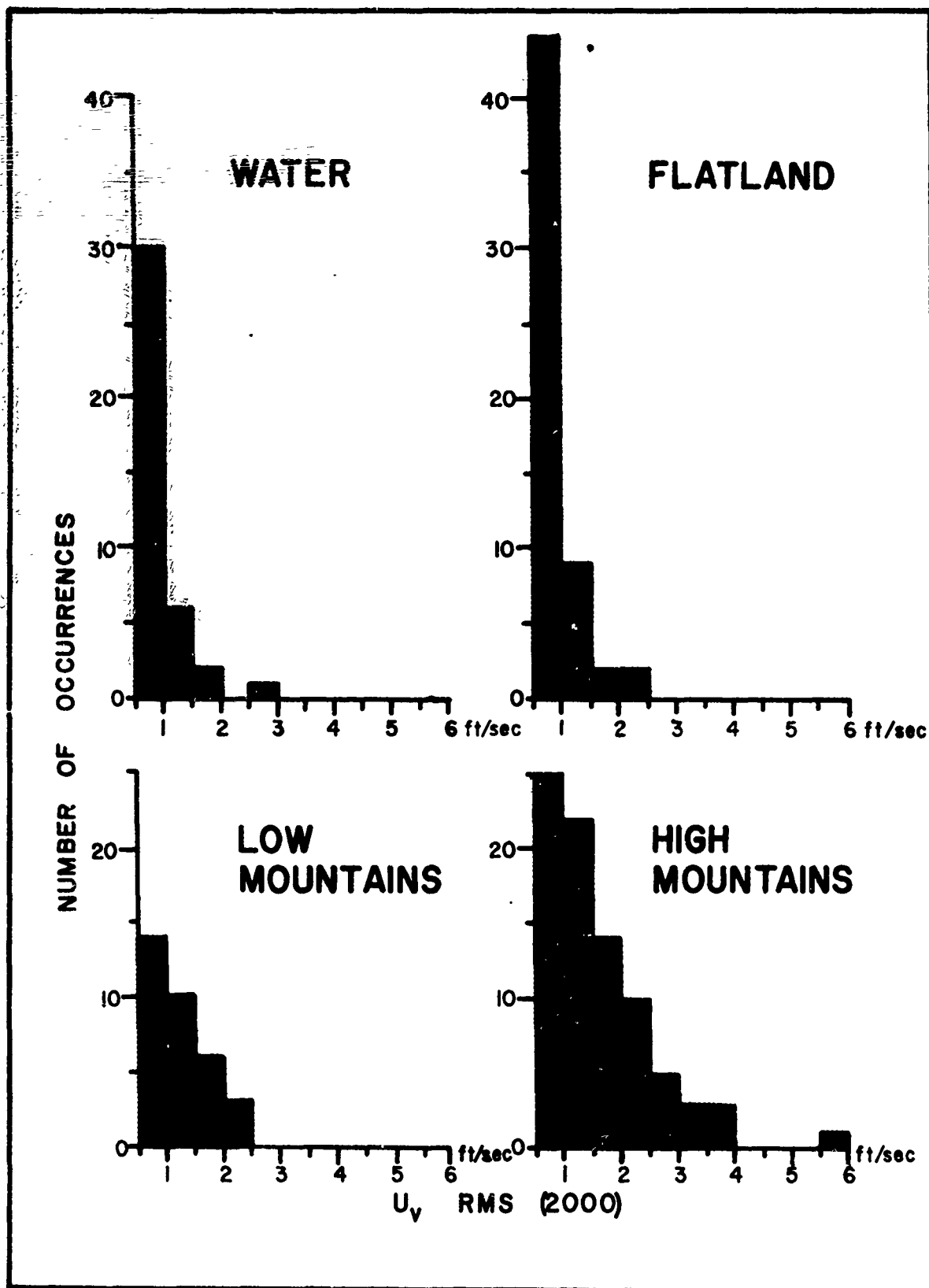


Figure 20. Distribution of the Number of Observations of Turbulence by RMS (2000) Magnitude and Topography.

Figures 21, 22 and 23 show the results obtained from this analysis. The curves provide evidence that the underlying topography and the exceedance data of RMS (2000) are correlated. For the flights over mountains the higher values of RMS (2000) occur relatively more frequently than is the case for flights over flatland or water.

Figure 24 shows the exceedance curves for the RMS (2000) data resulting from using only two categories of topography. This produces larger samples and increases the statistical reliability. The data may adequately be represented by the following equations:

$$\begin{array}{c} \text{Water and Flatlands} \\ \text{Percentage Exceedance RMS (2000)} = 9.4 \exp [-2.5 \text{ RMS (2000)}] \quad (2) \end{array}$$

$$\begin{array}{c} \text{Low and High Mountains} \\ \text{Percentage Exceedance RMS (2000)} = 8.1 \exp [-1.3 \text{ RMS (2000)}] \quad (3) \end{array}$$

In the following section analogous exceedance curves for RMS (2000) drawn for subsets defined by season and altitude indicate that season and altitude also may be significantly related to the distribution of the true gust velocities. At the present time no definite statement can be made on the importance of Equations (2) and (3) taken alone without giving proper weight to seasonal or altitude effects.

Variation of U_v with Topography and Altitude

Table IV shows the ratios of RMS (2000)/RMS (1000), RMS (4000)/RMS (1000), and RMS (10,000)/RMS (1000) for turbulent regions that were below 59,000 ft and above 59,000 ft altitude. These figures indicate no significant difference in the ratios with altitude and this in turn implies that there is no significant change in shape of the spectra with altitude of the turbulent region. These figures are based on mountain samples only.

TABLE IV

AVERAGE VALUES OF THE RATIO OF U_v RMS (2000), RMS (4000), AND RMS (10,000) TO U_v RMS (1000) FOR GIVEN ALTITUDE BANDS			
		< 59,000 ft	> 59,000 ft
λ_{\max} 4000 ft	Samples	(20)	(21)
	RMS (2000)	1.31	1.27
	RMS (4000)	1.67	1.64
λ_{\max} 10,000 ft	Samples	(7)	(8)
	RMS (2000)	1.30	1.27
	RMS (4000)	1.65	1.62
	RMS (10,000)	2.10	2.06

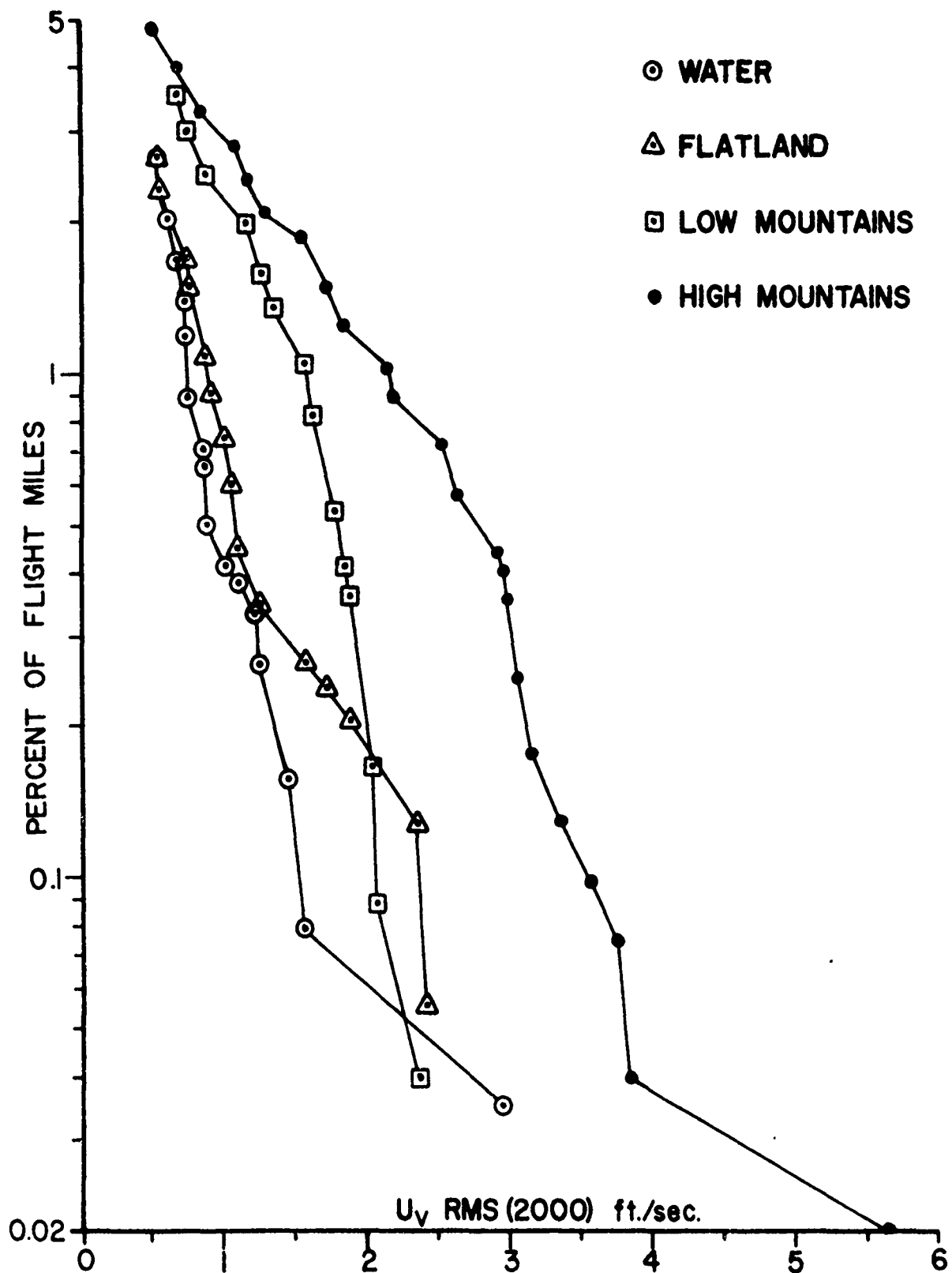


Figure 21. Percentage Exceedance of RMS (2000) for the U_v Component for Four Categories of Topography.

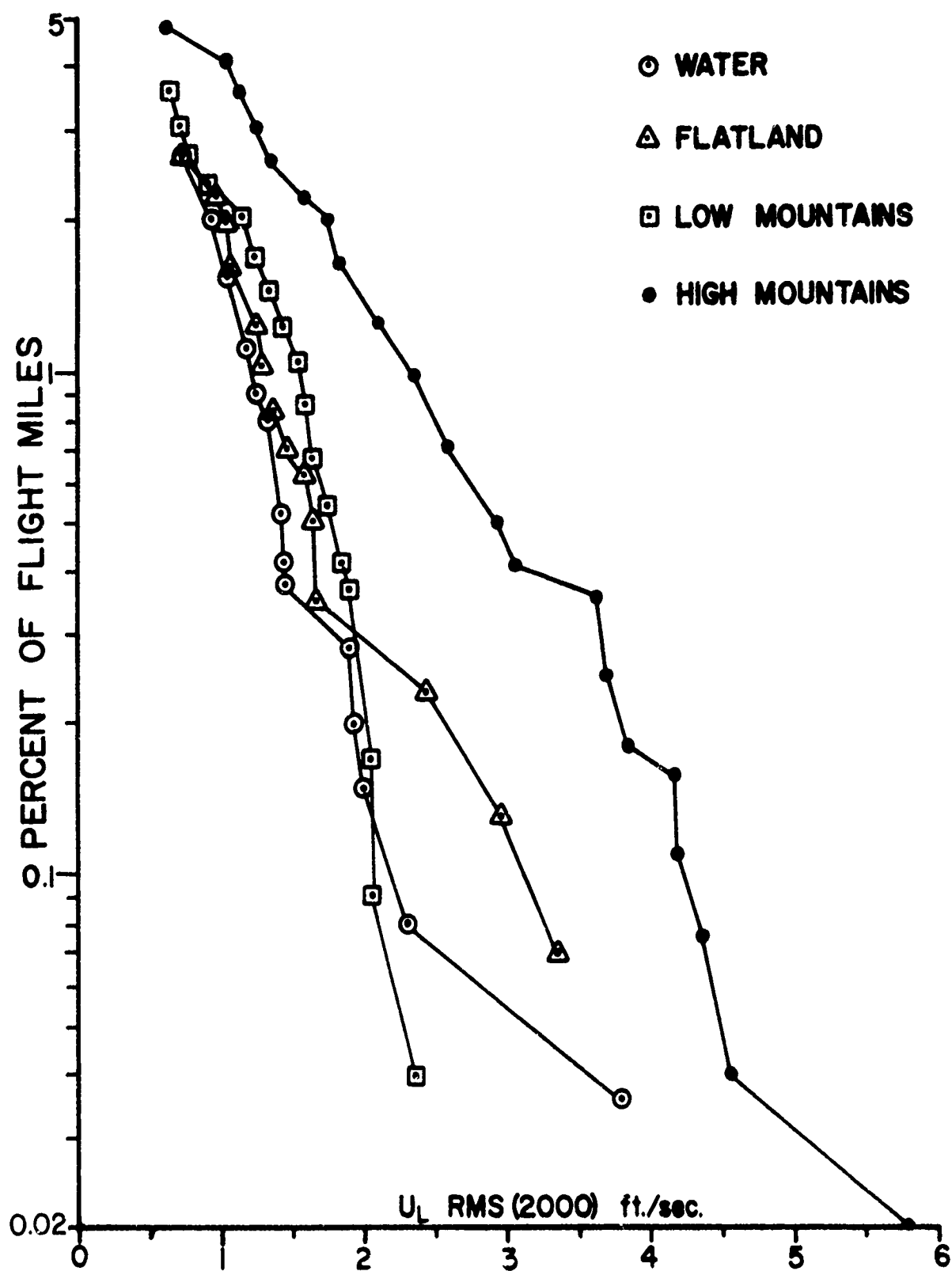


Figure 22. Percentage Exceedance of RMS (2000) for the U_L Component for Four Categories of Topography.

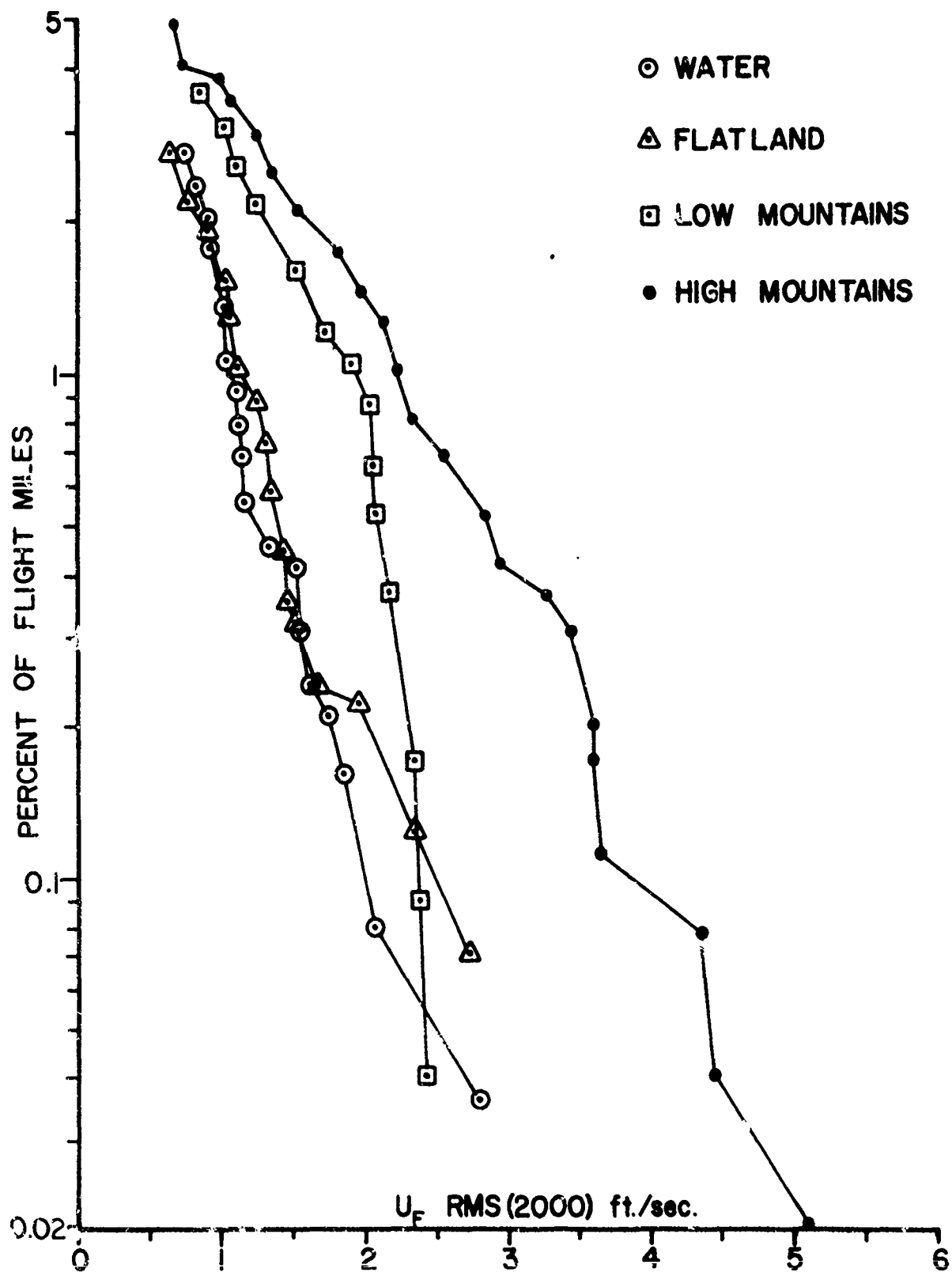


Figure 23. Percentage Exceedance of RMS (2000) for the U_F Component for Four Categories of Topography.

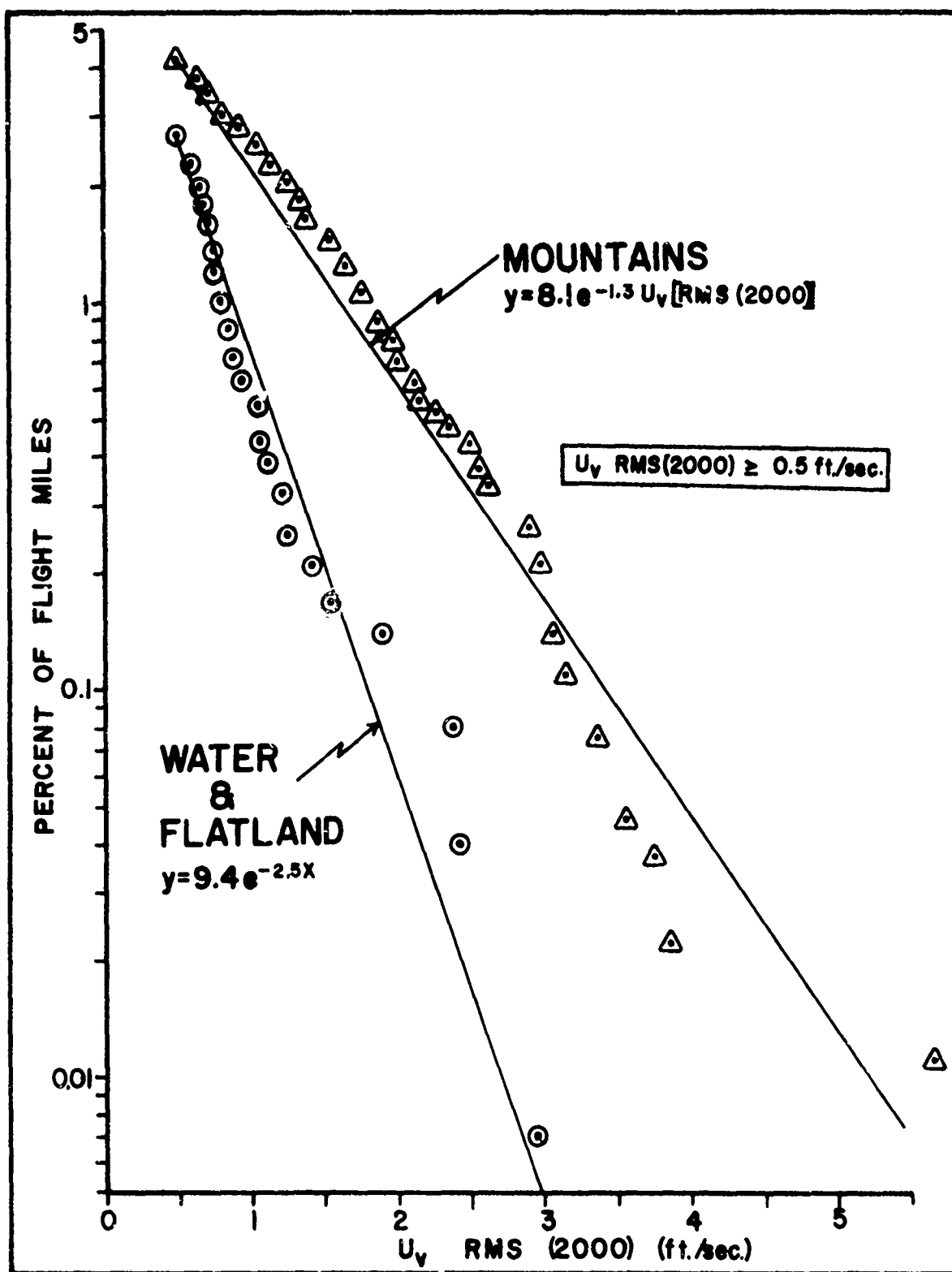


Figure 24. Percentage Exceedance of RMS (2000) for the U_v Component for Two Categories of Topography.

The variation in the number of observations of the RMS (2000) of the U_V component of the gust velocity that exceed given values is shown in Table V. These figures indicate that there was a significant decrease with increasing altitude in the number of observations of turbulence over water and flatland but no significant change with altitude over mountains. However, this conclusion is only justified if the assumption is made that the distribution of flight miles by altitude and topographic category is approximately uniform. Detailed records of flight miles by altitude band and topographic category were not prepared but an examination of carefully selected flights indicated that the distribution of flight miles by altitude band and topography is such that the conclusion reached from the figures given in Table V appears to be valid.

TABLE V

NUMBER OF OCCURRENCES BY TERRAIN OF RUNS WITH U_V RMS (2000) GREATER THAN LISTED VALUES FOR GIVEN ALTITUDE BANDS						
	Water, Flatland (100 Samples)			Mountains (120 Samples)		
	Altitude Band			Altitude Band		
U_V RMS (2000)	< 55K	50-60K	> 60K ft	< 55K	50-60K	> 60K ft
> 0.5 ft/sec	68	28	4	32	35	33
> 1.0 ft/sec	16	6	0	20	20	25
> 1.5 ft/sec	4	4	0	13	10	15
> 2.0 ft/sec	2	1	0	10	5	7
> 2.5 ft/sec	1	0	0	7	2	2

SECTION IV THE DISTRIBUTION OF LENGTHS OF HIGH ALTITUDE CLEAR AIR TURBULENT REGIONS

Summary

In the HICAT flight program 732 regions of turbulence were observed when the U-2 aircraft was in level flight. The percentage of cases that a given length, d , was exceeded may be expressed as follows:

$$\begin{aligned} P_d &= 109 e^{-0.038 d} && \text{for the total sample} \\ P_d &= 116 e^{-0.041 d} && \text{for the moderate turbulence cases} \\ P_d &= 173 e^{-0.055 d} && \text{for the severe turbulence cases} \end{aligned}$$

In each case the length of the turbulent region, d , cannot be less than that which makes P_d equal to 100.

Discussion

Crooks et al (1) used the results of the analysis of HICAT flights 39-175 to determine some measures of the size of high altitude clear air turbulence regions. In this section the new data from flights 180-285 have been combined with the older data to provide the basis for a determination of the distribution of lengths of high altitude clear air turbulent regions.

A total of 732 samples for which the flight path was level and the turbulence was indicated to be greater than very light were used to determine the distribution of lengths of the turbulent regions. The percentages of exceedances were computed for the total sample for cases of moderate or greater turbulence (144 cases) and for severe turbulence (16 cases). The mean lengths of the turbulent regions by altitude interval and season are given in Tables VI and VII. The data from these tables indicate that the lengths of the turbulent regions decrease with increasing altitude and that the lengths of the turbulent regions are greater in winter than in the other three seasons.

TABLE VI

MEAN LENGTHS OF TURBULENT REGIONS AS A FUNCTION OF ALTITUDE		
Altitude Range	No. of Cases	Mean Length
45,100 - 50,000 ft	71	24.5 nm
50,100 - 55,000 ft	299	24.5 nm
55,100 - 60,000 ft	234	22.0 nm
60,100 - 65,000 ft	128	17.0 nm

TABLE VII

MEAN LENGTHS OF TURBULENT REGIONS AS A FUNCTION OF SEASON		
Season	No. of Cases	Mean Length
Winter	219	29.5 nm
Spring	196	22.5 nm
Summer	81	22.5 nm
Autumn	236	21.5 nm

The distributions of the lengths of the turbulent regions were such that the percentage of the total number of cases, P_d , may be adequately represented by an equation of the form

$$P_d = a e^{-b d} \quad (4)$$

where a is a constant equal to 109 for all turbulent cases, 116 for the turbulent cases classified as moderate turbulence, and 173 for the severe turbulent cases. The constant b is equal to 0.038, 0.041, and 0.055 for the three categories respectively. The length of the turbulent patch is represented by d expressed in nautical miles. In each case d has a minimum value greater than zero because P_d cannot exceed 100.

The usefulness and the interpretation of the results presented in Equation (4) depend, to a significant degree, upon the definitions of a turbulent region that were used in preparing the Test Summary Tables of References 1 and 2. The definitions given by Crooks (1) are paraphrased as follows: The selection of clear air turbulence samples was based upon an edit of the flight measurements recorded upon a "quick look" oscillogram. Turbulence samples were selected primarily from an evaluation of the cg normal acceleration response of the aircraft. If continuous rapid cg acceleration disturbances in excess of ± 0.05 g were observed, turbulence was considered to be present. A turbulent region thus defined was considered to be significant (i.e. the data worth processing) if frequent cg acceleration peaks of 0.10 g or more were observed. In this event sample (called run and given a number) start and stop times were noted to the nearest five seconds. Samples of less than ten seconds duration were ignored. Each edited sample was also placed into one of the following categories:

Frequency Occurring Peak g Increment	Descriptive Term
± 0.05 to ± 0.10	very light
± 0.10 to ± 0.25	light
± 0.25 to ± 0.50	moderate
± 0.50 to ± 0.75	severe
± 0.75 or greater	extreme

These criteria were used for sample selection only. The correlation between these criteria and computed gust velocity is good but not perfect.

It is obvious from the definitions given in the above paragraph that the subjective element in the selection of turbulence samples was not negligible. Subjective judgment was used to determine, for example, if the oscillogram traces indicated one long turbulent region or two or more closely spaced turbulent regions. Throughout the HICAT program more than one person edited the oscillogram records. Even though a strong effort was made to obtain uniformity in judgment, individual differences in judgment probably were not eliminated. In addition, changes in judgment on the length of a run undoubtedly occurred as individual experience was gained. A relatively high number of samples at the even four, six, seven and ten minutes indicates some personal bias. An arbitrary upper limit of 1,000 seconds was established because of the data processing computer program. Thus, the statistical information represented by Equation (4) is biased because of the elimination of the very short and the very long turbulent regions, because the pilot, in a few cases, turned the aircraft before completely penetrating the turbulent regions and because the criteria for the intensity of turbulence do not include the gust velocities. On the whole, however, the results represented by Equation (4) probably provide an adequate representation of the relative frequencies of occurrence of the turbulent regions whose lengths are in the intermediate range.

Further measurements and analysis are required to answer relevant questions such as: What are the horizontal shapes of the turbulent regions? How do the shapes and lengths change in time with respect to axes fixed to the earth and with respect to axes fixed to a volume element of the atmosphere?

SECTION V

HICAT FLIGHTS AND THUNDERSTORMS

Summary

A review of the HICAT flight data indicated that there were 41 specifically documented flights over thunderstorms in which clear air turbulence was observed above the thunderstorm and one flight over a thunderstorm that was smooth. The length of the turbulent regions and the RMS of U_{de} both decreased with increasing altitude above the thunderstorm.

Discussion

A detailed review of the data presented by Crooks et al (1,2) and of the recordings of the statements made by the pilots of the HICAT flights indicated that there were 41 distinct cases (0.14% of total flight miles) of high altitude clear air turbulence in level flight above thunderstorm clouds. In each of these cases the pilot specifically stated that he flew over a thunderstorm and he estimated his altitude above the cloud top. Only once did the pilot specifically state that he flew over a thunderstorm and found no turbulence. In this instance the pilot estimated that he was 10,000 ft above the cloud top.

These 42 cases were categorized by altitude above the thunderstorm cloud top and the mean length of the turbulent regions, the U_{de} (max), and the RMS U_{de} were determined. The results obtained are as follows.

TABLE VIII

CHARACTERISTICS OF TURBULENCE ABOVE THUNDERSTORMS				
Estimated Altitude Above R_c	No. of Cases	Mean Length of Turbulent Region	U_{de} (max)	RMS U_{de}
1000-3000 ft	16	22 nm	7.0	1.60
4000-5000 ft	13	17 nm	4.9	0.92
6000-9000 ft	12	10 nm	2.5	0.76
> 9000 ft	1	0 nm	-	-

The true gust velocities were not included in Table VIII because they were computed for only four of the 41 cases.

The figures presented in Table VIII indicate that the mean length of the turbulent regions, the U_{de} (max) and the RMS U_{de} all decrease with increasing height above the thunderstorm cloud top. In a qualitative sense these results appear to be reasonable but the explanation of the absolute lengths of the turbulent regions is not obvious. Byers and Braham (4) published data relating to the mean horizontal cross-sectional area of thunderstorms as a function of altitude. The areas given refer to the areas

from which radar echoes are obtained and not necessarily to the areas of the visible clouds. They state that the cirrus clouds that form the anvil and much of the top portion of the thunderstorm cloud are not detected by the radar but the horizontal area of the visual cloud was approximately 19% greater than that of the radar cloud at 10,000 ft altitude.

If it is assumed that the thunderstorms are conical then the mean diameter of the region producing radar echoes for thunderstorms whose radar top is 47,000 ft is approximately 9 nm at 10,000 ft altitude and 3 nm at 45,000 ft altitude. The mean length of the turbulent region immediately above the thunderstorm is, however, 22 nm. This relatively large difference between the diameter of the thunderstorms and the length of the turbulent region above the thunderstorm could be interpreted as indicating (1) a disturbed region that is much larger than the thunderstorm, (2) a distinct difference in the samples of thunderstorms, (3) the HICAT flights were predominantly made parallel to squall line thunderstorms, or (4) that HICAT regions and thunderstorms are independently spaced and that the 41 cases of overlap was strictly fortuitous. At the present time there are insufficient data readily available to establish which of these or, perhaps, other alternatives would be the more probable. This work is being continued.

SECTION VI

CORRELATION OF HICAT WITH FUNCTIONS OF ATMOSPHERE TEMPERATURES AND WINDS

Summary

Chi-square and Kolmogorov tests were used to determine the extent to which HICAT was correlated with each of eight functions of atmospheric temperature and wind. These tests indicated that all eight of the functions were significantly correlated with HICAT. Both tests indicated that Richardson's Number and the minimum vertical gradient of the potential temperature within the layer ± 1000 ft of the flight altitude were the most highly correlated with HICAT. The relative rankings of the other six functions varied for the two tests of statistical significance.

In-flight measurements of the ambient temperature clearly showed that large changes generally accompanied moderate or severe turbulence although the characteristics of the changes depended upon individual circumstances.

Selection of the Sample and Description of the Tests

The following criteria were used to select turbulent and non-turbulent cases:

1. A case was put into the turbulent category if a turbulent sample (run) of intensity \geq light was within 100 miles and six hours of a radiosonde observation.
2. Non-turbulent cases were chosen from segments of flights where the U-2 flew within 50 miles and six hours of a radiosonde observation and no "run" of intensity \geq very light within 150 miles of the radiosonde station was listed in references 1 or 2 and the pilot did not report turbulence \geq light.

A total of 138 turbulent and 152 non-turbulent cases were selected.

The following statistical tests were employed to indicate the degree to which the turbulent and non-turbulent cases may have come from differing populations:

1. Chi-square (χ^2) tests with four degrees of freedom. The critical value of χ^2 is 13.3. The degrees of freedom are one less than the number of classes into which the data is distributed. For a χ^2 value calculated from the observed data greater than 13.3, the hypothesis that the two frequency distributions are from the same population is rejected at the 99% confidence level.
2. Kolmogorov-Smirnov tests with a critical value of 1.63. The hypothesis that the two distributions come from the same population is rejected at the 99% level. If the critical statistic obtained from the observed data is less than 1.63, the null hypothesis is accepted (the two distributions are assumed to come from the same distribution).

Results of Applying Chi-Square and Kolmogorov Tests

The chi-square and Kolmogorov tests for correlation between HICAT and the eight following functions of temperature and wind are presented in Table IX.

- (a) $(\Delta T/\Delta z)_{\max}$ The maximum temperature gradient in any layer within ± 1000 ft of the flight level. A ± 1000 ft deviation was allowed primarily to partially compensate for height errors in balloon and aircraft measurements. Although the vertical gradient is positive if the temperature increases with height, the maximum gradient in any layer can of course be negative if no positive gradient is present.
- (b) $|\Delta T/\Delta z|_{\max}$ The maximum absolute value of the vertical temperature gradient in any layer within ± 1000 ft flight level.
- (c) $|(\Delta T/\Delta z)_1 - (\Delta T/\Delta z)_2|_{\max}$ The absolute value of the maximum change in the vertical gradient at any level within ± 2000 ft above and below flight level. Δz_1 and Δz_2 are two adjacent layers.
- (d) $(\Delta \theta/\Delta z)_{\min}$ The minimum vertical potential temperature gradient in any layer within ± 1000 ft of flight level.
- (e) V Interpolated wind speed at flight level.
- (f) $\Delta V/\Delta z$ Vertical scalar wind shear.
- (g) $|\Delta \vec{V}/\Delta z|$ Magnitude of vertical vector wind shear.
- (h) Ri (Richardson's number) $(g/\theta) [(\Delta \theta/\Delta z)_{\min} / (|\Delta \vec{V}/\Delta z|)^2]$

The Δz used in the temperature gradient computations varied from a few hundred feet to several thousand feet, depending on the number of significant levels, and in the wind gradient computations from 1000 to 10,000 ft.

The distributions of these functions are shown in Figures 25 and 26. Unequal bands in the abscissa result from maintaining the turbulent and non-turbulent cases approximately constant for each class interval. This reduces the variability that occurs in test results due to arbitrarily selecting intervals.

These tests and the cumulative frequency curves given in Figures 27 and 28 indicated that all eight of the functions were significantly correlated with HICAT. Both tests indicated that Richardson's number and the minimum vertical gradient of the potential temperature within the layer ± 1000 ft of the flight altitude were the most highly correlated with HICAT. The relative rankings of the other six functions varied with the two tests of statistical significance. It is important to note, however, that less than 4% of the HICAT turbulent runs for which Ri could be computed had an Ri less than one. This appears to be in conflict with the conclusions reached by Briggs and Roach (5) and Endlich and Mancuso (6) from an examination of the data applicable for altitudes flown by the commercial airlines. This difference in results obtained for flights in the stratosphere and flights in the upper tropopause may be explained in part by the

TABLE IX

CHI-SQUARE (χ^2) AND KOLMOGOROV-SMIRNOV (K-S) TESTS APPLIED TO METEOROLOGICAL VARIABLES FOR HICAT FLIGHTS			
Equation	Explanation	χ^2	K-S
$(\Delta T/\Delta z)_{\max}$	Critical value (probability = .99)	13.3	1.63
	Max vertical temperature gradient (layer \pm 1000 ft of flight level)	49.2	1.83
$ \Delta T/\Delta z _{\max}$	Max absolute value of vertical temperature gradient (layer \pm 1000 ft of flight level)	48.4	2.93
$ (\Delta T/\Delta z)_{\Delta z_1} - (\Delta T/\Delta z)_{\Delta z_2} _{\max}$	Absolute value of max change in vertical temperature gradient (layer \pm 2000 ft of flight level)	56.4	2.55
$(\Delta \theta/\Delta z)_{\min}$	Min vertical potential temperature gradient (layer \pm 1000 ft of flight level)	85.4	3.78
V	Interpolated wind speed at flight level	63.7	3.02
$\Delta V/\Delta z$	Vertical scalar wind shear	54.6	3.14
$ \Delta \vec{V}/\Delta z $	Magnitude of vertical vector wind shear	70.6	3.14
R1	$\frac{g}{\theta} \frac{(\Delta \theta/\Delta z)_{\min}}{(\Delta \vec{V}/\Delta z)^2}$	114.7	4.34

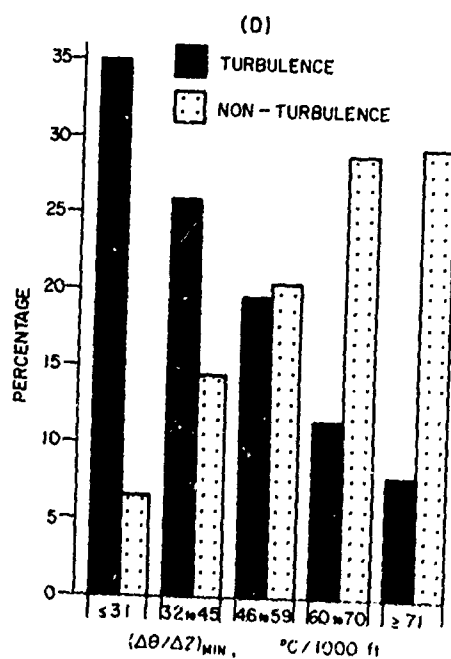
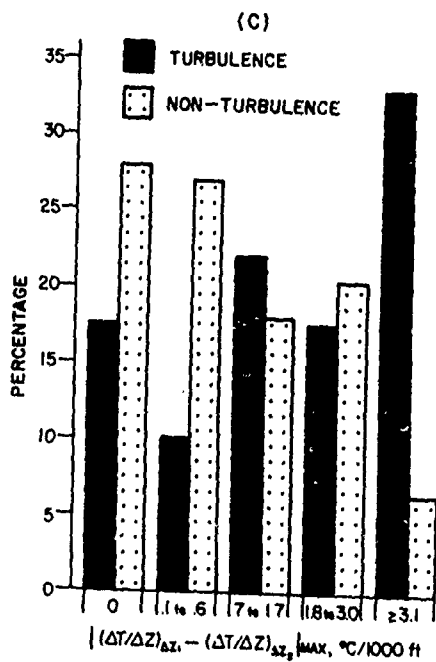
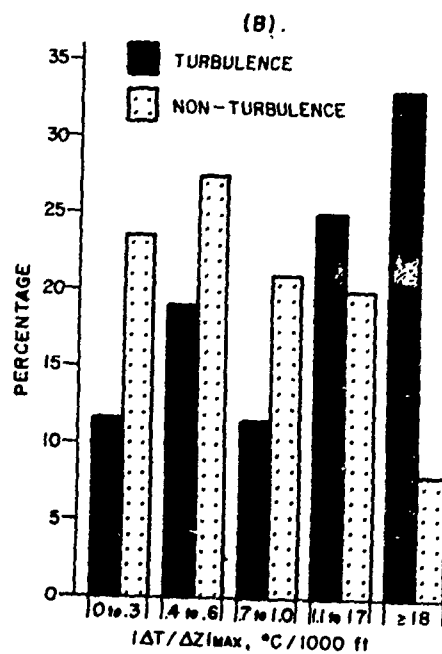
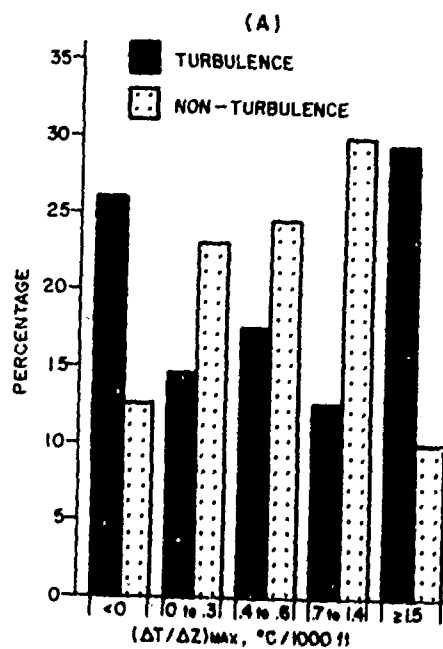


Figure 25. Histograms of Temperature Variables for Turbulent and Non-Turbulent Cases.

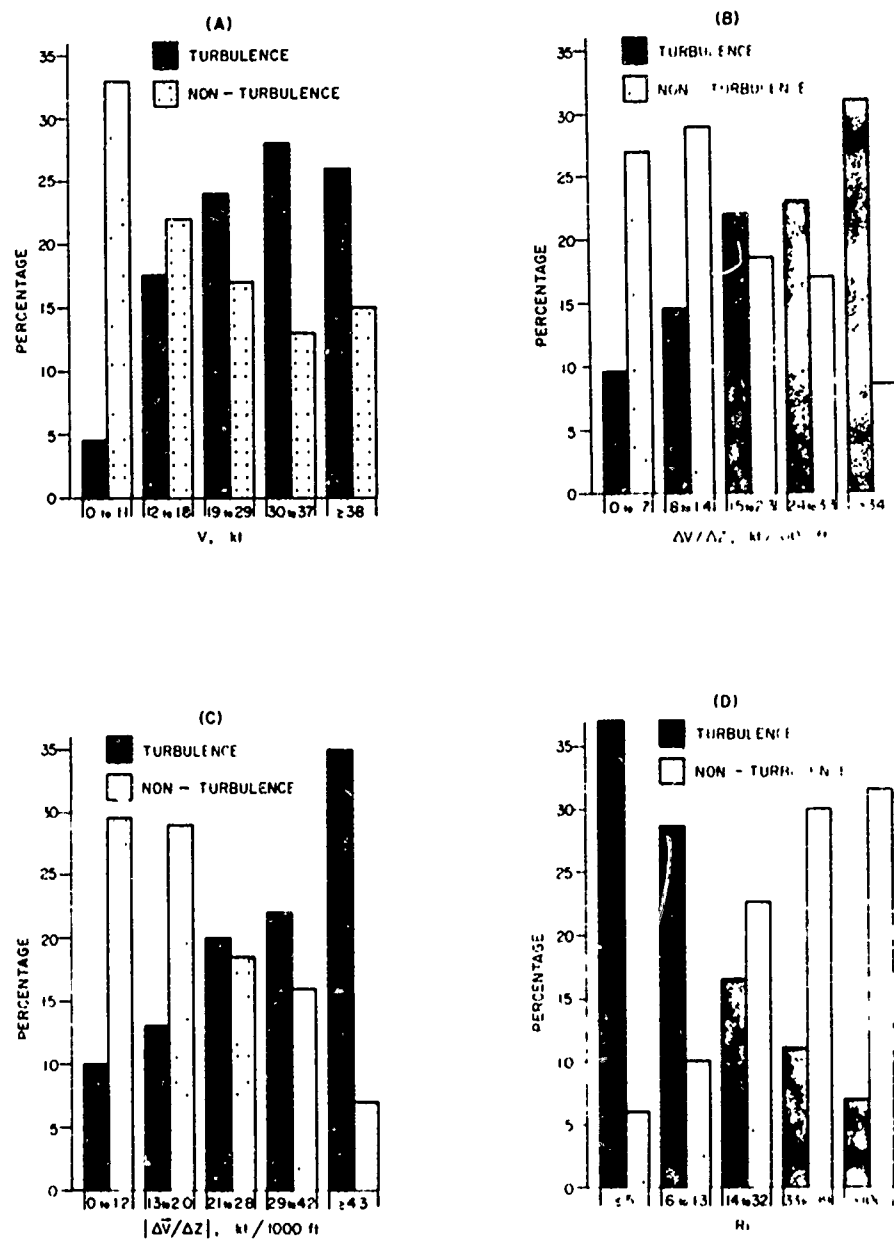


Figure 26. Histograms of Wind Variables and Richardson's Number for Turbulent and Non-Turbulent Cases.

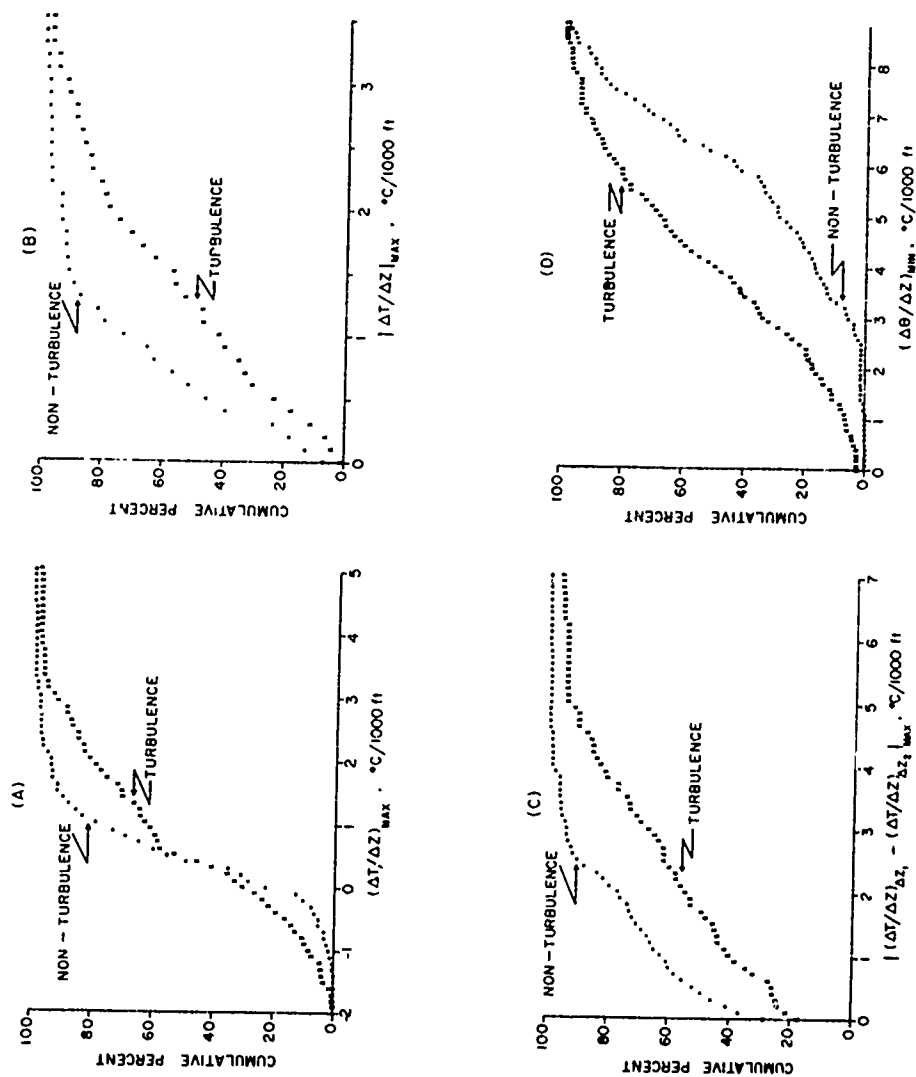


Figure 27. Cumulative Frequency Distribution of Temperature Variables for Turbulent and Non-Turbulent Cases.

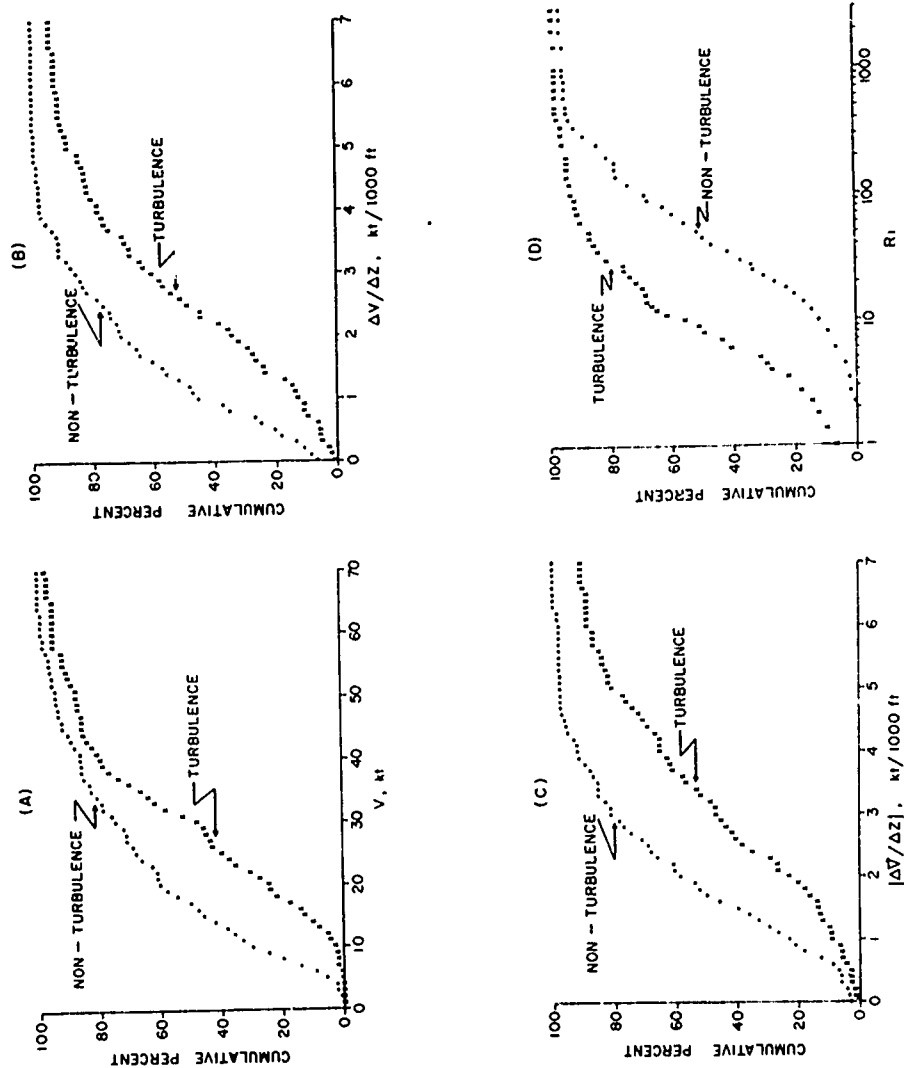


Figure 28. Cumulative Frequency Distribution of Wind Variables and Richardson's Number for Turbulent and Non-Turbulent Cases.

lack of knowledge of the wind shear over small altitude increments for the stratosphere and also the usual relatively large change of potential temperature with altitude at the HICAT flight altitudes.

In Figure 29 $|\Delta \vec{V}/\Delta z|$ and $(\Delta \theta/\Delta z)_{\min}$ were plotted, one as a function of the other. Then a straight line was drawn which best separated the turbulent cases (right side) from non-turbulent ones (left side). A total of 72% of the turbulent cases are to the right of the line and only 17% of the non-turbulent cases. It may be implied from the graph that turbulence occurs in layers where the wind shear is relatively weak providing there is a sufficiently large decrease or even an increase in temperature with height existing in the presence of turbulence.

In-Flight Measured Temperature Gradients

Approximately 25 hours of ambient temperature and true gust velocity time histories were available for analysis from the 232 HICAT flights. In-flight temperatures were measured with a Rosemount Engineering Model 102 total temperature probe mounted in the U-2's nose. Various correlations were derived between one and all of the gust velocity components and true air temperature variations. The method yielding the highest correlation was as follows:

- (a) Each turbulence encounter or "run" was counted as one sample. The largest temperature change over 20 seconds was calculated for each run. The altitude change for this 20 second period was restricted to less than 100 ft.
- (b) The largest gust velocity change during any 10 second period of a run was determined for each component. These changes were usually but not necessarily within the 20 second period described in (a).
- (c) The quantity $(\Delta U_F^2 + \Delta U_L^2 + \Delta U_V^2)^{1/2}_{\max}$ was computed, where ΔU_F , ΔU_L , and ΔU_V are changes in the lateral, longitudinal, and vertical components, respectively. The degree of correlation was established between this term and the maximum temperature change. The results appear in Figure 30.

The high correlation coefficient (.79) does not reflect the complexity of the temperature changes for individual cases. Selected time histories illustrating this are presented in Figures 31 to 35. A comparison of two time histories obtained from HICAT flights over the Cobar, Australia area is illustrated in Figure 31. One without turbulence (Figure 31a) shows nearly isothermal conditions and one with moderate turbulence (Figure 31b) shows short time interval temperature changes of 2.5°C accompanying the turbulence. The runs were separated in time by 1-1/2 hours.

The variability of temperature preceding turbulence contrasted to that within turbulence is seen in Figure 32a. These measurements were made above relatively flat terrain between Laverton and Cobar in southeastern Australia. The temperature scale has been enlarged to emphasize changes during turbulence.

The largest temperature change for any HICAT flight occurred during severe turbulence over the mountains northwest of Albuquerque, New Mexico. An 11.5°C change in four miles was recorded (Figure 32b).

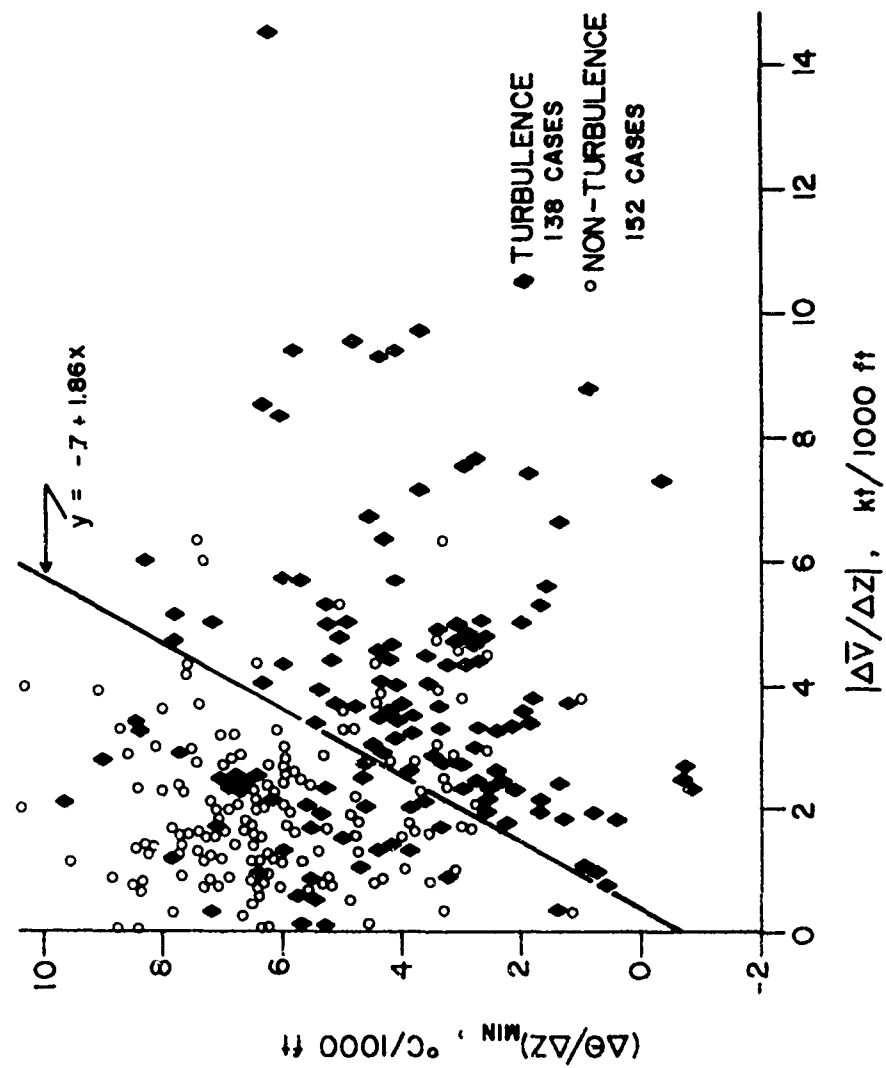


Figure 29. Minimum Vertical Potential Temperature Gradient as a Function of Vertical Vector Wind Shear.

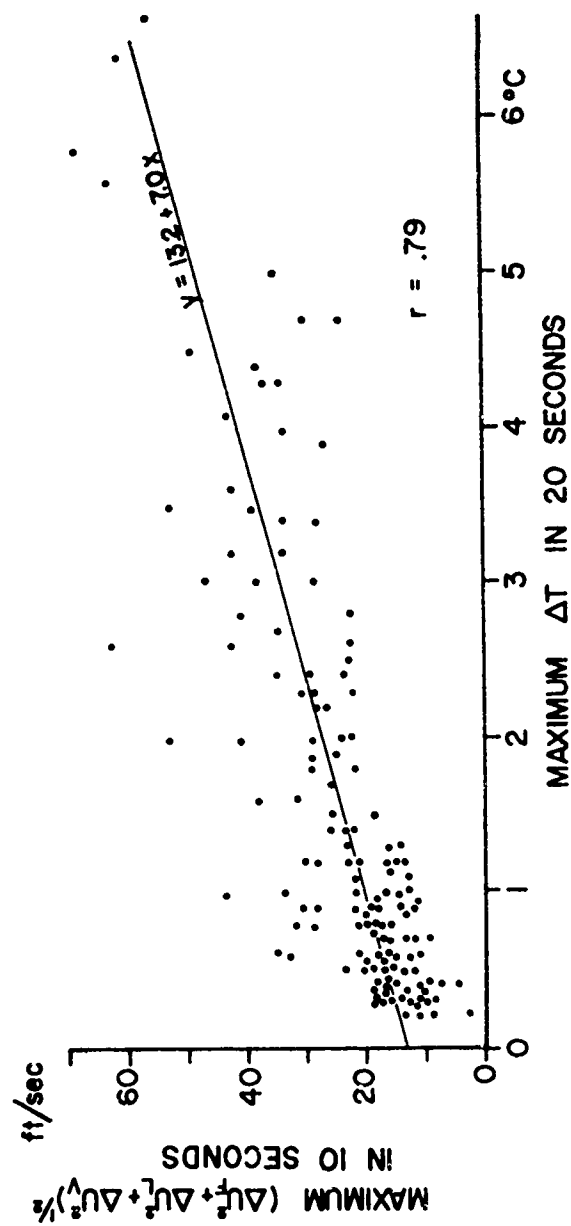


Figure 30. Correlation Between In-Flight Measured Temperature and Gust Velocity Changes.

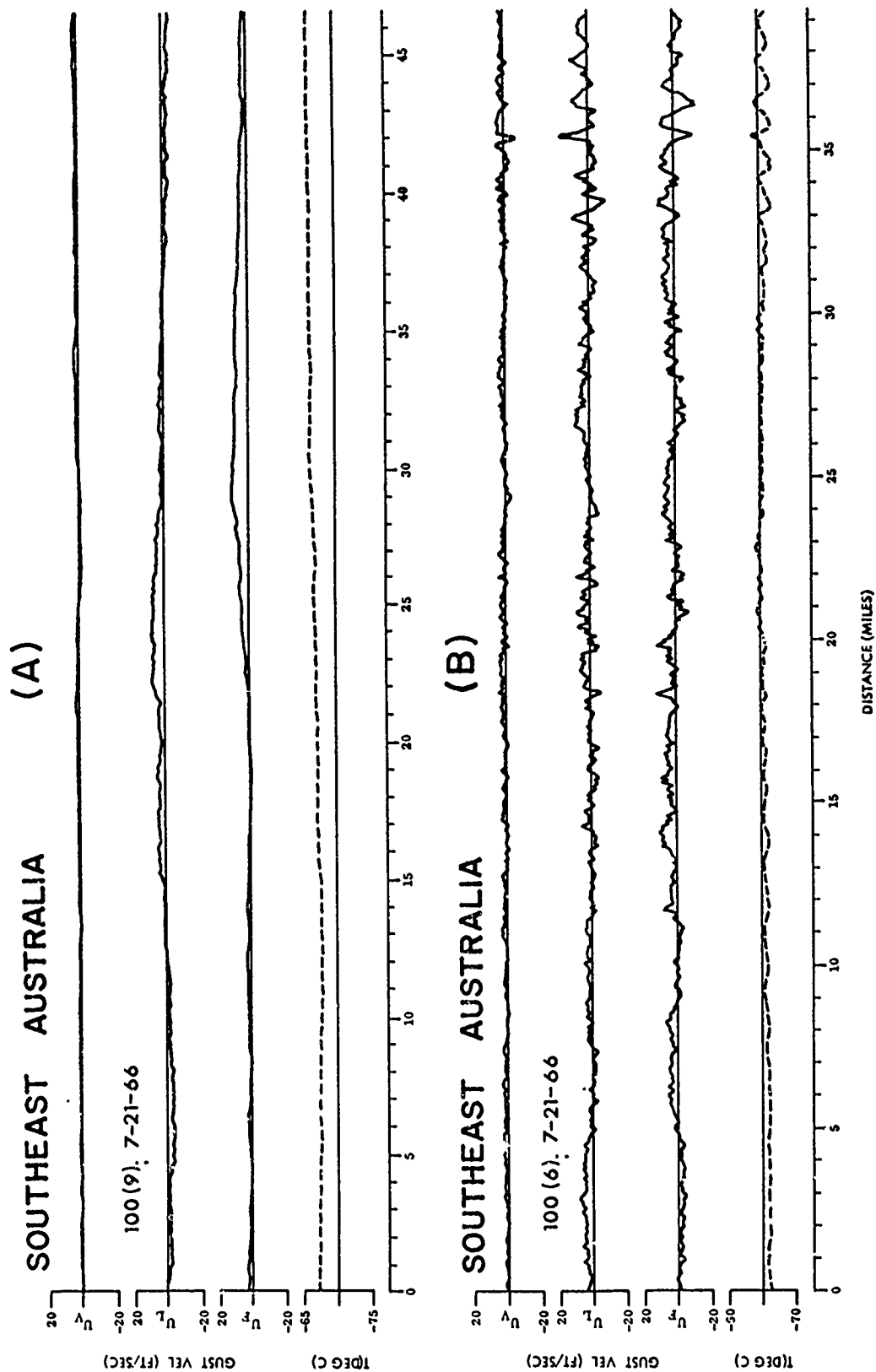


Figure 31. Time Histories of Gust Velocity and Temperature Variations for Smooth (A) and Turbulent (B) Flights Over Southeast Australia.

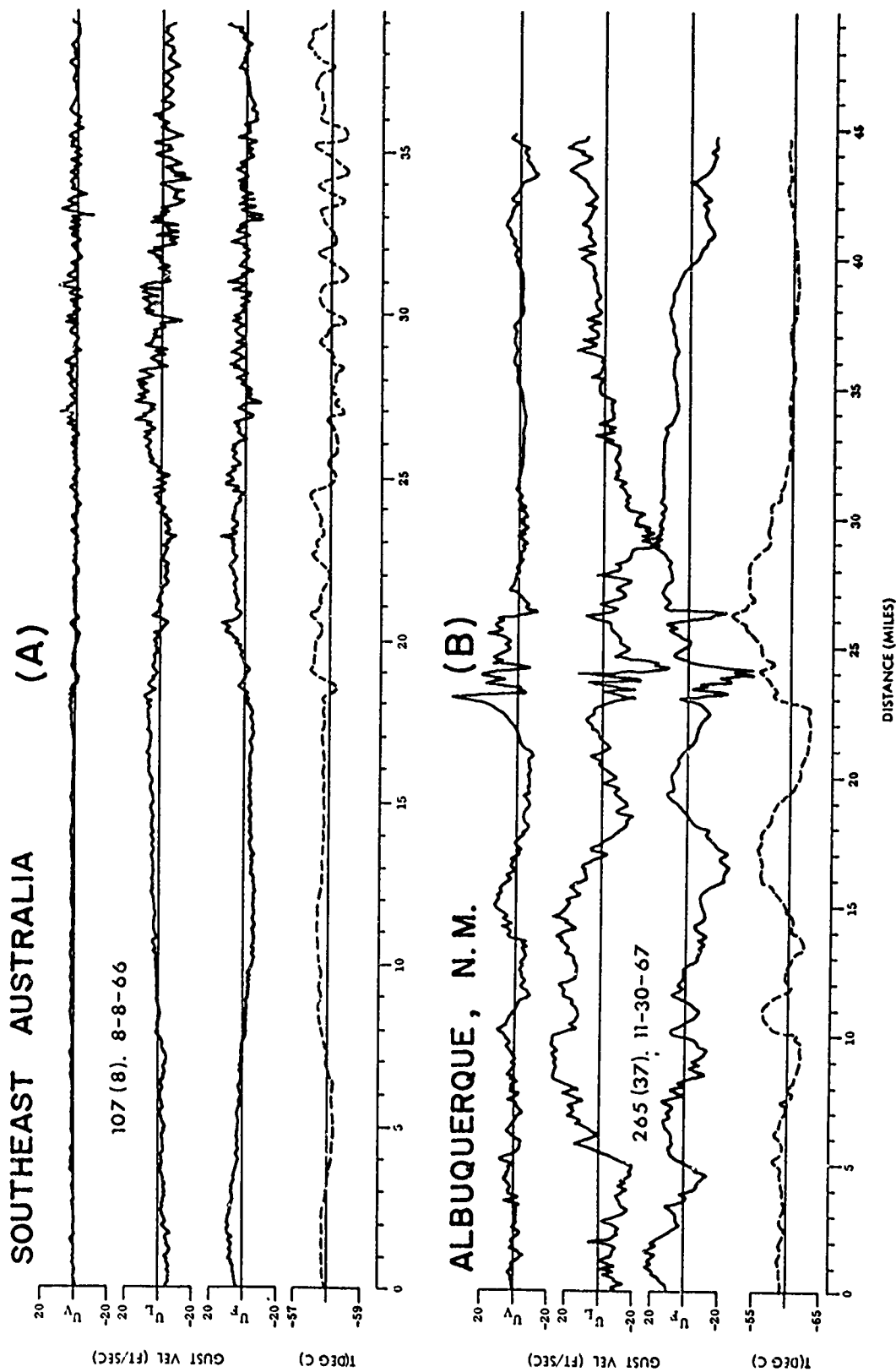


Figure 32. Time Histories of Gust Velocity and Temperature Variations for Flights Over Southeast Australia (A) and Albuquerque, New Mexico (B).

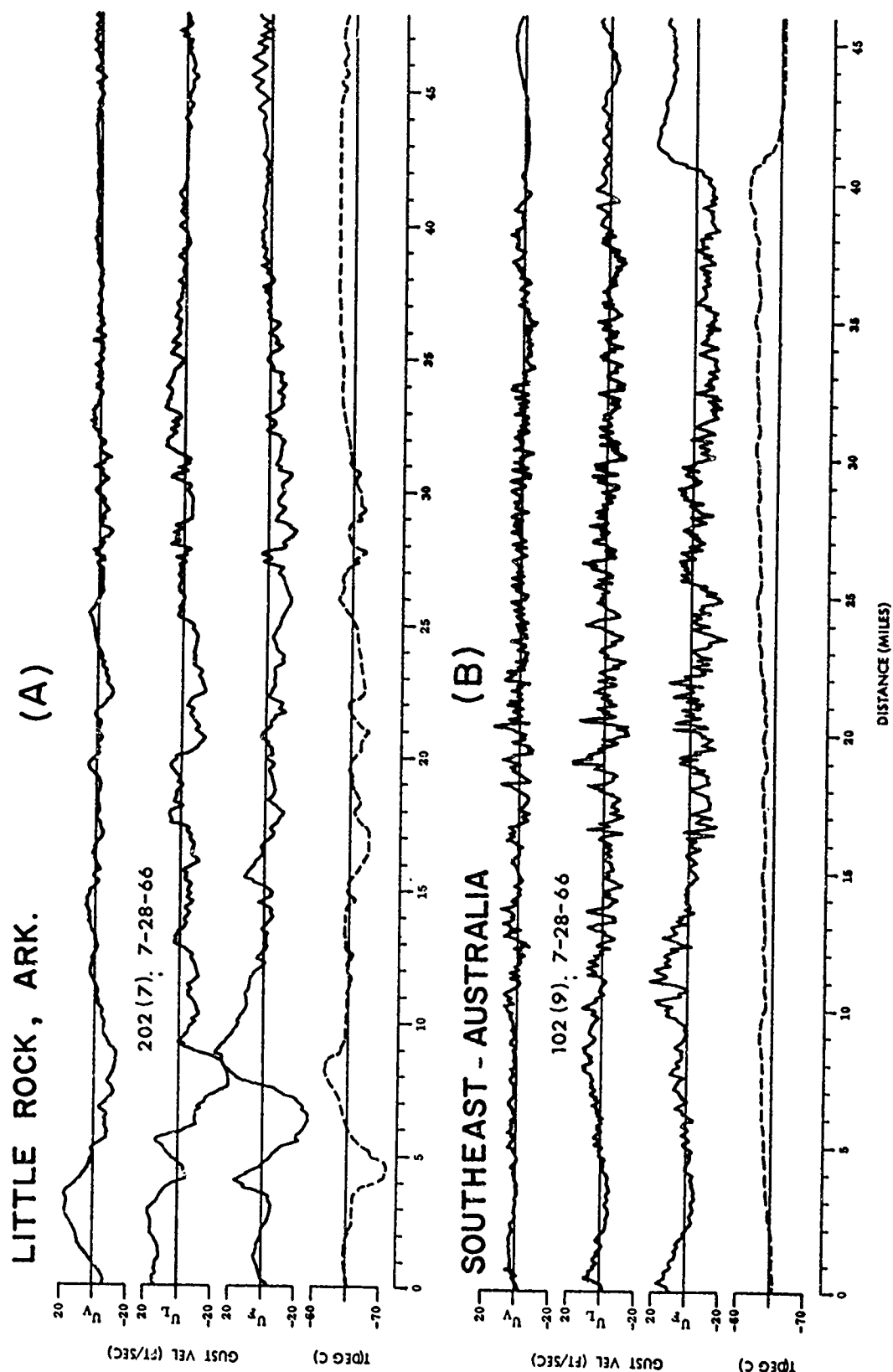


Figure 33. Time Histories of Gust Velocity and Temperature Variations for Flights Over Little Rock, Arkansas (A) and Southeast Australia (B).

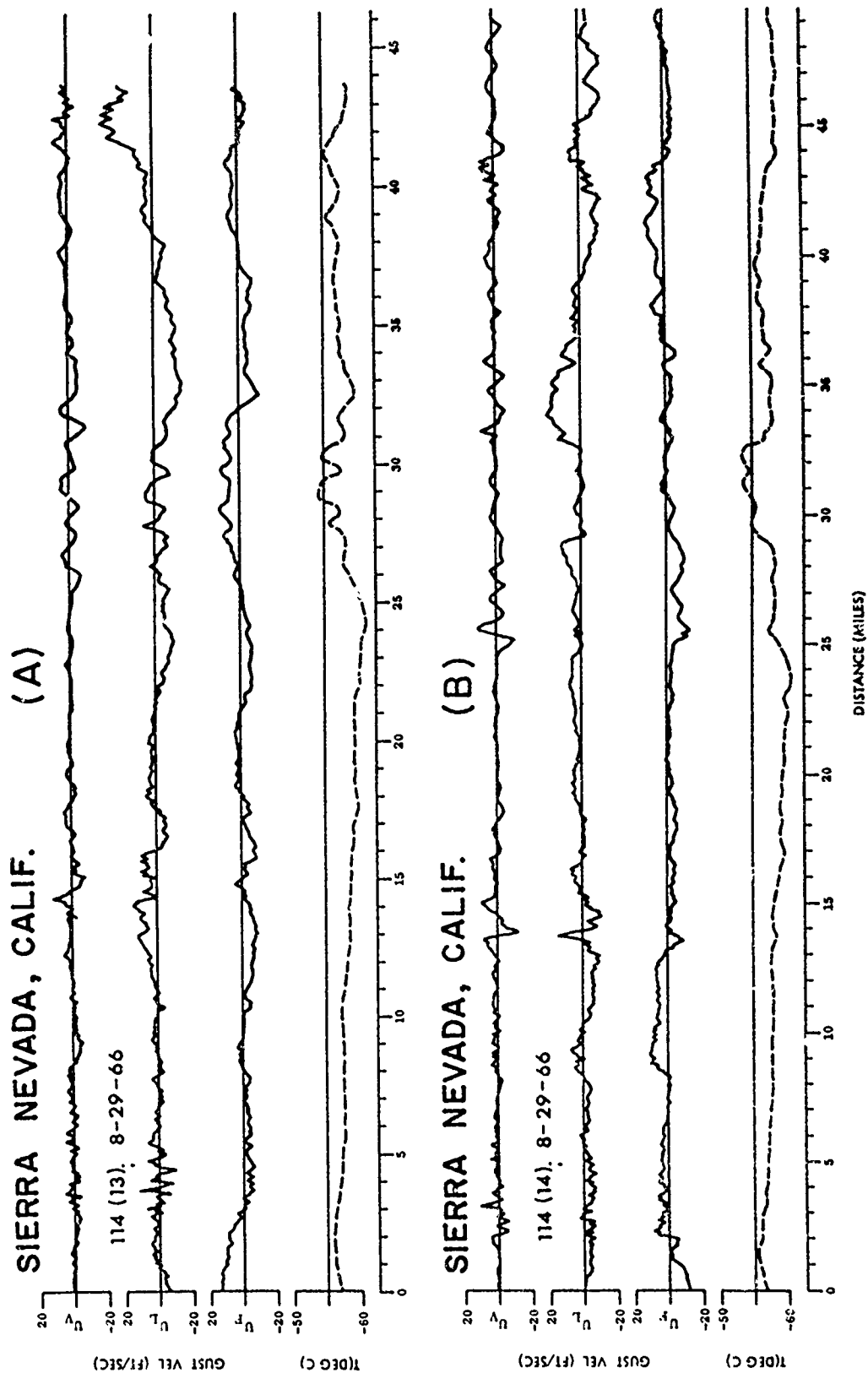


Figure 34. Time Histories of Gust Velocity and Temperature Variations for Two Flights Over the Lee Side of the Sierra Nevada Mountains, California.

DENVER, COLO.

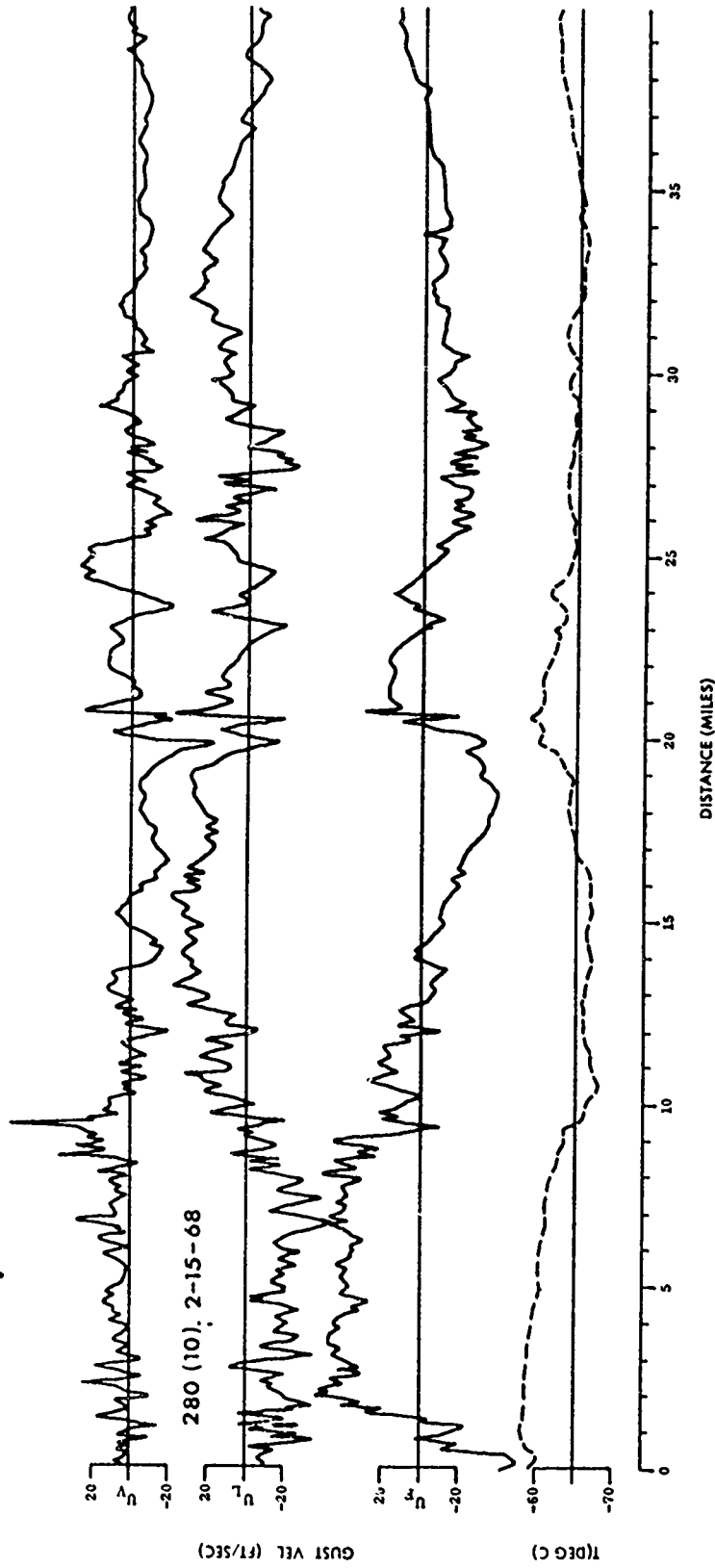


Figure 35. Time Histories of Gust Velocity and Temperature Variations for a Flight Over the Lee Side of the Rocky Mountains Near Denver, Colorado.

Although some statistical studies, like the present, have suggested a strong relationship between turbulence and atmospheric temperature changes (Helvey (7), Kadlec (8), Moore and Krishnamurti (9)), the characteristic of the change varies considerably from case to case. For example, Figure 33a shows a temperature change of 9°C in three miles recorded during moderate turbulence above thunderstorm activity in Arkansas. Figure 33b records a gradual rise in temperature over a distance of several miles and a drop in the temperature of 5°C in $2\frac{1}{2}$ miles near the end of the run. Moderate turbulence accompanied this flight at 61,000 ft on the lee side of the Great Dividing Range in southeast Australia. There was a strong jet at 36,000 ft with winds exceeding 150 kt. This case illustrates that the effectiveness of a remote sensing device may depend upon the relative flight direction. Had the aircraft flown at 180° to the actual heading the sharp temperature change would have probably preceded the turbulence. It is reasonable to assume this type of change could be detected more readily than a gradual one.

The temperature variation for a flight east of the ridge line of the Sierra Nevada Mountains in California (Figure 34) is indicative of a mountain wave situation. The heading in Figure 34a was into the wind (towards the ridge) and with the wind (away from the ridge) in Figure 34b. Both runs were at right angles to the ridge, nearly overlapping and separated by a few minutes. Time histories for Figure 34b are plotted in reverse to correspond with the wind flow which was west-southwest and perpendicular to the ridge both at mountaintop and flight level.

A trough-ridge structure in the horizontal temperature field is discernible for both runs. The distance between crests is approximately 9 to 10 miles, with the exception of the first wave which has a wavelength about three times as long. In a detailed report on 1962 U-2 measurements in the same general area Helvey (7) concluded that the temperature troughs, or cold zones, were associated with crests in the mountain wave. Turbulence was found to be concentrated in the zone between the warm and cold axis, the warm axis being oriented upwind from the cold. The Sierra HICAT flights do not supply any conclusive evidence to verify this. There is, however, a case of severe turbulence in the Denver, Colorado area (Figure 35) where the maximum gusts occurred in the zone designated by Helvey (7). The Albuquerque flight (Figure 32) also verifies this.

It is reasonable to conclude from the evidence presented that variations in the horizontal temperature along the flight path are quite commonly synchronous with clear air turbulence and proportional to the magnitude of the turbulent gusts.

SECTION VII

CORRELATION BETWEEN HICAT AND HEAD WIND AND TAIL WIND

Summary

In the HICAT flight program there were 376 observations of high altitude clear air turbulence for which the winds were computed from inertial platform data. A histogram of the differences between aircraft heading and wind direction shows a pronounced maximum for those cases 0-30° from a headwind and a minimum for those cases 0-30° from a tailwind.

Discussion

The HICAT Test Summary Tables published by Crooks et al (1, 2) listed 376 cases for which winds and aircraft heading were both listed. Figure 36 consists of a histogram of the difference between the aircraft heading and the wind direction. This histogram shows that for all turbulent classes, the turbulence was observed most frequently when the aircraft was heading into the wind and least frequently when there was a tailwind. The relative frequency of occurrence of turbulence with other differences in angle between the heading and wind showing a decrease from headwind to tailwind.

The correlation between the difference in aircraft heading and wind direction indicated by Figure 36 may be real or it may be the result of a systematic error in the wind measurements derived from the inertial platform data. If the second of these hypotheses were more nearly true than a non-zero correlation would be expected between the change in heading of successive "runs" made on the same flight and the change in wind direction. Figure 37 indicates that the correlation coefficient is near zero and hence supports the first hypothesis.

A second test of the two hypotheses consisted of a determination of the mean wind of the 376 wind observations. The mean wind consists of the vector sum of the means of each of the two horizontal components (west-east and south-north) of the winds. This mean wind was 23.5 knots from 262°. This value corresponds closely to the mean wind at the HICAT flight levels for most of the areas of flight. For example, the mean wind at 53,000 ft altitude over Ely, Nevada, a representative station for flights based at Edwards AFB, is 22.5 knots from 267°. Thus, this test also supports the first hypothesis. The HICAT flight data indicate that light turbulence was found more frequently with a head wind than with a tail wind.

Table X is a contingency table showing detailed subsets defined by wind direction and aircraft heading categories. The total number of cases is 349 rather than 376 because the cases for which the wind speed was 10 knots or less were eliminated from the sample. The sums on the borders of the table indicate in detail that the maximum number of occasions of turbulence occurred with a headwind for all directions of the wind.

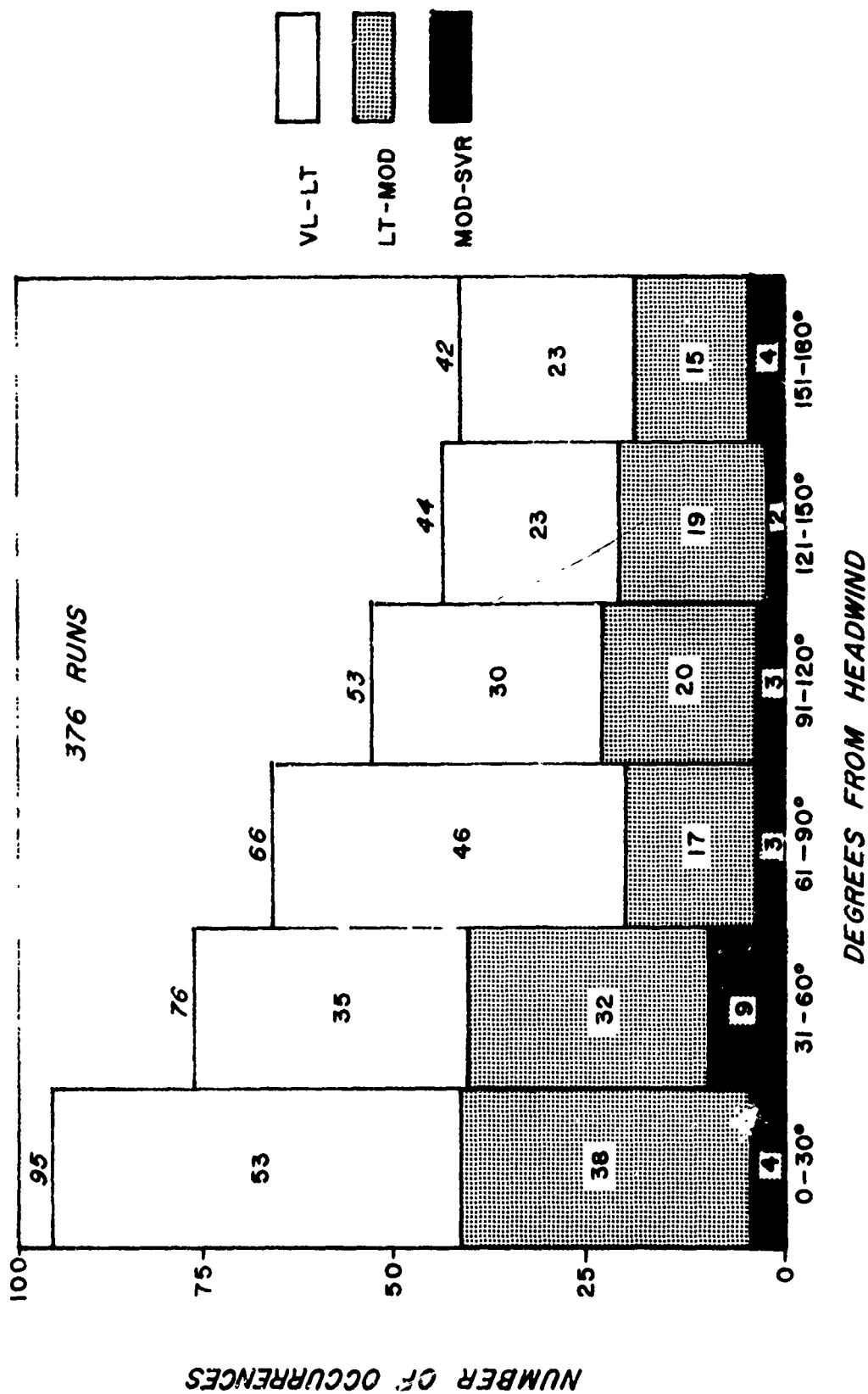


Figure 36. Histogram of the Difference in Angle Between Heading and Wind for the H(CAT) Turbulence Cases.

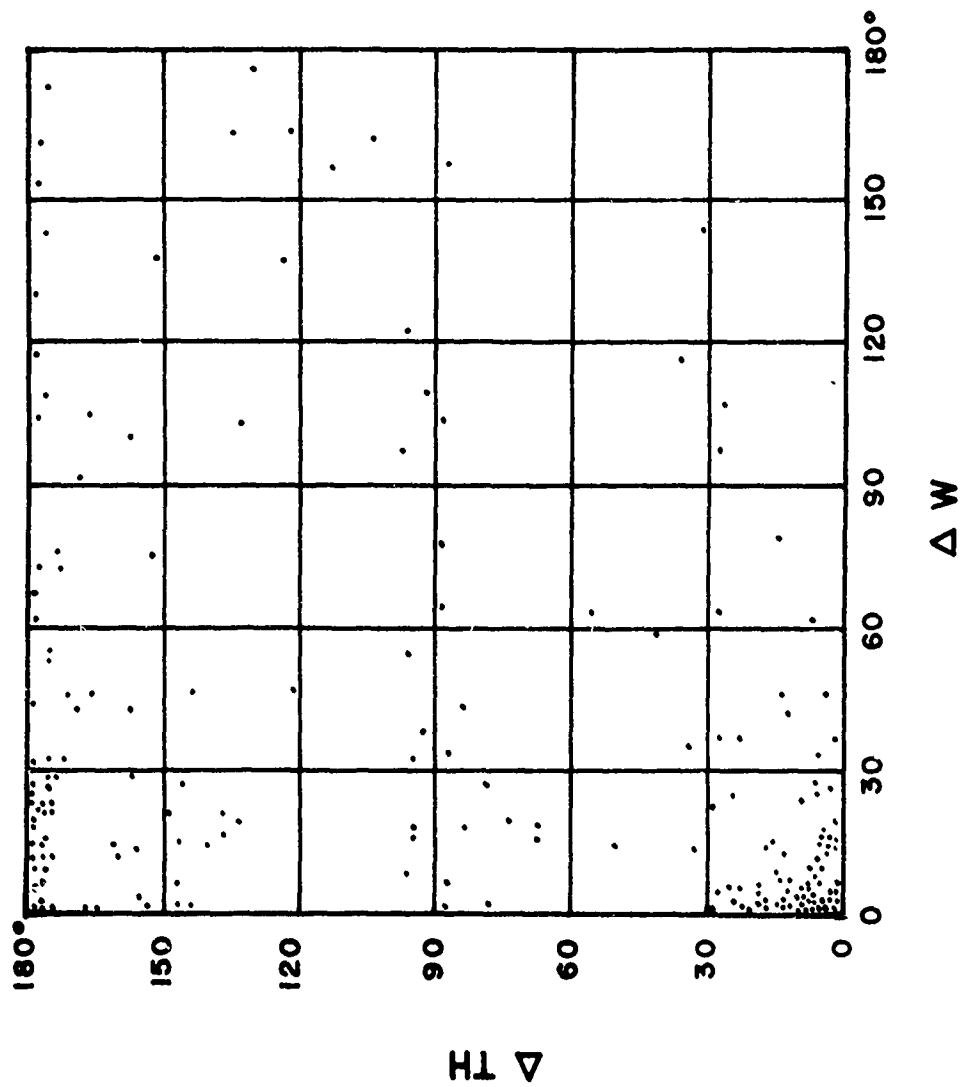



Figure 37. Change in WU-2 Observed Wind Direction (ΔW) as a Function of Change in Aircraft True Heading (ΔTH) for All Runs with Change in Altitude ≤ 1000 feet and Wind Velocity ≥ 10 knots.

TABLE X

CONTINGENCY TABLE SHOWING WIND DIRECTION
AND AIRCRAFT HEADING CATEGORIES (349 RUNS)

	10.6	9.7	10.3	8.6	15.8	16.6	12.6	15.8		
	37	34	36	30	55	58	44	55		
316-360°	5	1	4	0	2	11	6	5	34	9.7
271-315°	7	8	8	5	14	11	16	14	83	23.8
226-270°	15	5	9	8	21	20	9	16	103	29.5
181-225°	7	8	1	11	12	11	6	7	63	18.1
136-180°	1	2	3	3	2	1	0	5	17	4.9
91-135°	0	1	6	2	1	0	0	3	13	3.7
46-90°	0	8	2	1	3	2	4	0	20	5.7
1-45°	2	1	3	0	0	2	3	5	16	4.6
	1-45°	46-90°	91-135°	136-180°	181-225°	226-270°	271-315°	316-360°		

WIND DIRECTION

AIRCRAFT HEADING

SECTION VIII

EXCEEDANCE PROBABILITY OF RMS (2000) FOR THE THREE COMPONENTS OF THE GUST VELOCITY BY SEASON AND BY ALTITUDE

Summary

Gust velocity data are analyzed in terms of a log-normal cumulative frequency distribution. Velocity exceedance probabilities are tabulated for all four seasons and for four altitude bands.

Discussion

Exceedance curves of the RMS (2000) for the three gust velocity components can be approximated by a variety of non-linear type of curves. However, one type of mathematical equation which most generally gives a linear relationship, especially at the high values of velocity (low probabilities of exceedance), can be expressed as

$$P = e^{-a(x)^m} \quad (5)$$

where, P is the probability of equaling or exceeding a given value of x , the RMS velocity.

a and m are constants to be determined.

If the distribution is log-normal, then the cumulative percentages yield a straight line when plotted on log probability paper. In this case, the velocity is plotted on a logarithmic scale along the ordinate and the abscissa is a probability scale linear in terms of σx . In the special case when $m=2$, the expression equals Rice's equation, and, of course, if $m=1$ the expression reduces to a simple semi-logarithmic one.

All three velocity components for RMS (2000) were available for analysis for 125 individual turbulence runs. The percentage exceedance curves for all three components are shown in Figure 38. As may be noted, the median values (50% probability) range from 1.1 ft/sec for the vertical component, to 1.3 and 1.4 ft/sec for the longitudinal and lateral components, respectively. Percentagewise, the difference between the RMS gust velocity components is greatest at low velocities and appears to steadily diminish at higher velocities. Values for a and m were computed from the curves in Figure 38 and are summarized in Table XI below.

TABLE XI

CALCULATED VALUES FOR CONSTANTS IN EXCEEDANCE EQUATION		
Component	a	m
U_L	0.16	2.98
U_F	0.26	2.62
U_V	0.41	2.33

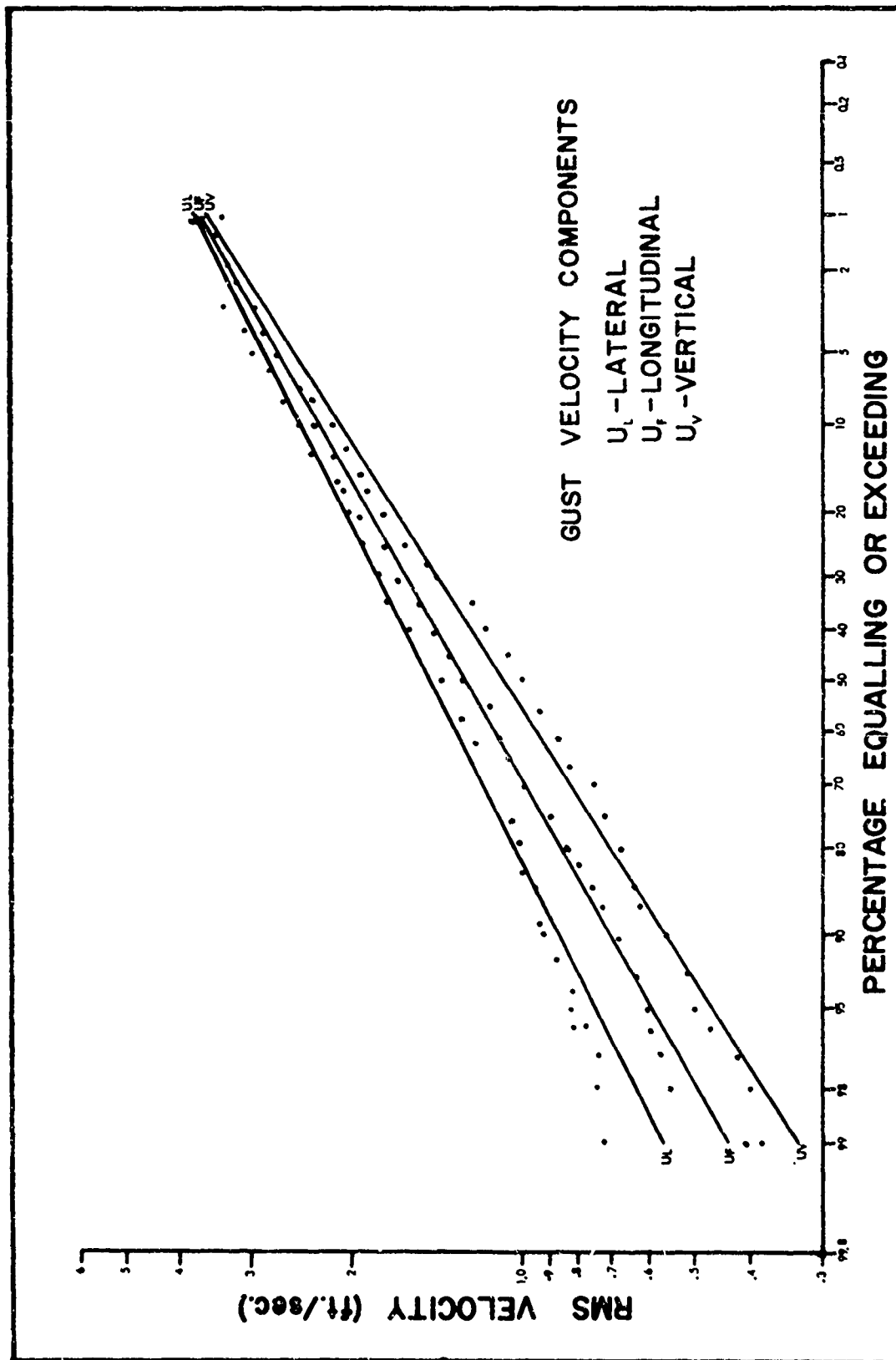


Figure 38. Cumulative Distribution of RMS (2000) Gust Velocity.

The data were also analyzed according to season and altitude and similar curves were prepared. Values for the 50% and 10% velocity exceedance levels are tabulated in Table XII along with the estimated 1% exceedance velocities obtained by extrapolating the best eye-fitted straight line. The most obvious features in the table are that all three gust components are less intense in summer and less intense between 45,000 and 50,000 ft compared to other seasons and altitude bands, although both sample sizes are small.

In the section on topographic effects a ratio between the total RMS value and the truncated RMS (2000) was derived. An apparent relationship between the PSD shapes and topography made it possible to use definite theoretical curves to determine this ratio and the scale length, L . Seasonal and altitude effects do not appear to be sufficiently strong to outweigh the topographic effects. Thus, at present, no ratio between the total and the truncated RMS area of the PSD for seasonal and altitude effects has been determined. The sample size of the union of the subsets determined by topography, season, and altitude appear to be too small to achieve statistically significant results.

TABLE XII

RMS (2000) EXCEEDANCE GUST VELOCITIES (FT/SEC)

SEASON	NO. OF RUNS	VERTICAL			LATERAL			LONGITUDINAL		
		50%	10%	1%	50%	10%	1%	50%	10%	1%
Winter	69	1.1	2.1	3.6	1.5	2.4	3.6	1.3	2.4	3.6
Spring	27	1.0	2.0	3.8	1.4	2.8	5.0	1.3	2.1	3.1
Summer	7	0.7	1.3	2.2	1.0	1.8	3.1	0.7	1.5	3.1
Autumn	22	1.4	2.5	4.2	1.7	3.1	4.5	1.7	3.1	4.5

ALTITUDE												
45-50 k ft	12	1.0	1.2	1.4	1.5	2.0	2.5	1.2	1.5	1.9		
50-55 k ft	48	1.0	2.0	3.6	1.3	2.8	5.2	1.1	2.4	4.5		
55-60 k ft	36	1.2	2.3	4.1	1.3	2.5	4.1	1.3	2.4	3.8		
60-65 k ft	23	1.6	2.6	3.7	1.9	3.1	4.5	1.9	3.1	4.5		

SECTION IX

DISTRIBUTION OF HICAT FLIGHT MILES AND TURBULENT FLIGHT MILES IN THE UNITED STATES

Summary

Total flight miles, miles in all classes of turbulence and miles in moderate or severe turbulence were determined for each of the sectors 5° longitude by 5° latitude for continental United States. The three sectors covering the area from central California to central Colorado show the largest number of flight miles. These areas also had a relatively high percentage of turbulence. The highest percentage of turbulence was found in the Oklahoma area.

Discussion

The distribution of HICAT flight miles and the percentages of flight miles that were turbulent is shown in Figure 39. The upper figure in each 5° x 5° sector gives the total miles flown in the sector. The second figure gives the percentage of the total miles that were turbulent. The third figure gives the percentage of the total flight miles for which the intensity of the turbulence was classified as moderate or severe. All flight miles (including patterns) were counted. This was done to obtain as large a sample as possible and to avoid the selection of a "particular" run in a pattern as being "representative". The highest percentages of turbulence were found to be in the central Rocky Mountain and central Plains areas. The turbulence in the central Plains area was largely associated with thunderstorms and squall lines.

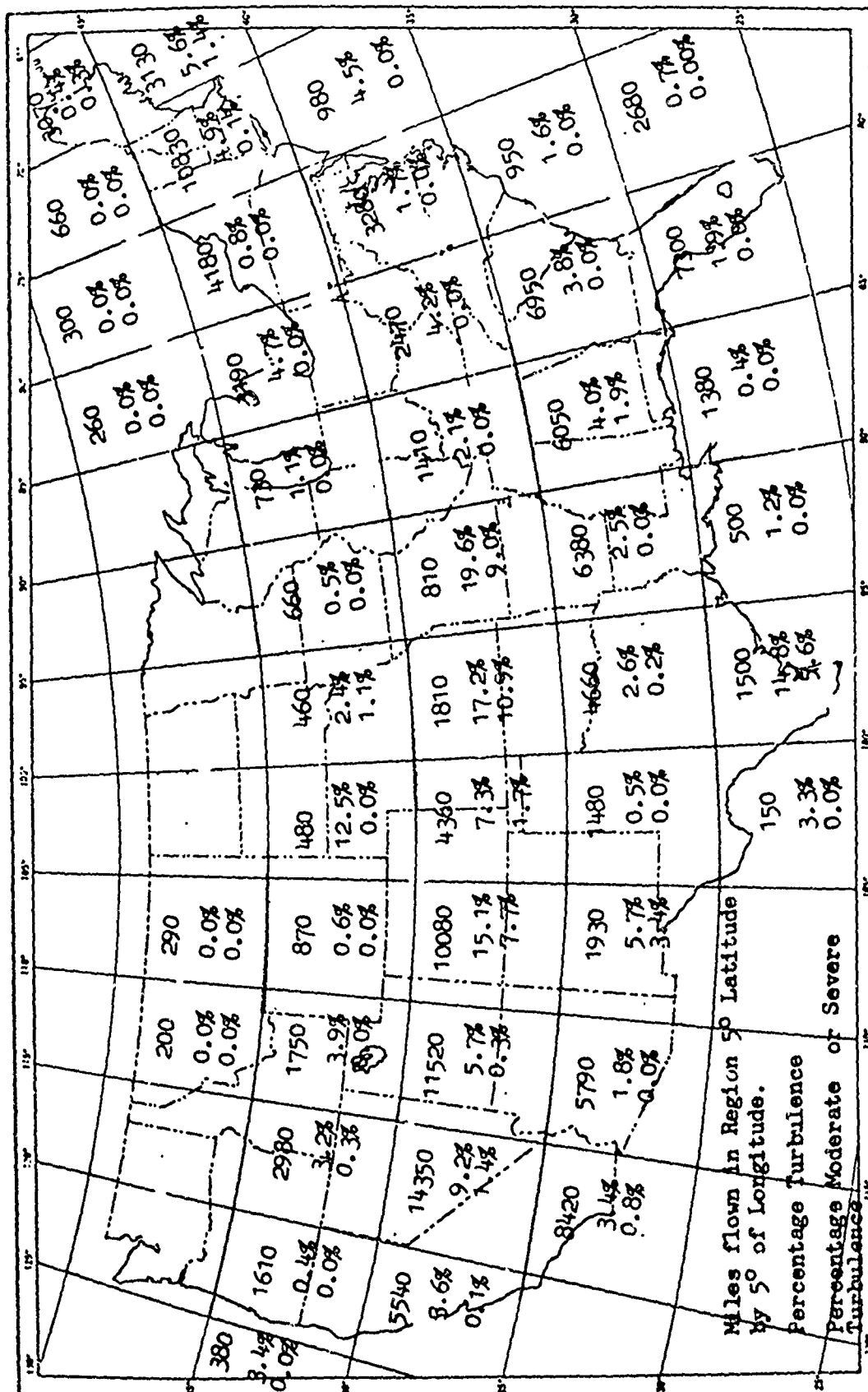


Figure 39. Distribution of HICAT Flight and Turbulent Flight Miles in the United States.

SECTION X

MODELS AND EXAMPLES

Summary

Models of the percentage of the flight miles in turbulence for given values of σ_w are given for topographic and altitude.

Frequency of Gust Encounters

The results described in the previous sections were used as a basis for the following models. Figure 47 presents a model for use in determining the relative frequency of occurrence of gust intensities where σ_w^2 is used as a measure of the gust intensity. The lower limit of σ_w^2 in this model is 0.25 (ft/sec)^2 . This model indicates a relatively large difference in the relative frequency of a given value of σ_w^2 for the four classes of topography. This conclusion, however, is not firmly established because the HICAT observations over mountains were almost exclusively winter and autumn flights and the flights over water and flatland were largely made during the spring and summer. The model is not complete because insufficient data were available for all seasons and for high latitudes. The model also does not apply for extensive flights over the intertropical convergence zone.

The main features of the model are as follows:

- (a) Flights in the 45,000–65,000 ft altitude interval in autumn and winter over high mountains have the highest percentage of flight miles with relatively high values of σ_w^2 .
- (b) The percentage exceedance curves of σ_w^2 vary with altitude for flights over water and flatland but do not vary with altitude for flights over mountains.

Examples

Location	Season	Percentage of Flight Miles		
		$\sigma_w^2 \geq 10 \text{ (ft/sec)}^2$	$\sigma_w^2 \geq 50 \text{ (ft/sec)}^2$	$\sigma_w^2 \geq 100 \text{ (ft/sec)}^2$
Trans-Pacific	Spring	0.03	<0.01	<0.01
Western U.S.	Winter	1.7	0.12	0.026
Central U.S.	Spring	0.14	0.01	<0.01
Appalachian Area	Autumn	0.4	0.022	<0.01

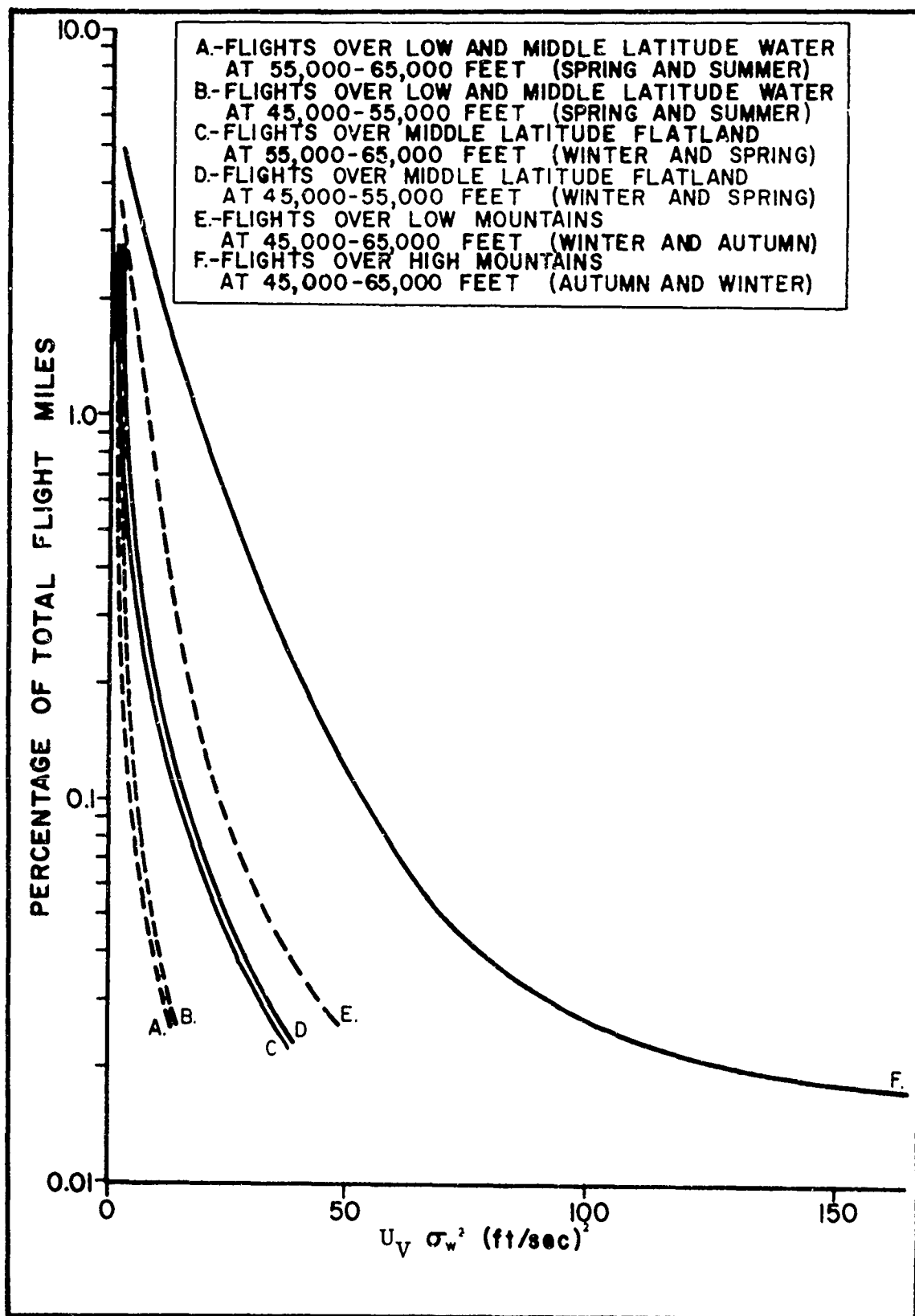


Figure 40. Percentage of Flight Miles for Which Given Value of σ_w^2 is Equaled or Exceeded.

SECTION XI

CONCLUSIONS

The principal conclusions that were presented in this report are:

1. The equations for the probability of the RMS (2000) for U_L , U_F and U_V equaling or exceeding a given value x respectively are

$$P = e^{-0.16 x^{2.98}} \quad (\text{for } U_L)$$

$$P = e^{-0.26 x^{2.62}} \quad (\text{for } U_F)$$

$$P = e^{-0.41 x^{2.33}} \quad (\text{for } U_V)$$

2. All three gust components are less intense in summer and between 45,000 and 50,000 ft compared to other seasons and altitude bands.
3. The mile knee equation (Equation (1) page 23) best fits the power spectral density curves.
4. The "scale lengths" for U_V power spectral density curves are 4000 ft for flights over high mountains, 2000 ft for low mountains and 500 ft for flatlands.
5. There was no significant change in scale length with flight altitude for either the mountain or the flatland cases.
6. The ratio of turbulent flight miles to total flight miles varied from 0.027 for flights over water to 0.049 for flights over high mountains.
7. The intensity and the frequency of occurrence of turbulence decreased with altitude above 55,000 ft over low relief terrain but did not change with altitude over mountains.
8. The probability, P_d , of the length of turbulent regions equaling or exceeding a given length, d , may be represented by

$$P_d = 1.09 e^{-0.038 d}$$

When only regions of severe turbulence are considered then the relevant equation is

$$P_d = 1.73 e^{-0.055 d}$$

(The length, d , is not less than that value that makes $P_d = 1.0$.)

9. The occurrence of clear air turbulence is associated with variations in the atmospheric temperature along the flight path and the magnitudes of the gust velocities and the temperature changes are nearly proportional.
10. The mean lengths of the turbulent regions and the intensity of the turbulence decrease with increasing altitude above thunderstorms. No turbulence was observed when the flight altitude was 10,000 ft above a thunderstorm.
11. Turbulence was observed approximately twice as often with head winds as tail winds.

REFERENCES

1. Crooks, Walter M., Frederic M. Hoblit, David T. Prophet, et al, "Project HICAT. An Investigation of High Altitude Clear Air Turbulence, " Air Force Flight Dynamics Laboratory Technical Report AFFDL-TR-67-123 (November 1967).
2. Crooks, Walter M., Frederic M. Hoblit, Finis A. Mitchell, et al, "Project HICAT High Altitude Clear Air Turbulence Measurements and Meteorological Correlations, " Air Force Flight Dynamics Laboratory Technical Report AFFDL-TR-68-127 (November 1968).
3. Ashburn, Edward V., David T. Prophet, and David E. Waco, "High Altitude Clear Air Turbulence Models for Aircraft Design and Operation, " Air Force Flight Dynamics Laboratory Technical Report AFFDL-TR-79 (July 1968).
4. Byers, Horace R., and Roscoe R. Braham Jr., "The Thunderstorm, " (U.S. Dept. Commerce, Washington D.C. 1949).
5. Briggs, J. and W.T. Roach, "Aircraft Observations Near Jet Streams, " Quart. J. Roy. Meteorol. Soc. 89, 225-47 (1963)
6. Endlich, R.M. and R.L. Mancuso, "On the Analysis of Clear Air Turbulence, " Proc. National Air Meeting on Clear Air Turbulence, Soc Automatic Engineers, New York (1966) pp. 172-80.
7. Helvey, R.A., "Observations of Stratospheric Clear-Air Turbulences and Mountain Waves Over the Sierra Nevada Mountains, " Final Report, Contract AF 19(628)-4146, Dept. of Meteorology, U.C.L.A., (1967) 60 pp.
8. Kadlec, P.W., "Atmospheric Temperature Gradients Related to Clear Air Turbulence in the Upper Troposphere and Lower Stratosphere, " NASA Contract No. NAS 4-1194, Eastern Air Lines, Inc., (1967) 15 pp.
9. Moore, R.L. and T.N.Krishnamurti, "A Theory of Generation of Clear Air Turbulence, " Proc. National Air Meeting on Clear Air Turbulence, Society Automotive Engineers, New York, (1966) pp 462-464.

Unclassified

Security Classification

DOCUMENT CONTROL DATA - R & D		
<i>(Security classification of title, body of abstract and indexing annotation must be entered when the overall report is classified)</i>		
1. ORIGINATING ACTIVITY (Corporate author) Lockheed-California Company P.O. Box 551 Burbank, California		2a. REPORT SECURITY CLASSIFICATION Unclassified
		2b. GROUP
3. REPORT TITLE DEVELOPMENT OF HIGH ALTITUDE CLEAR AIR TURBULENCE MODELS		
4. DESCRIPTIVE NOTES (Type of report and inclusive dates) Final Report 30 September 1968 - 30 September 1969		
5. AUTHOR(S) (First name, middle initial, last name) Edward V. Ashburn, David E. Waco, Finis A. Mitchell		
6. REPORT DATE September 1969	7a. TOTAL NO. OF PAGES 82	7b. NO. OF REFS 10
8a. CONTRACT OR GRANT NO. F33615-69-C-1033	9a. ORIGINATOR'S REPORT NUMBER(S) LR22630	
b. PROJECT NO. c. 1367 d.	9b. OTHER REPORT NO(S) (Any other numbers that may be assigned this report)	
10. DISTRIBUTION STATEMENT This document is subject to special export controls and each transmittal to foreign governments or foreign nationals may be made only with prior approval of the Air Force Flight Dynamics Laboratory (FDTR), Wright-Patterson AFB, Ohio 45433		
11. SUPPLEMENTARY NOTES	12. SPONSORING MILITARY ACTIVITY Flight Dynamics Laboratory Air Force Systems Command Wright-Patterson Air Force Base, Ohio	
13. ABSTRACT <p>The high altitude clear air turbulence (HICAT) data were divided into subsets defined by season, altitude, topography, and flight heading. The shape of the power spectral density curves are shown to be a function of topography with the corresponding "scale lengths" 500 feet for flights over water and flatland and increasing to 6000-8000 feet for flights over high mountains. Curves representing the percentage exceedance of the RMS of the area under the truncated PSD curves are logarithmic curves for the subsets defined by topography but are not simple logarithmic curves for the subsets defined by season or altitude. Ratios of the total RMS of the area under the PSD curves to the truncated area truncated at $\lambda = 2000$ feet are given for the various scale lengths. Eight functions of atmospheric temperature and wind were shown to be significantly correlated with high altitude clear air turbulence. A significantly greater number of the observations of turbulence occurred with headwinds than with tailwinds. The percentage exceedance of the lengths of turbulent regions was shown to be a logarithmic function. The length of the turbulent regions and the intensity of the turbulence decreased with altitude above the turbulence cloud top.</p>		

DD FORM 1473
1 NOV 65

Unclassified

Security Classification

Unclassified

Security Classification

14	KEY WORDS	LINK A		LINK B		LINK C	
		ROLE	WT	ROLE	WT	ROLE	WT
	1. High altitude clear air turbulence						
	2. Clear air turbulence						
	3. Power spectral density curves, clear air turbulence and topography						
	4. Meteorological and geophysical conditions for clear air turbulence						
	5. HICAT						

Unclassified

Security Classification